INFORMATION TO USERS

This manuscript has been reproduced from the microfilm master. UMI films the text directly from the original or copy submitted. Thus, some thesis and dissertation copies are in typewriter face, while others may be from any type of computer printer.

The quality of this reproduction is dependent upon the quality of the copy submitted. Broken or indistinct print, colored or poor quality illustrations and photographs, print bleedthrough, substandard margins, and improper alignment can adversely affect reproduction.

In the unlikely event that the author did not send UMI a complete manuscript and there are missing pages, these will be noted. Also, if unauthorized copyright material had to be removed, a note will indicate the deletion.

Oversize materials (e.g., maps, drawings, charts) are reproduced by sectioning the original, beginning at the upper left-hand corner and continuing from left to right in equal sections with small overlaps. Each original is also photographed in one exposure and is included in reduced form at the back of the book.

Photographs included in the original manuscript have been reproduced xerographically in this copy. Higher quality 6" x 9" black and white photographic prints are available for any photographs or illustrations appearing in this copy for an additional charge. Contact UMI directly to order.

UMI

University Microfilms International
A Bell & Howell Information Company
300 North Zeeb Road Ann Arbor MI 48106-1346 USA
313 761-4700 800 521-0600

Order Number 9510737

Modulation spectroscopy study of strained-layer semiconductor microstructures

Yin, Yichun, Ph.D.

City University of New York, 1994

U·M·I
300 N. Zeeb Rd.
Ann Arbor, MI 48106

MODULATION SPECTROSCOPY STUDY OF STRAINED-LAYER SEMICONDUCTOR MICROSTRUCTURES

by

Yichun Yin

A dissertation submitted to the Graduate Faculty in Physics in partial fulfillment of the requirements for the degree of Doctor of Philosophy, The City University of New York

1994

This manuscript has been read and accepted for the Graduate Faculty in Physics in satisfaction of the dissertation requirement for the degree of Doctor of Philosophy.

May 15, 1994
Date

Fred H. Pollak
Chair of Examining Committee

June 21, 1994
Date

Edward R. Zysman
Executive Officer

Distinguished Professor Fred H. Pollak

Professor Steven G. Greenbaum

Dr. Mark S. Hybertsen

Professor Micha Tomkiewicz

Supervisory Committee

THE CITY UNIVERSITY OF NEW YORK

Abstract

MODULATION SPECTROSCOPY STUDY OF STRAINED-LAYER SEMICONDUCTOR MICROSTRUCTURES

by

Yichun Yin

Advisor: Distinguished Professor Fred H. Pollak

Strained-layer semiconductor microstructures are of great importance for both fundamental interest and technological applications. A study of such systems can reveal a great amount of information of the physics of reduced dimensionality, strain effects, as well as knowledge for material and structural characterization. In this thesis, electroreflectance, photoreflectance and piezoreflectance modulation spectroscopy methods were employed to investigate a number of strained microstructures.

We have for the first time positively identified the optical features in modulation spectroscopy associated with the two-dimensional electron gas properties in the pseudomorphic modulation-doped quantum well structures. We have proposed a proper modulation spectroscopy lineshape function for the intersubband transitions in a modulation-doped quantum well with two-dimensional electron gas. This lineshape allows us to extract the Fermi level position relative to the electron subband in addition

to the intersubband transition energies and broadening, which in turn yields the sheet electron density present in the well channel.

We have measured the Ge composition dependence of the E_1 and "E_0'" (will be defined later in chapter 5) transition energies at 300K in a series of strained $Si_{1-x}Ge_x$/Si layers ($0<x<0.23$) using photoreflectance. In our strained samples the energy of the E_1 peak is essentially the same as in unstrained material, in agreement with deformation potential theory. The "E_0'" feature, which exhibits only a very weak variation with Ge content, may also contain a strain-shifted $E_1+\Delta_1$ component.

We have investigated a number of short-period strained Si-Ge microstructures fabricated on (001) Ge using piezoreflectance, photoreflectance and Schottky barrier electroreflectance at 77K. In addition to bulk Ge these samples consisted of Ge quantum wells sandwiched between ordered short-period strained Si-Ge superlattice regions. No evidence for pseudodirect transitions in the Si-Ge superlattices was found by any of the above measurements although quantum transitions in the Ge quantum wells were observed in piezoreflectance. The photoreflectance and Schottky barrier electroreflectance spectra measured to date derive from the bulk-like Ge regions of the sample, in contrast to previously published data on similar samples.

Dedication

To my parents, my wife Kequn and my sons Albert and Jack

Acknowledgements

I wish to express my greatest appreciation to my thesis advisor, Distinguished Professor Fred H. Pollak. Without his guidance, support, and encouragement, this dissertation would have been impossible. His enthusiasm and creativity in exploring and understanding physics were an inspiration. His valuable friendship and his constant interest in my progress has given me more than one could hope for in mentor.

I would like to express my deep gratitude to the other members of my thesis advisory committee, Professor Steven G. Greenbaum of Hunter College, Dr. Mark S. Hybertsen of AT&T Bell Labs, and Professor Micha Tomkiewicz of Brooklyn College for agreeing to serve on my committee and for their careful reading and of this manuscript and helpful advice. I want to especially thank Dr. Mark S. Hybertsen, who was our collaborator in part of the work in this thesis, for his many inspiring discussions with me.

I am deeply indebted to my colleagues at Brooklyn College, Dr. Dong Yan, Dr. Hao Qiang, Dr. Xiaomin Yin and Dr. Edward Look, for their support, encouragement and friendship. The experience of working in this group has left me with wonderful memories that I will ever cherish. In particular I want to thank Dr. Dong Yan, who is my source of all kinds of help during the years of my graduate study. I want to thank

Prof. Y. S. Huang at National Taiwan Institute of Technology for his friendship, encouragement and support.

I wish to acknowledge with gratitude the Department of Physics of Brooklyn College, the City University of New York for providing me with this opportunity and support. I want to thank the faculty of this department for the wonderful lectures. I want to express my deep gratitude to Professor Victor Franco for his encouragement, support, inspiring discussions and friendship during my years of stay at Brooklyn College. I want sincerely thank Ms. Pearl Coyne and Ms. Laura Incampo for their friendship and support for all those years.

My sincere gratitude and great appreciation to my wife Kequn are beyond description. Without her support and sacrifice during the years of my graduate study this work would never have been possible. I also want to thank my sons Albert and Jack for their understanding and support during my hardworking years of graduate study.

TABLE OF CONTENTS

ACRONYMS

1D	one-dimensional
2D	two-dimensional
2DEG	two-dimensional electron-gas
3D	three-dimensional
AP	Auger profilometry
BZ	Brillouin zone
CER	contactless electroreflectance
EBER	electron-beam electroreflectance
EM	Electromodulation
ER	electroreflectance
FDGL	first-derivative Gaussian lineshape
HBT	heterojunction bipolar transistors
HEMT	high electron mobility transistor
HH	heavy-hole
HRXRD	high resolution x-ray diffraction
HJ	heterojunctions
LCAO	linear combination of atomic orbital
LH	light-hole
LPE	liquid phase epitaxy
MBE	molecular beam epitaxy
MDQW	modulation-doped quantum well
MDHJ	modulation-doped heterojunction
MIS	metal-insulator-semiconductor
MKPM	modified Kronig-Penney model
ML	monolayers
MODFET	modulation-doped field effect transistor
MQW	multiple quantum well
NID	not-intentionally doped
OMCVD	organometallic chemical vapor deposition
OMVPE	organometallic vapor phase epitaxy
PHEMT	pseudomorphic high electron mobility transistor
PMDQW	pseudomorphic modulation doped quantum well
PR	photoreflectance
PzR	piezoreflectance
QW	quantum well
RTCVD	rapid thermal chemical vapor deposition
SBER	Shottky barrier electroreflectance
SCR	space-charge region
SDHT	selectively doped heterostructure transistor
SL	superlattices
SLSPSL	strained-layer short period superlattice
SQW	single quantum well

TEGFET	two-dimensional electron-gas field effect transistor
TEM	transmission electron microscopy
TR	thermoreflectance
VNDF	variable neutral density filter
VPE	vapor phase epitaxy

LIST OF TABLES

LIST OF FIGURES

Chapter 1. INTRODUCTION

Semiconductor microstructures such as heterojunctions (HJ), quantum wells (QW), multiple quantum wells (MQW), superlattices (SL), etc., have been receiving great deal of attention and considerable research efforts ever since the pioneer work of Esaki and Tsu in 1970 (Esaki and Tsu 1970). The study and application of these semiconductor microstructures have greatly enriched our understanding of the fundamental physics of semiconductor materials and brought about tremendous technological progress. Using modern thin film growth techniques such as molecular beam epitaxy (MBE), organometallic vapor phase epitaxy (OMVPE), gas phase MBE, liquid phase epitaxy (LPE), etc., various structures can be grown in a precisely controlled way (See, for example, Bauer *et al.* 1990, Bean 1988, and references therein). These structures can be composed of ultra thin layers of thicknesses varying from several atomic layers to several hundred Å (typical thickness of 100 Å) of different composition, of alternating doping or a combination of them. Also heterointerfaces can be either lattice-matched or strained. The reduced dimensionality in such systems alters the behavior of electrons and holes in the synthetic semiconductor systems at the quantum mechanical level, bringing about a large number of phenomena that are not available in the natural bulk semiconductors. The novel electronic and optical properties of these structures have made possible many high performance devices such as heterojunction bipolar transistors (HBT), high electron mobility transistors (HEMT), quantum well lasers, etc. Because of the great scientific significance of these microstructures and their potential applications in electronics and optoelectronics, efforts to better understand the

physical properties of these systems and to obtain better materials and devices from these systems continue to thrive.

For about a decade in the beginning years, works on semiconductor microstructures mostly focused on those grown from lattice-matched materials. Early attempts to grow strained microstructures had failed due to the large densities of dislocations at the heterointerfaces arising from strain relaxation between the mismatched layers. Although strained-layer semiconductor microstructures were first proposed by Mathew and Blakeslee in 1976 (Matthews and Blakeslee 1976), they did not acquire considerable attention until Osbourn pointed out in 1982 that the growth of thin layers (typical thickness of 100 Å), which is necessary to achieve sizeable quantum confinement effects, in fact relaxes the requirement of lattice matching between host materials inasmuch as any lattice mismatch could be elastically accommodated by strains of the host layers (Osbourn 1982). Since then there has been increasing interest and research in this field. Since the requirement for the host materials to be lattice-matched is relaxed, we have more materials to choose from for the host materials of our artificial structures. In addition the strain in these structures can also be a controlling parameter (Bir and Pikus 1974, Pollak 1990). In these strained-layer microstructures we have both quantum size-effects and strain-induced effects. Together, they can produce novel physical phenomena that are not available in lattice-matched systems. Great progress in the understanding and the application of strained semiconductor microstructures has been achieved (see, for example, Pearsall 1989b, Pollak 1990b, Marzin and Gerard

1990, People and Jackson 1990). More and more interesting and challenging topics are still to be explored. Both experimental investigation and theoretical research in this field will continue to expand rapidly.

Modulation spectroscopy has proven to be a powerful tool in studying and characterizing the electronic levels in semiconductor materials and semiconductor microstructures (see, for example, Cardona 1969, Aspnes 1980, Pollak 1981, Pollak and Glembocki 1988, Pollak 1991, 1992, Glembocki and Shanabrook 1992, Pollak and Shen 1993). It deals with the measurement and interpretation of changes in the optical response of a sample which are caused by modifying in some way the measurement conditions. This can easily be accomplished by periodically modulating (a) some parameter applied to the sample ("external" modulation) or (b) the measurement conditions themselves ("internal" modulation). The observed normalized changes are usually small so that the difference signals are closely related to a derivative of the absolute spectrum with respect to the modifying parameter. The derivative nature of modulation spectroscopy emphasizes structures localized in the photon energy region of interband (intersubband) transitions of semiconductors (semiconductor microstructures) and suppresses uninteresting background effects. Also weak features that may not have been detected in the absolute spectra are often enhanced. Because of this derivative-like nature, a large number of sharp spectral features can be observed, even at elevated temperatures. The measured spectra can be fitted to appropriate lineshapes to accurately determine the peak energies and broadening parameters of the relevant transitions. This

fitting procedure is made possible by the derivative nature of this method. Unlike absolute optical spectra where the interpretation involves a calculation of full spectra, the features in modulation spectroscopy are localized in photon energy, greatly simplifing the analysis. These two key aspects, i.e., sensitive experimental spectrum and the ability to accurately determine the physical parameters from lineshape fitting, have established modulation spectroscopy as a superior experimental technique.

In this thesis, the optical properties of four types of very important strained-layer semiconductor microstructures will be investigated using modulation spectroscopy. They are GaAlAs/InGaAs/GaAs pseudomorphic modulation-doped quantum wells (MDQW) structures, strained SiGe Si-rich alloy films grown on (001) Si substrate, strained-layer Si-Ge short period superlattices (SLSPSL) grown on (001) Ge and Ge/SiGe quantum wells grown on (001) Ge.

Modulation doping of heterostructures was first implemented by Stormer and Dingle *et al.* (Dingle *et al.* 1978, Stormer *et al.* 1979) on n-type modulation-doped samples. The underlying idea is that, at equilibrium, charge transfer occurs across a heterojunction to equalize the Fermi level on both sides. For example, n-doping the wide-bandgap side of the GaAlAs/GaAs heterojunction causes electrons to be transferred to the GaAs layer until equilibrium is reached. The charge-transfer effect makes possible an old dream of semiconductor technologists, i.e., getting conducting electrons in a high-purity, high-mobility semiconductor without having to introduce mobility-limiting donor impurities. Since then, modulation doping has been applied to a number of situations

involving various semiconductor pairs and also to hole modulation doping. The impressive development of the subject is due to the applicability both to basic science (many-body physics, reduced dimensional electron gas system, quantum Hall effect, etc.) and to very high-performance devices called equivalently HEMT, two-dimensional electron-gas (2DEG) field effect transistor (TEGFET), selectively doped heterostructure transistor (SDHT), and modulation-doped field effect transistor (MODFET) (See, for example, Morkoc and Unlu 1987, Smith P. M. *et al.* 1990, Schaff *et al.* 1990). A lot of work was directed to the study and characterization of such structures using modulation spectroscopy (Snow *et al.* 1988, Mendonca *et al.* 1990, Novellino *et al* 1991, Sydor *et al* 1991a, 1991b, 1992), but the 2DEG effects were not completely understood.

The GaAlAs/InGaAs/GaAs pseudomorphic modulation doped quantum well (PMDQW) has many advantages compared to the GaAlAs/GaAs modulation doped system. The InGaAs channel is beneficial in many respects. This material produces an excellent conduction profile, forming a quantum well that provides good confinement of the electrons. Larger conduction band discontinuity, which allows high two-dimensional electron gas densities in the well channel, can be achieved for a given Al composition in the GaAlAs/InGaAs/GaAs system than in the GaAlAs/GaAs structures. This also overcomes the problem in GaAlAs/GaAs systems due to the DX centers in the GaAlAs (with Al mole fraction over 15%) (see, for example, Morkoc and Unlu 1987, Schaff *et al.* 1990). The GaAlAs/InGaAs/GaAs PMDQW structure is also best suited to be used in the investigation of the properties of the two-dimensional electron gas (2DEG) present

in the InGaAs channel. The smaller band gap of the InGaAs channel enhances the electron confinement. The transition energies in the 2DEG are lower than that from the GaAs substrate, hence, the features of interest stand out clean and clear. The traces due to the 2DEG in modulation spectroscopy have very unusual lineshapes which were not given a satisfactory explanation. A detailed knowledge of these lineshapes will further enrich our understanding of modulation spectroscopy, and is extremely important to the application of modulation spectroscopy to the investigation and characterization of the properties of the PMDQW.

The group IV materials silicon and germanium are both indirect gap semiconductors. They are also the most technologically important materials. They both have been extensively studied and reasonably well understood in their bulk forms. But the properties of microstructures using Si and Ge as host materials are not as clear at the present stage. The relative lattice mismatch $\Delta a/a$ is 4.2%. Strain in such microstructures can be tuned in a large range and hence plays a very important role. The growth technique of SiGe strained-layer microstructures has received considerable attention and has been greatly improved since it was reported that the critical thickness of these layers greatly exceeds the predictions of equilibrium models (Bean *et al.* 1984a, 1984b). Various high quality strained-layer SiGe microstructures are now readily obtainable. The most interesting topic in this field is to search for a direct gap semiconductor from the artificial structures of these indirect group IV materials. Modifications in the band gap which come about from the alloying of Si and Ge as well

as from the strain, and the effect of the superlattice potential in these materials and their alloys have raised the hope that a direct band gap material may be achievable in a group IV semiconductor system, according to earlier theoretical calculations (Gnutzmann and Clausecker 1974). Such perspectives have stimulated a considerable amount of experimental effort (see, for example, Bevk *et al.* 1986, Pearsall *et al.* 1987, 1989a, 1989c, Pearsall 1990b, Dafesh *et al.* 1990a, 1990b, Asami *et al.* 1990, Gell *et al.* 1990, Mencziger *et al.* 1991), and intensive further theoretical research (see, for example, Froyen *et al.* 1987, People and Jackson 1987, Hybertsen and Schluter 1988, Godby *et al.* 1988, Schmid *et al.* 1991, 1992). Modulation spectrosocpy has been applied to investigate (001) SiGe SLSPSL structures fabricated on Si substrate (Pearsall *et al.* 1987, 1989a, Asami *et al.* 1990), Ge substrate (Pearsall *et al.* 1989c, 1989d, Pearsall 1990b, Gell *et al.* 1990, Mencziger *et al.* 1991, Yin Y. *et al* 1991, 1992), and GeSi buffer (Dafesh *et al.* 1990a, 1990b). Evidence of pseudodirect transitions in such SLSPSL has been reported (Pearsall *et al.* 1987, Pearsall *et al.* 1989c, Pearsall 1989d, Pearsall 1990b, Asami *et al.* 1990, Gell *et al.* 1990, U. Mencziger *et al.* 1991, Dafesh *et al* 1990a, 1990b), but are not conclusive. Work is continuing to determine more definitively the nature of the band gap in these structures and its dependence on the lattice constant of the substrate, the periodicity of the structure and other material parameters.

Ge/SiGe quantum wells can be used to study many interesting physical properties, such as band offset, electron-phonon interaction in the group IV reduced dimensional systems, etc. SiGe Alloys are promising materials for the design of novel and high-

performance devices (Iyer *et al* 1989, King C. A. *et al* 1989). Their fundamental (indirect) band gaps span the 1.3 μm to 1.55 μm range, and can be applied to long wavelength integrated optoelectronics grown on Si (see, for instance, People 1986 and references therein). There is much literature on the properties of these alloys in early works (See, for example, Tauc and Abrahám 1961, Kline *et al.* 1968). Great progress has been made in semiconductor material growth techniques since then. Today's high quality SiGe alloy samples will provide better conditions and allow more precise determination of many important physical parameters. Moreover, strain can be used to control the properties of the alloy film, such as the bandgap. The reexamining of some very fine, intriguing aspects of these high quality strained alloy films will greatly enrich our knowledge about them and speed up their application.

This thesis consists of seven chapters. In Chapter 2, some theoretical aspects about semiconductors and semiconductor microstructures, including methods for calculating quantum levels in microsctructures, strain effects and temperature dependence of band gaps and broadening parameters are briefly reviewed. Principles and techniques of modulation spectroscopy are discussed in Chapter 3. In particular, lineshapes associated with the 2DEG of modulation spectroscopy will be considered. Chapter 4 deals with pseudomorphic modulation-doped quantum well, emphasizing the 2DEG effects. An investigation of a series of Si rich thin SiGe films grown on (001) Si substrate is reported in Chapter 5. The work on strained SiGe microstructures grown on (001) Ge is reported in Chapter 6, including a study of the temperature dependence

of the transition energy and broadening of the fundamental direct gap of (001) bulk Ge and the intersubband transitions in a SiGe/Ge quantum well. A summary and conclusions are given in Chapter 7.

Chapter 2. THEORETICAL CONSIDERATIONS

In this chapter I intend to briefly review some theoretical aspects of semiconductors and semiconductor microstructures directly related to this thesis work. Methods for calculating the electronic states in semiconductor microstructures are discussed in Section 2.1, including the Schrödinger-Poisson self-consistent approach for calculating the electronic levels and the sheet density of the 2DEG in a MDQW. Strain effects and their theoretical descriptions will be discussed in Section 2.2. The temperature dependence of energy gaps and broadening parameters is considered in Section 2.3.

2.1 Electronic states in microstructures

The quantum levels in semiconductor microstructures can be calculated in a number of ways. I will limit the discussion to the approaches used in this thesis. The simplest and most frequently used methods are based on the envelope function approximation (see, for example, Bastard 1982, Weisbuch 1987). In what follows in this section, I will first introduce the envelope function approximation, and then review two simple but important models, the modified Kronig-Penney model (MKPM) and the Bastard model. Finally I will outline the self consistent approach for calculating the quantum levels and the sheet density of the 2DEG in a n-type modulation-doped quantum well.

2.1.1. Envelope function approximation

In the one-electron approximation, the Schrödinger equation for the motion of an electron in an unperturbed crystal is:

$$H_0\psi_{nk}(r) = E_n(k)\psi_{nk}(r) \tag{2.1}$$

where n is the band index, k is the crystal wave vector which is restricted to the first Brillouin zone, H_0 is the one-electron Hamiltonian of the crystal with a periodic potential $V(r)$:

$$H_0 = \left[-\frac{\hbar^2}{2m_0}\right]\nabla^2 + V(r) \tag{2.2}$$

where m_0 is the free electron mass, and $\psi_{nk}(r)$ is the Bloch function with energy eigenvalue $E_n(k)$, and

$$\psi_{nk}(r) = u_{nk}(r)e^{ik.r} \tag{2.3}$$

where $u_{nk}(r)$ is a periodic function with the periodicity of the crystal lattice.

In the presence of some perturbation potential $U(r)$, the Schrödinger equation of the system becomes:

$$[H_0 + U(r) - E]\Psi(r) = 0 \tag{2.4}$$

where E is the energy, and $\Psi(r)$ is the one-electron wave function. $U(r)$ is assumed to be slowly varying compared to the crystal periodicity. When $U(r)=0$ Eq. (2.4) reduces to Eq. (2.1). Assuming that the energy eigenvalues $E_n(k)$ and the Bloch wave functions $\psi_{nk}(r)$ are given, it can be shown that (Kohn 1957, Altarelli 1986), if:

(a) $U(r)$ is slowly varying on the scale of the lattice parameter a of the semiconductor, i.e., its Fourier transform $U(k)$ is appreciably non-zero only in a region around $k=0$ of extension Δk, with $\Delta k \ll 2\pi/a$,

(b) $U(r)$ is weak, i.e., $|<\psi_{nk}|U|\psi_{n'k}>| \ll |E_n(0)-E_{n'}(0)| \quad (n \neq n')$,

(c) we are considering eigenvalues in the neighborhood of a simple parabolic band edge n, well separated from all others:

$$E_n(k) = E_n(0) + \frac{\hbar^2 k^2}{2m^*} \tag{2.5}$$

where m^* is the effective mass of the electron (or hole), then the problem of Eq. (2.4) can be reduced to solving the following effective-mass equation:

$$\left[-\frac{\hbar^2}{2m^*}\nabla^2 + U(r)\right]F_n(r) = [E-E_n(0)]F_n(r), \tag{2.6a}$$

$$\Psi_n(r) = F_n(r)\psi_{n0}(r) \tag{2.6b}$$

where $F_n(r)$ is the so-called envelope function.

As can be seen from Eqs. (2.6a)-(2.6b), the unperturbed properties of the bulk semiconductor enter the calculation via two parameters: the effective mass m^* and the band edge energy $E_n(0)$. Equation (2.6b) shows that the wave function in the presence of $U(r)$ is a slowly varying "envelope" function modulating the rapidly varying unperturbed Bloch function.

Semiconductor microstructures in general contain more than one constituent material. Assuming the growth direction to be along the z-axis, the effective masses and band gaps will vary as a function of z. The z-dependent $E_n(0)$ can be considered as $U(r)$, i.e., $U(r)=E_n(0,z)$. Depending on how the bands in the host materials are lined up, such potentials for a specific pair of conduction-valence bands (for example, the electron-heavy hole bands) in the microstructure may have either a type I profile, which means the potentials for electrons and holes have their minimum values in the same layer of material, or a type II profile, which means the electrons and holes have their minimum potentials in different host layers. Shown in Fig. 1 is an illustration of the two types of potential profile in the case of a quantum well.

In the case of semiconductor microstructures Eq. (2.6a) is generalized to read:

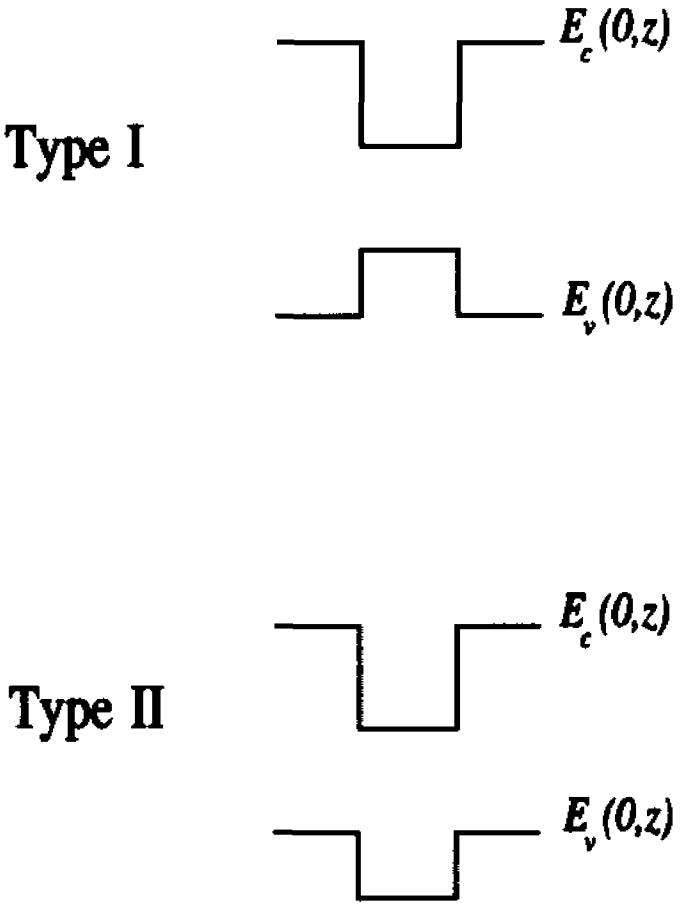

Fig. 1. Illustration of type I and type II potential profile in the case of a quantum well.

$$\left[-\frac{\hbar^2}{2}\frac{d}{dz}\left(\frac{1}{m^*(z)}\frac{d}{dz}\right)+E_n(0,z)\right]F_{n,s}(z) = E_s F_{n,s}(z), \qquad (2.7)$$

where the index s is used to label the quantized levels of envelope function F_n. The kinetic energy term in Eq. (2.7) has been rewritten, for a z-dependent mass, in a way

which restores the Hermitian character of the Hamiltonian (Harrison 1961, Ben-Daniel and Duke 1966). The boundary conditions at the heterointerfaces are given by

$$F_{n,s}(z) \quad \textit{continuous at interface},$$
$$\frac{1}{m^*}\frac{\partial F_{n,s}(z)}{\partial z} \quad \textit{continuous at interface} \tag{2.8}$$

These boundary conditions require that the periodic factor u_{n0} of the Bloch wave function on both sides of the heterointerface be approximately the same, and ensure the current density conservation. Equations (2.7) and (2.8) serve as the starting point for the calculation methods to be discussed in this section. Their solutions give a series of subband energy levels E_s, $s=1,2\ldots$, and the wave (envelope) functions F of the relevant levels. Equation (2.7) and the boundary conditions Eq. (2.8) are also known as the Ben-Daniel-Duke model.

2.1.2. Modified Kronig-Penney model

The Kronig-Penney model has been described in quantum mechanics textbooks (see, for example, Merzbacher 1970). It deals with the one-dimensional periodic square well potential problem and illustrates the consequences of the periodicity in potential. In the limit of infinite barrier width it gives the results of uncoupled multiple quantum wells.

In a semiconductor superlattice, the periodic potential is due to the band alignment of the alternating thin layers of host materials along the growth direction (z). Since the host materials of a compositional superlattice are usually different, the effective masses of the particles (electrons in the conduction band, or holes in the valence band) also undergo a periodic change. In the envelope function approximation the equation of motion and the boundary conditions at the interfaces in such cases are modified according to Eqs. (2.7) and (2.8), as given by the Ben-Dannial-Duke model. In addition, due to the translational symmetry along the growth direction we have the Born-von Karman periodic condition. Using Eqs. (2.7), (2.8) and the Born-von Karman periodic condition the superlattice miniband structure can be found. This is the so-called modified Kronig-Penney model.

Let E_g^I, m_I^*, d_I and E_g^{II} m_{II}^*, d_{II} be the energy gap, effective mass and layer thickness in well and barrier materials, respectively. Consider the case of type I band alignment and define V_o as the energy gap difference:

$$V_o = E_g^{II} - E_g^I \tag{2.9}$$

V_o is divided in one part $V_{o,c}$ that appears as a discontinuity in the conduction band $E_c(z)$ and another part $V_{o,v}$ which modulates valence band edge $E_v(z)$, such that

$$V_{o,c} + V_{o,v} = V_o \tag{2.10}$$

This is illustrated in Fig. 2.

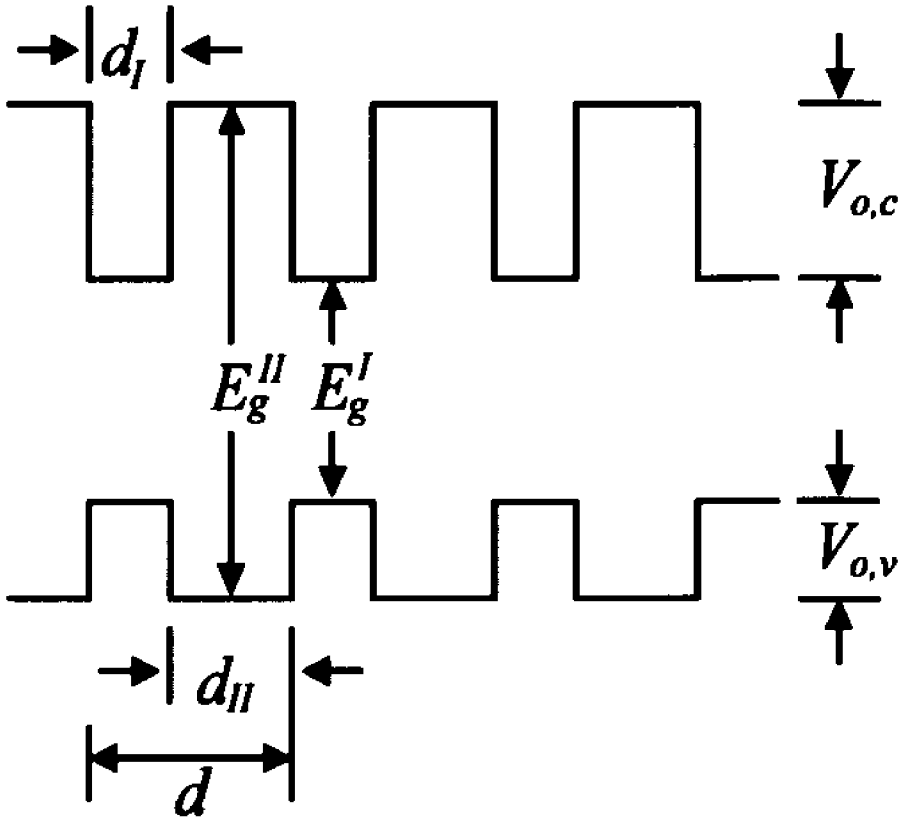

Fig. 2. Schematic representation of the potential profile of a superlattice.

The solution is given by the modified Kronig-Penney equation:

$$\cos(qd) = \cos(k_I d_I)\cos(k_{II} d_{II}) - \frac{1}{2}(\chi + \frac{1}{\chi})\sin(k_I d_I)\sin(k_{II} d_{II}) \qquad (2.11)$$

where

$$d = d_I + d_{II} \tag{2.12a}$$

$$\chi = \frac{k_I m_{II}^*}{k_{II} m_I^*} \tag{2.12b}$$

$$k_I^2 = (2m_I^* E/\hbar^2) - k_\perp^2 \tag{2.12c}$$

$$k_{II}^2 = \left[2m_{II}^* (V_{o,i} - E)/\hbar^2\right] - k_\perp^2 \tag{2.12d}$$

with $i = c$, *or* v

with $k_\perp^2 = k_x^2 + k_y^2$, the momentum perpendicular to the superlattices growth direction; and q is the wave vector associated with the superlattice periodicity, i.e., the one-dimensional Bloch wave vector in the growth direction of the superlattice.

In the case of type II band alignment Eq. (2.10) should be modified to read:

$$|V_{o,c} - V_{o,v}| = V_o \tag{2.13}$$

The quantum levels in a type II superlattice are calculated in the same way since in this model each band is treated independently. For type II multiple quantum wells the electrons and holes are confined in different layers. The transitions between these states are spatially indirect. The intensity of such transitions is much weaker than its counterpart in the type I case.

The Kronig-Penney model is the simplest case and is still the one most commonly used in the design of superlattices. However, it frequently introduces errors for the higher-lying subbands. This is because of the non-parabolicity of the bulk band structure, the mixing of the superlattices bands when they are close in energy and the mixing of the valence bands of light and heavy hole character for **k** not equal to zero.

2.1.3. Bastard model

The Bastard model (the multiband envelope function method) made a big improvement in calculating microstructure electronic levels over the MKPM, yet without introducing much more computation effort (Bastard 1981, 1982). It uses the Kane model (Kane 1966) to describe the host material band structures. The 8 × 8 Kane Hamiltonian matrix that describes the electron ***k.p*** interaction within the lowest conduction, highest valence and spin-orbit split bands are decoupled into two 1 × 1 matrices for the heavy holes and two 3 × 3 matrices for the light particles (electrons, light holes and spin-orbit split holes). Heavy holes are thus treated separately, as in the MKPM. However, the 3 × 3 system introduces a small modification to the MKPM, that is, m_I^* and m_{II}^* are replaced by $m_I(E)$ and $m_{II}(E)$, where

$$m_I(E)^{-1} = 1 + \frac{2P^2}{3}\left[\frac{2}{E+E_g^I} + \frac{1}{E+E_g^I+\Delta_I}\right]$$

$$m_{II}(E)^{-1} = 1 + \frac{2P^2}{3}\left[\frac{2}{E+E_g^{II}-V_{o,v}} + \frac{1}{E+E_g^{II}+\Delta_I-V_b}\right] \qquad (2.14)$$

where P is the momentum matrix element between the conduction and valence bands, Δ_s is the spin-orbit splitting and V_0 is the band offset of the split-off band. This model is also called the three-band Kane model. Sometimes the spin-orbit split band is neglected by setting Δ_s to infinite; this is called the two-band model.

The advantage of the Bastard model is that at almost no cost in terms of computational effort, it gives quite satisfactory results. The calculated energy levels are in quantitative agreement with those obtained from more sophisticated methods such as linear combination of atomic orbital (LCAO) (Bastard 1982). The mixing of the conduction and light-hole bands is considered and the nonparabolicity of the bands is included in a natural way. The disadvantage of the Bastard model is that it allows no mixing of bulk heavy and light holes in the superlattice wave function. This approximation is realistic only when superlattice heavy- and light-hole states are sufficiently separated in energy.

2.1.4. Quantum levels and 2DEG in a modulation-doped quantum well

In modulation-doped quantum-well structures there are two-dimensional electron gases in well channels. The potential in which electrons move will be significantly affected by their own presence due to the direct and exchange interactions among them (band gap renormalization). To the lowest order, the many-body interaction is treated in the Hartree approximation by using an average one-electron potential. The envelope function method can then be applied. However, since the confining potential is affected

by the electron distribution (wave function), the Schrödinger equation and the Poisson equation that determines the Coulomb static potential form a coupled system have to be solved self-consistently. The single electron Schrödinger equation for the conduction band can be expressed as (Ando *et al.* 1982):

$$\left[-\frac{\hbar^2}{2m_e^*}\frac{d^2}{dz^2}+V_b(z)+V_{sc}(z)+V_{xc}(z)+V_{IM}(z)\right]\ F_n(z)=E_nF_n(z) \tag{2.15}$$

where, E_n and F_n are the energy and (envelope) wave function of the n^{th} level, $V_b(z)$ is the heterostructure conduction band discontinuity, $V_{sc}(z)$ is the static Coulomb potential that is determined by the Poisson equation. V_{xc} originates from the non-local exchange potential due to Pauli principle, and is usually approximated by the local density approximation as a localized potential. One such example is (Ando *et al.* 1982):

$$V_{xc}(z)=-\left[1+0.7734x(z)\ln\left(1+\frac{1}{x(z)}\right)\right]\left[\frac{1}{\pi br_s(z)}\right]R_y,$$

with

$$a_s=\frac{4\pi\epsilon_0\kappa\hbar^2}{m_0q^2},\quad r_s=\left[\frac{4}{3}\pi a_s^3n(z)\right]^{-\frac{1}{3}},\quad x=\frac{r_s}{21},$$

$$b=\left[\frac{4}{9\pi}\right]^{\frac{1}{3}},\qquad R_y=\frac{q}{8\pi\epsilon_0\kappa a_s}. \tag{2.16}$$

where ϵ_0 is the permittivity of free space, κ is the dielectric constant of the material, q is the unit charge, $\hbar$ is the Plank constant and $n(z)$ is the number density of electrons. In Eq. (2.15) V_{IM} is the contribution from the image charges across the interface due to

different dielectric constants κ of the different material layers. For GaAs/AlGaAs material systems it is believed to be very small since the κ deviation is small.

In the Eq. (2.16) the static Coulomb potential term V_{sc} is determined by the Poisson Equation:

$$\frac{d^2V_{sc}(z)}{dz^2} = -\frac{e}{\epsilon_0 \kappa(z)} n_{total}(z) \tag{2.17}$$

with

$$n_{total}(E_F;z) = \sum_i n_i(E_F)\,|F_i(z)|^2 - p(E_F;z) - N_D^+(E_F;z) + N_A^-(E_F;z) \tag{2.18}$$

where E_F is the Fermi energy, the four terms on the right side of the equation represent the contributions from the free electrons (n_i), free holes (p), ionized donors (N_D^+), and ionized acceptors (N_A^-), respectively. For a MDQW structure, they are:

$$n_i(E_F) = \frac{k_B T}{\pi \hbar^2} \ln[1 + \exp(\frac{E_F - E_i}{k_B T})] \tag{2.19a}$$

$$p(E_F;z) \approx 0 \tag{2.19b}$$

$$N_D^+(E_F;z) = \frac{N_D}{\frac{1}{2} + \exp(\frac{E_D(z) - E_F}{k_B T})} \tag{2.19c}$$

$$N_A^-(E_F;z) = \frac{N_A}{\frac{1}{2}+\exp(\frac{E_F-E_A(z)}{k_BT})} \approx 0 \qquad (2.19d)$$

where E_i is the electron subband level determined by the Schrödinger equation, E_D, E_A, and E_F are the donor level, acceptor level, and Fermi level, respectively, and k_B is the Boltzmann constant. The expression for the n_i is deduced from the step-like 2D density of state distribution. For 2DEG MDQW structures, the contributions from the free holes and acceptors can be neglected. The total electron sheet density N_e is then obtained from:

$$N_e(E_F) = \sum_i n_i(E_F) \qquad (2.20)$$

The Fermi level E_F is determined from the charge neutrality requirement:

$$\int_{-\infty}^{\infty} n_{total}(E_F; z)dz = 0 \qquad (2.21)$$

The nature of this problem makes it impossible to achieve an analytical solution. We used numerical methods to solve this type of problem in our work on PMDQWs. The details of such numerical calculations can be found in Qiang 1993. The output results include the electron and hole levels and their respective wave functions, the potential profile, electric field distribution, sheet electron density and Fermi energy.

2.2. The effects of strain

2.2.1. Introduction

Strain has very significant effects on the electronics states of semiconductor materials (Pollak 1973, Bir and Pikus 1974, Pollak 1990). It produces changes in the lattice parameter and in some cases, in the symmetry of the material. These in turn produce significant changes in the electronic band structure. The vibrational modes in the crystal will be affected also (Pollak 1990), but will not be discussed in this thesis.

All configurations of homogeneous strain can be divided into two contributions: the isotropic or hydrostatic component, which give rise to a volume change without disturbing the crystal symmetry, and the anisotropic component, which in general reduces the symmetry present in the strain-free lattice. The energy gaps are altered, and in some cases, degeneracies are removed. Effective masses are affected by the variations in energy gaps as well as by changes in interband matrix elements. The strain dependence of electronic levels can be characterized by deformation potentials, i.e., the energy shift per unit strain, which are typically from 1 to 10 eV. In strained microstructures, the effects of strain can be used to produce desired effects. This greatly increases the ability to control the electronic and optical properties of such structures.

To fully describe the electronic energy levels of such strained microstructures, it is important to have information about the effects of strain on the properties of the host

materials. These include strain-induced changes in the energy gaps, splittings due to the lowering of symmetry, and variations in effective masses.

In this section the main results of the strain effects on bulk electronic band structure will be presented.

2.2.2 Strain dependence of critical points at $k=0$

2.2.2.A Strain dependence of energy gaps

Without strain or spin-orbit splitting, the valence-band edge at $k=0$ in diamond- and zincblende-type materials is a sixfold degenerate multiplet with orbital symmetry $\Gamma_{25'}$ (diamond) or Γ_{15} (zincblende). The spin-orbit interaction lifts this degeneracy into a fourfold degenerate (including spin) $P_{3/2}$ multiplet ($J=3/2$, $M_J=\pm 3/2, \pm 1/2$ in spherical notation) and a $P_{1/2}$ multiplet ($J=1/2$, $M_J=\pm 1/2$) as shown in detail in Fig. 3. Also given in Fig. 3 is the double group notation for the spin-orbit bands as well as the lowest conduction bands [$\Gamma_{2'}(\Gamma_1)$] in diamond- and zincblende-type semiconductors. Because of the $J=3/2$ degeneracy, the valence bands have warped energy surfaces (Hensel and Feher 1963, Pollak 1990).

The fundamental direct gap, i.e., the energy difference between the $\Gamma_6^-(\Gamma_6)$ conduction and $\Gamma_8^-(\Gamma_8)$ valence bands, is denoted as E_0. The spin-orbit splitting is Δ_0, and $E_0+\Delta_0$ is the transition energy between $\Gamma_6^-(\Gamma_6)$ and the spin-orbit split $\Gamma_7^+(\Gamma_7)$ bands.

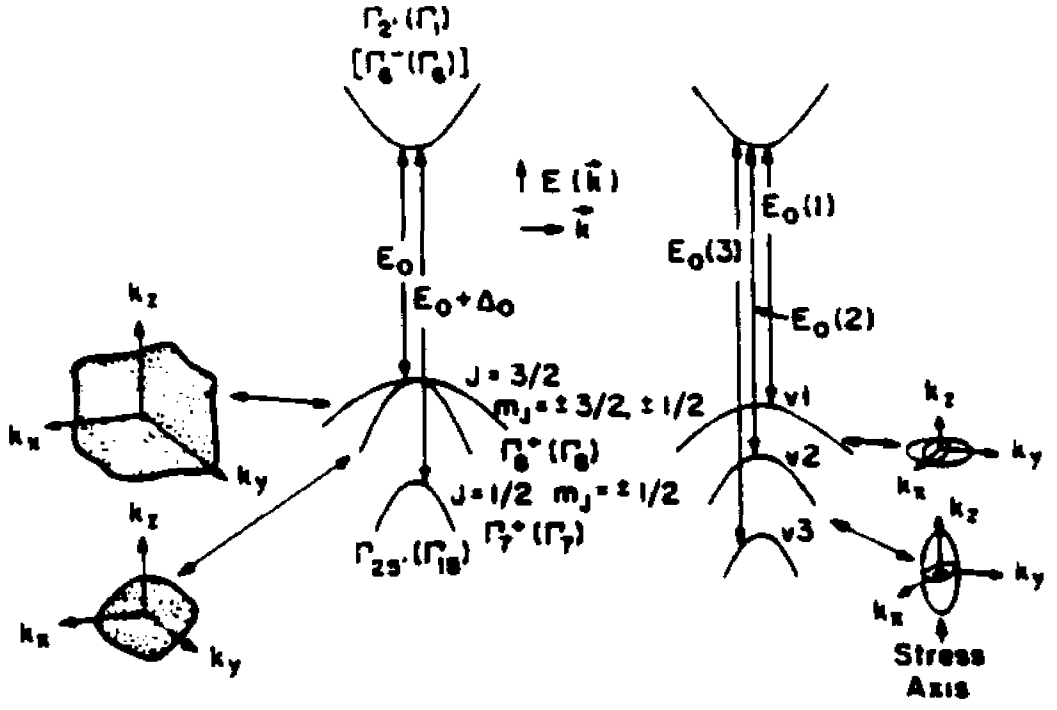

Fig. 3 Valence bands and lowest conduction band in diamond- and zincblende-type semiconductors for unstrained (left-hand) and strained (right-hand) crystal (see text).

A strain with a uniaxial component splits the $J = 3/2$ multiplet into a pair of degenerate Kramers doublets (Kleiner and Roth 1959, Hensel and Feher 1963, Pollak 1973, Bir and Pikus 1974, Pollak 1990). The three valence bands for the case of compressive uniaxial stress along (001) is shown schematically in Fig. 3, where the

bands are labelled v_1, v_2, and v_3. In addition, the hydrostatic component of the strain will shift the energy gap between valence bands and the lowest lying conduction band. The transition between the conduction band and the v_i valence band is denoted $E_0(i)$, where i=1, 2, 3. The removal of the J=3/2 degeneracy produces energy surfaces that are ellipsoids of revolution around the L_z axis (Hensel and Feher 1963, Pollak 1990).

It has been shown that strain Hamiltonian $H_\varepsilon^{(v)}$ for a P-like valence-band multiplet can be expressed as (Pollak 1973, 1990)

$$H_\varepsilon^{(v)} = H_\varepsilon^{(1,v)} + H_\varepsilon^{(2,v)} \tag{2.22}$$

where $H_\varepsilon^{(1,v)}$ is the orbital-strain Hamiltonian and $H_\varepsilon^{(2,v)}$ is the strain-dependent spin-orbit Hamiltonian.

The orbital-strain Hamiltonian $H_\varepsilon^{(1,v)}$ of the valence bands can be written as (Pollak 1973, 1990):

$$\begin{aligned} H_\varepsilon^{(1,v)} = & -a_1 Tr(\varepsilon) - 3b_1[(L_x^2 - \frac{1}{3}L^2)\varepsilon_{xx} + cp] \\ & -\sqrt{3}\, d_1[(L_xL_y + L_yL_x)\varepsilon_{xy} + cp] \end{aligned} \tag{2.23}$$

where ε_{ij} denotes the components of the strain tensor, $\boldsymbol{L}$ is the angular momentum operator and cp denotes cyclic permutation with respect to the indices x, y, z. The quantity a_1 represents the intraband (absolute) shift of the orbital valence bands due to

the hydrostatic component of the stress (intraband or absolute hydrostatic deformation potential), while b_1 and d_1 are orbital uniaxial deformation potentials appropriate to strains of tetragonal and rhombohedral symmetries, respectively.

The contribution from strain-dependent spin-orbit Hamiltonian $H_\varepsilon^{(2,v)}$ is very small compared to that of $H_\varepsilon^{(1,v)}$. It will be ignored in the following discussion (Pollak 1990).

At $\boldsymbol{k}=\mathbf{0}$ the conduction-band minima for the diamond- and zincblende-type solids (except for Si and "zero" bandgap materials such as α-Sn and HgTe) is an antibonding s-state with symmetry $\Gamma_2(\Gamma_1)$. The effects of a strain is to produce a hydrostatic shift given by:

$$H_\varepsilon^{(c)} = a_c Tr(\varepsilon) \tag{2.24}$$

where a_c is the intraband (absolute) hydrostatic deformation potential of the $\Gamma_2(\Gamma_1)$ conduction band.

To explore the structure of the conduction and valence bands near $\boldsymbol{k}=\mathbf{0}$, we shall use the $\boldsymbol{k.p}$ perturbation approach where the Hamiltonian is given by (Kane 1966):

$$H_k = H_0 + \left[\frac{\hbar^2 k^2}{2m_0}\right] + \left[\frac{\hbar}{m_0}\right] \boldsymbol{k}\cdot\boldsymbol{p} \tag{2.25}$$

where H_0 is given in Eq.(2.2), and p is the momentum operator. Therefore, the total Hamiltonian including the spin-orbit interaction H_{so} can be written as:

$$H = H_k + H_{so} + H_c^{(c)} + H_c^{(1,v)} \tag{2.26}$$

We choose the set of wave functions that make H_{so} diagonal. These are functions that have the same transformation properties as the eigenfunctions of the total angular momentum operator **J** (=**L**+**S**), i.e., $|J, M_J\rangle$. For the s-like Γ_2^- (Γ_1) conduction band these wave functions are (Kane 1966):

$$|1/2,1/2\rangle_c = |S\uparrow\rangle \tag{2.27a}$$

$$|1/2,-1/2\rangle_c = |S\downarrow\rangle \tag{2.27b}$$

while for the P-like Γ_8^+ (Γ_8), Γ_7^+ (Γ_7) valence bands, they can be written as:

$$|3/2,3/2\rangle = (1/\sqrt{2})(X+iY)\uparrow \tag{2.27c}$$

$$|3/2,1/2\rangle = (1/\sqrt{6})(X+iY)\downarrow - (\sqrt{2/3})Z\uparrow \tag{2.27d}$$

$$|3/2,-1/2\rangle = -(1/\sqrt{6})(X-iY)\uparrow - (\sqrt{2/3})Z\downarrow \tag{2.27e}$$

$$|3/2,-3/2\rangle = -(1/\sqrt{2})(X-iY)\downarrow \tag{2.27f}$$

$$|1/2,1/2\rangle = (1/\sqrt{3})(X+iY)\downarrow + (1/\sqrt{3})Z\uparrow \tag{2.27g}$$

$$|1/2,-1/2\rangle = (1/\sqrt{3})(X - iY)\uparrow - (1/\sqrt{3})Z\downarrow \qquad (2.27h)$$

Using these basis wave functions, the 8×8 matrix of the Hamiltonian Eq. (2.26) can be written down explicitly (Pollak 1990). By solving the eigenvalue problem of this Hamiltonian matrix, the strain-dependent dispersion relation of the band structure near $\mathbf{k}=0$ and the corresponding eigenfunctions can be found.

For (001) built-in biaxial strain of magnitude ε, which is the case of strained-layer microstructures involved in this thesis, the 8×8 strain Hamiltonian becomes two decoupled identical 4×4 matrices (Pollak 1973, 1990):

$$[H_\varepsilon] = \begin{array}{c} \begin{array}{cccc} |S\uparrow\rangle & |3/2,3/2\rangle & |3/2,1/2\rangle & |1/2,1/2\rangle \end{array} \\ \begin{bmatrix} E_0+\delta E_H^c & 0 & 0 & 0 \\ 0 & -\delta E_H^v-\delta E_s & 0 & 0 \\ 0 & 0 & -\delta E_H^v+\delta E_s & \sqrt{2}\,\delta E_s \\ 0 & 0 & \sqrt{2}\,\delta E_s & -\Delta_0-\delta E_H^v \end{bmatrix} \end{array} \qquad (2.28)$$

where δE_H^c, δE_H^v, δE_S are defined as:

$$\begin{aligned} \delta E_H^c &= a_c(2-\lambda)\varepsilon \\ \delta E_a^v &= a_1(2-\lambda)\varepsilon \\ \delta E_s &= b_1(1+\lambda)\varepsilon \end{aligned} \qquad (2.29)$$

with

$$\lambda = 2C_{12}/C_{11} \tag{2.30}$$

where C_{12} and C_{11} are the elastic stiffness constants. These constants and the interband hydrostatic pressure deformation potential a of E_0 and the shear deformation potentials can be found in the literature (Landolt-Börnstein 1982, Pollak 1990). The strain-dependent transition energies between the conduction band the valence bands can be written as (Pollak 1990):

$$E_0(2) = E_0 + \delta E_H + \delta E_s \tag{2.31a}$$

$$E_0(1) = E_0 + \delta E_H + \frac{\Delta_0 - \delta E_s}{2} - \frac{1}{2}\sqrt{\Delta_0^2 + 2\Delta_0 \delta E_s + 9(\delta E_s)^2} \tag{2.31b}$$

$$E_0(3) = E_0 + \delta E_H + \frac{\Delta_0 - \delta E_s}{2} + \frac{1}{2}\sqrt{\Delta_0^2 + 2\Delta_0 \delta E_s + 9(\delta E_s)^2} \tag{2.31c}$$

where

$$\delta E_H = (a_1 + a_c)(2 - \lambda)\varepsilon = a(2 - \lambda)\varepsilon \tag{2.32a}$$

$$\delta E_s = -b_1(1 + \lambda)\varepsilon = -b(1 + \lambda)\varepsilon \tag{2.32b}$$

where a is the interband hydrostatic pressure deformation potential of E_0 and b is the shear deformation potential. The strain-dependent wave functions for the three valence bands are given by (Laude *et al.* 1971):

$$|v_2\rangle = |3/2, \pm 3/2\rangle \tag{2.33a}$$

$$|v_1\rangle = \alpha\,|3/2, \pm 1/2\rangle + \beta\,|\pm 1/2\rangle \tag{2.33b}$$

$$|v_3\rangle = -\beta\,|3/2, \pm 1/2\rangle + \alpha\,|1/2, \pm 1/2\rangle \tag{2.33c}$$

where

$$\alpha = 2\sqrt{2}\,|\delta E_s|/q \tag{2.34a}$$

$$\alpha = \frac{(n-p)\delta E_s}{q\,|\delta E_s|} \tag{2.34b}$$

with

$$\begin{aligned} p &= \Delta_0 + \delta E_s \\ n &= \sqrt{p^2 + 8(\delta E_s)^2} \\ q &= \sqrt{2n(n-p)} \end{aligned} \tag{2.34c}$$

2.2.2.B. Strain dependence of effective mass

The band structure in the presence of an arbitrary strain is quite complicated, because momentum matrix elements as well as energy gaps are strain dependent (Aspnes and Cardona 1978). I define $k_{||}$ as the component of k-vector along the z-direction (out of the layer plane) and $k_{\perp}$ ($= k_x^2 + k_y^2$) as the in-plane component. In the case of (001)

biaxial strain, it can be shown that for the v_2 band ($|3/2, \pm 3/2>$) the effective masses are

$$m/m_{\parallel}^{*}(v_2) = (A_2 - B_2),\ out\text{-}of\text{-}plane\ mass, \tag{2.35a}$$

$$m/m_{\perp}^{*}(v_2) = (A_2 + \tfrac{1}{2}B_2),\ in\text{-}plane\ mass. \tag{2.35b}$$

The subscript on the mass parameters A, B introduced in the above equations reflects the fact that they are different for the v_1, v_2, and v_3. Since, for the diamond- and zincblende-type semiconductor, A and B have the same sign (Landolt-Börnstein 1982), $m_{\parallel}^{*}$ (v_2) is heavy-hole like, while $m_{\perp}^{*}$ (v_2) is light-hole like.

For v_1 and v_3 bands, the effective masses are given by:

$$m/m_{\parallel}^{*}(v_1) = \alpha^2(A_1 + B_1) - 2\sqrt{2}\,\alpha\beta B_1 + \beta^2 A_{so} \tag{2.36a}$$

$$m/m_{\perp}^{*}(v_1) = \alpha^2(A_1 - \tfrac{1}{2}B_1) + \sqrt{2}\,\alpha\beta B_1 + \beta^2 A_{so} \tag{2.36b}$$

$$m/m_{\parallel}^{*}(v_3) = \alpha^2 A_{so} + 2\sqrt{2}\,\alpha\beta B_1 + \beta^2(A_1 + B_1) \tag{2.36c}$$

$$m/m_{\perp}^{*}(v_3) = \alpha^2 A_{so} - \sqrt{2}\,\alpha\beta B_1 + \beta^2(A_1 - \tfrac{1}{2}B_1) \tag{2.36d}$$

The mass parameters A_1, B_1, A_2, B_2, A_{so} are defined in Pollak 1990.

2.2.3 Effects of strain on critical points at $k \neq 0$

For band extrema or interband critical points at $k \neq 0$, the shear component of the applied uniaxial stress can cause three effects (Pollak 1990): (1) band states of different k vector, which are degenerate because of the symmetry of the crystal, may have their degeneracy reduced depending on the projections of their k vectors on to the stress direction (interband splitting), (2) a splitting of degenerate orbital bands whose k vector are not parallel to the stress, and (3) a stress-induced coupling between neighboring bands. The second and the third effects mentioned above are denoted as intraband splitting.

Deformation-potential theory for many-valley cubic semiconductors (Brooks 1955, Herring and Vogt 1956, Kane 1970) gives the following expression (in the notation of Brooks) describing the stress-induced hydrostatic shift and interband splitting of a band-extrema interband critical point due to effect (1) above plus the hydrostatic pressure component (Pollak 1973, Pollak 1990):

$$\Delta E = \hat{n} \cdot \left\{ \Xi_1 Tr(e) + \Xi_2 \left[e - \tfrac{1}{3} Tr(e) \mathrm{I} \right] \right\} \cdot \hat{n} \qquad (2.37)$$

where $\hat{n}$ is a unit vector in the direction of the band extrema or critical point in k-space, I is the unit diadic, and Ξ_1 and Ξ_2 are the hydrostatic and shear deformation potentials, respectively. The intraband effects will depend on the specific bands under consideration.

The silicon conduction band minima are in the six equivalent $<100>$ directions at a distance of 85% of the Brillouin zone from Γ-point. In the presence of a [001] biaxial strain, there will be no intraband splitting since there are no nonvanishing off diagonal elements of the strain tensor. The interband effects will split the six equivalent minima into two groups according to their orientation with respect to the biaxial strain axis [001]. From Eq. (2.37) the shift of the conduction band minima along the [001] direction is given by

$$\Delta E^{S}(\Delta_1) = \mathscr{E}_1(2-\lambda)\varepsilon - \mathscr{E}_2(1+\lambda)(2\varepsilon/3) \tag{2.38a}$$

while for the [100] and [010] bands, the strain-dependent energy shifts are:

$$\Delta E^{D}(\Delta_1) = \mathscr{E}_1(2-\lambda)\varepsilon + \mathscr{E}_2(1+\lambda)(\varepsilon/3) \tag{2.38b}$$

Germanium is an indirect gap material with degenerate conduction band minima along $<111>$. Since there are not other bands near L_1, the intraband mixing can be neglected. Only Eq. (2.37) applies. Again, we consider only the case of (001) biaxial strain. The degeneracy of the L_1 conduction band minima remains in this case, hence there is only a hydrostatic pressure shift given by

$$\Delta E(L_1) = \mathscr{E}_1(2-\lambda)\varepsilon \tag{2.39}$$

Another important set of bands are the Λ_1 conduction bands and the Λ_3 valence bands, which occur along the equivalent $<111>$ directions of the Brillouin zone. The orbital degeneracy of Λ_3 is removed by the spin-orbit splitting. The spin-orbit split transitions between Λ_3 and Λ_1 are denoted as E_1 and $E_1+\Delta_1$, where Δ_1 is the spin-orbit splitting of Λ_3.

A (001) biaxial strain does not remove the k-space degeneracy of these bands (no interband splitting) but does cause an intraband effect, i.e., a strain dependence of the separation between of Λ_3 orbital bands. The energies of the E_1 and $E_1+\Delta_1$ transitions are given by

$$\Delta E_1 = \frac{\Delta_1}{2} + \delta E_{H,\Lambda} - \tfrac{1}{2}\sqrt{\Delta_1^2 + 4(\delta E_{s,\Lambda})^2} \tag{2.40a}$$

$$\Delta(E_1+\Delta_1) = -\frac{\Delta_1}{2} + \delta E_{H,\Lambda} + \tfrac{1}{2}\sqrt{\Delta_1^2 + 4(\delta E_{s,\Lambda})^2} \tag{2.40b}$$

where

$$\begin{aligned} \delta E_{H,\Lambda} &= \mathscr{E}_2(2-\lambda)\varepsilon \\ \delta E_{s,\Lambda} &= \sqrt{2/3}\, D_3^3(1+\lambda)\varepsilon \end{aligned} \tag{2.40c}$$

The quantity D_3^3 is an intraband deformation potential for the Λ_3 valence band for a [001] uniaxial strain.

2.2.4. Effects of built-in strain on semiconductor microstructures

The most important effect of built-in strain in the stained layer microstructures is to change the one-dimensional superlattice potential profiles. The built-in biaxial strain will shift and split the energy bands (Pollak 1990). The band offsets also have some dependence on the strain (Priester *et al.* 1988). Depending on magnitude and sign of the strain the ordering of heavy- and light-hole levels can be switched. One can even have a type I potential profile for the heavy-hole band and a type II potential profile for the light-hole band, or vice versa. Therefore, depending on the strain in each material and on the band discontinuity, a large number of band alignment configurations may be obtained (Marzin and Gérard 1990, People and Jackson 1990). Some of them in the case of superlattices are shown in Fig. 4.

In polar material systems such as III-V, II-VI compounds there can also be piezoelectric effects for certain strain configurations in which there are non-vanishing off-diagonal elements of the strain tensor (Smith and Maihiolt 1987, People and Jackson 1990). These polar materials possess a nonvanishing piezoelectric constant e_{14}. The built-in strain along certain directions in the microstructures induces a polarization field, P_i, which in turn generates an electric fields. In III-V strained-layer structures, these strain induced fields approach 10^5 V/cm for lattice-mismatch strains -1%, and hence significantly modify the superlattice electronic structures and optical properties. Note, for example, that the electric fields will change the shape of the quantum well potentials, thereby changing subbband energy levels and wave functions. Consequently, one obtains

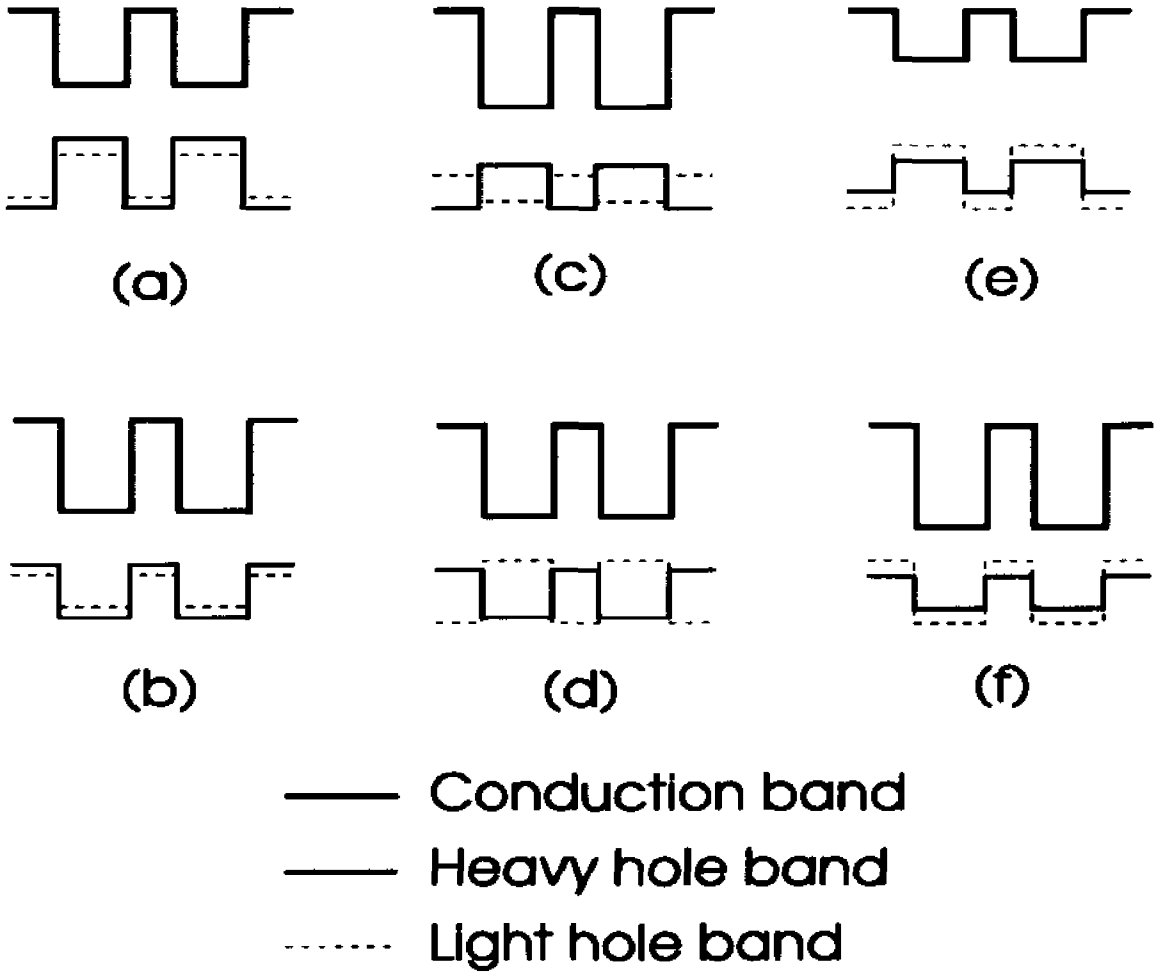

Figure 4. Possible band-extrema configurations for strained-layer superlattices.

modifications of optical transitions and oscillator strengths. The magnitude of these changes have been shown to be second order in the magnitude of the electric fields (second-order Stark effect) (People and Jackson 1990). The internal electric fields may be externally modulated by either (i) photo-pumping (since photogenerated carriers screen these internal fields), (ii) external electric fields, and (iii) external strain (Qiang *et al.*

1991, 1992). As a result of such modulations, one expects to observe large nonlinear optic, electro-optic, and piezo-optic effects.

In zincblende-type semiconductors, off-diagonal strains ε_{jk} (for example j=x, k=y) induce polarization fields, P_i, whose magnitude is given by (Nye 1957)

$$P_i = 2e_{14}\varepsilon_{jk} \tag{2.41}$$

Note that diagonal strains (ε_{xx}, ε_{yy}, ε_{zz}) do not induce a polarization. Hence, strained-layer microstructures grown on (001)-oriented substrates will not give rise to strain-induced polarization fields. For the (111) growth axis, $\boldsymbol{P}$ is along the superlattice direction, whereas for (110) growth, $\boldsymbol{P}$ lies in the superlattice plane.

Pseudomorphic microstructures are coherently grown such that the in-plane lattice constants of the thin layers composing the system are forced to match that of the substrate (or buffer) lattice constant. Usually only one type of the host materials is strained. For example, in the pseudomorphic InGaAs/GaAs quantum well structures and GaAlAs/InGaAs/GaAs asymmetric quantum well structures grown on GaAs substrate, only the InGaAs layer is under a biaxial strain. Assume a_S to be the bulk lattice constant of the substrate (or buffer) and a_T to be the bulk lattice constant of strained thin layer material, the biaxial strain ε present in the thin layer is given by:

$$\varepsilon = \frac{a_S - a_T}{a_T} \tag{2.42}$$

Since the stain effects are easily comparable with the level spacing due to size quantization, it is clear that they should be taken into account for quantitative interpretations of the electronic properties of strained layer heterostructures. For microstructures with built-in [001] biaxial strain, which is the case in this thesis, the approach is quite straight forward. It is accomplished by using the envelope function approach, such as modified Kronig-Penney model or Bastard Model, with the strain-effects incorporated by using the input material parameters modified by the built-in strain, such as strain-modified band gaps, strain modified band offsets and strain modified effective masses (Osbourn 1983, Voisin 1984, Osbourn 1985, Marzin 1985, Marzin and Gérard 1990).

2.3 Temperature dependence of the energy gaps and broadening parameters

The temperature dependence of energy gaps [$E_g(T)$] and broadening parameters [$\Gamma(T)$] can provide important information about the electron-phonon interaction, exciton effects, etc. It is well known that the electron-phonon interaction contributes to both the temperature shift of the energy gap and to the increase of the lifetime broadening. Cardona *et al.* have made extensive microscopic analysis of these temperature dependent shifts and broadening for such semiconductors as Ge (Allen and Cardona 1981, 1983, Lautenschlager *et al.* 1985), Si (Allen and Cardona 1981, 1983, Lautenschlager *et al.* 1985, 1986) and GaAs (Lautenschlager *et al.* 1987a) based on the renormalization of the band energies by the electron-phonon coupling. We illustrate here the treatment

presented by Cardona *et al.* (Allen and Cardona 1981, Lautenschlager *et al.* 1986, Gopalan *et al.* 1987), outlining the basic equations and physical implication.

Consider a crystal with atoms of species κ that occupy sites $\boldsymbol{R}(l, \kappa)$ and have displacements $\boldsymbol{u}(l, \kappa)$ from equilibrium, where l labels the unit cells. In order to describe the renormalization of the semiconductor band structure by the electron-phonon interaction, the electron-atom interaction $V[\boldsymbol{r}-\boldsymbol{R}(l, \kappa)-u(l,\kappa)]$ is Taylor expanded about the position $\boldsymbol{u}(l, \kappa)=\boldsymbol{0}$. The zeroth-order Hamiltonian H_0 gives the one-electron states $|\boldsymbol{k},n>$ and band energies ϵ_{kn} where $\boldsymbol{k}$, n are the wave vector and the band index, respectively. The first two terms of the expansion of $V[\boldsymbol{r}-\boldsymbol{R}(l,\kappa)-\boldsymbol{u}(l, \kappa)]$ in powers of $\boldsymbol{u}(l, \kappa)$ are (Allen and Heine 1976, Lautenschlager *et al.* 1986)

$$H_1 = \sum_{l,\kappa} \frac{\partial V}{\partial R_\alpha(l,\kappa)} u_\alpha(l,\kappa) \tag{2.43}$$

and

$$H_2 = \frac{1}{2} \sum_{l,\kappa,l',\kappa'} \frac{\partial^2 V}{\partial R_\alpha(l,\kappa)\partial R_\beta(l',\kappa')} u_\alpha(l,\kappa) u_\beta(l',\kappa') \tag{2.44}$$

where H_1 represents the electron-phonon interaction involving absorption or emission of one phonon, and H_2 represents the electron-phonon interaction involving absorption or emission of two phonons. The subscripts α, β denote Cartesian components which are

summed when repeated. The adiabatic approximation allows the neglect of time dependence of $u(l, \kappa)$. To second order in $u(l, \kappa)$ we obtain, in standard Rayleigh-Schrödinger perturbation theory (Allen and Heine 1976, Lautenschlager *et al.* 1986)

$$E_{kn}[u(l,\kappa)] = \epsilon_{k,n} + \langle k,n|H_2|k,n\rangle + \sum{}' \frac{|\langle k',n'|H_1|k,n\rangle|^2}{\epsilon_{k,n}-\epsilon_{k',n'}+i\Gamma} \qquad (2.45)$$

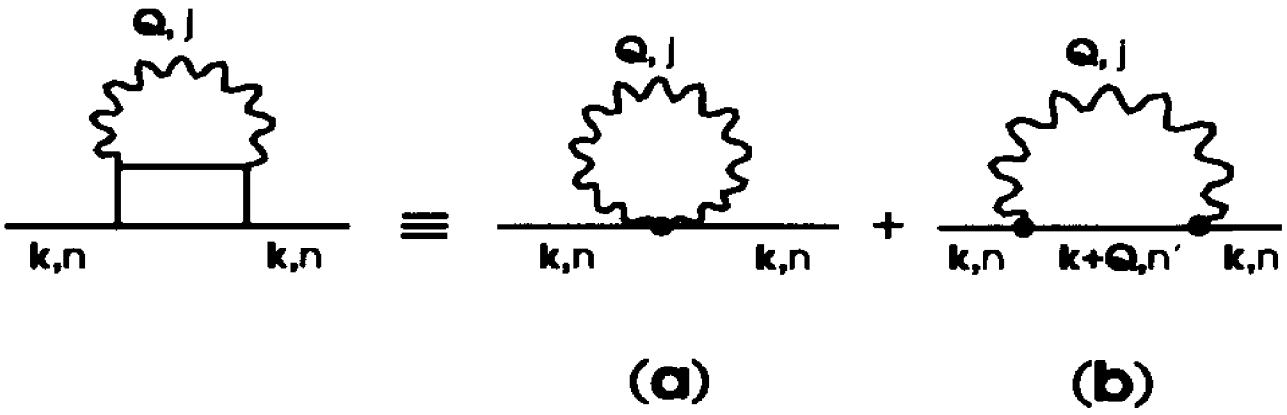

Figure 5. Self-energy graphs which give the temperature renormalization of the band energies to second order in atomic displacement. (a) represents the Fan term; (b) represents the lowest-order Debye-Waller correction.

The first and second order correction terms to the unperturbed energy of the initial state ϵ_{kn} are called "Debye-Waller" (Antoncik 1955), and "Fan" terms (Fan 1951, Cohen 1962), respectively. The Feynman diagram is shown in Fig. 5. The Debye-Waller term is purely real. This term will not contribute to life time broadening. In the Fan terms

the scattering process involves the electron-phonon interaction which induces transitions from initial state $|k, n>$ to intermediate state $|k', n'>$ and to initial state (see Fig. 5b). This term not only contributes to energy shift, but also to lifetime broadening. Equation (2.45) can be written as

$$E_{kn}(T) = \epsilon_{kn} + \Delta E_{kn} + i\Gamma(T) \tag{2.46}$$

where

$$\Delta E_{kn}(T) = \sum_j E(Q_j, |k,n\rangle) \left[n_{qj}(T) + \frac{1}{2} \right] \tag{2.47}$$

and

$$\Gamma_{kn}(T) = \sum_j \Gamma(Q_j, |k,n\rangle) \left[n_{qj}(T) + \frac{1}{2} \right] \tag{2.48}$$

where n_{qj} is the Bose-Einstein occupation factor:

$$n_{qj} = \frac{1}{\exp\left[\frac{\hbar\omega_{qj}}{k_B T} \right] - 1} \tag{2.49}$$

whereas $E(Q_j, |k,n>)$ is given by

$$E(Q_j,|kn\rangle)=\frac{\hbar}{N}\sum \frac{\langle kn|\partial V/\partial R_\alpha(\kappa)|k+Qn'\rangle\ \langle k+Qn'|\partial V/\partial R_\beta(\kappa')|kn\rangle}{\epsilon_{kn}-\epsilon_{k+Qn'}}$$

$$\times\exp[-iQ(\tau_\kappa-\tau_{\kappa'})](M_\kappa M_{\kappa'})^{(-1/2)}\epsilon_\alpha(-Q_{j\kappa})\epsilon_\beta(Q_{j\kappa'})$$

$$\times\exp[-iQ(\tau_\kappa-\tau_{\kappa'})](M_\kappa M_{\kappa'})^{(-1/2)}\epsilon_\alpha(-Q_{j\kappa})\epsilon_\beta(Q_{j\kappa'})\ -\qquad (2.50)$$

$$\frac{\hbar}{2N}\sum \frac{\langle kn|\partial V/\partial R_\alpha(\kappa)|kn'\rangle\ \langle kn'|\partial V/\partial R_\beta(\kappa')|kn\rangle}{\epsilon_{\ldots}-\epsilon_{\ldots}}\Big)_{j\kappa'})],$$

and $\Gamma(Q_j,\ |k,\ n>)$ is given by

$$\Gamma(Q_j,|k,n\rangle)=\frac{\pi\hbar}{N}\sum\ \langle kn|\partial V/\partial R_\alpha(\kappa)|k+Qn'\rangle\ \langle k+Qn'|\partial V/\partial R_\beta(\kappa')|kn\rangle \qquad (2.51)$$

$$\times\exp[-iQ(\tau_\kappa-\tau_{\kappa'})](M_\kappa M_{\kappa'}\omega_{Qj}^2)^{-1/2}\epsilon_\alpha(-Q_{j\kappa})\epsilon_\beta(Q_{j\kappa'})\delta(\epsilon_{kn}-\epsilon_{k+Qn'})$$

where M_κ is the mass of the atom κ located in the unit cell at position τ_κ, N is the number of unit cells in the crystal, $\hat{\epsilon}(Q_{j\kappa})$ is the polarization vector for the phonon Q_j of the atom κ. From the expression of $E(Q_j,\ |k,n>)$, it is found that all wave vectors of phonons (acoustic as well as optical phonons) make a contribution to the temperature shift of the band gap.

In Eq. (2.51) there is a $\delta(\epsilon_{kn}-\epsilon_{k+Q,n'})$ function in the term $\Gamma(Q_j,|k,n>)$. This δ-function means that only phonons which couple to an electronic state with the same energy $\epsilon_{k+Q,n'}$ as the initial state ϵ_{kn} can make a contribution to $\Gamma(Q_j,|k,n>)$.

With this theoretical treatment, if a group of phonons of frequencies close to $k_B\Theta_B/\hbar$ [$k_B\Theta/\hbar$] yields the dominant contribution to $\Delta E_{kn}(T)$ [$\Gamma_{kn}(T)$], respectively, then we have:

$$\Delta E_{kn}(T) = a_b' \left[1 + \frac{2}{e^{\Theta_e/T} - 1} \right] \tag{2.52}$$

and

$$\Gamma(T) = \Gamma_1' \left[1 + \frac{2}{e^{\Theta/T} - 1} \right] \tag{2.53}$$

where

$$a_b' = \frac{1}{2} \sum E(Q_j, |kn\rangle),$$

$$\textit{and} \tag{2.54}$$

$$\Gamma_1' = \frac{1}{2} \sum \Gamma(Q_j, |k,n\rangle).$$

To obtain the total shift and broadening at the critical point, the shift and broadening of the valence and conduction band states are added up, respectively. Therefore, we have the expressions for temperature dependence of energy gaps (E_g) due to electron-phonon interactions (Lautenschlager *et al* 1987a, 1987b):

$$E_g(T) = E_B(0) - a_B \left[1 + \frac{2}{e^{\Theta_e/T} - 1} \right] \tag{2.55}$$

where $E_B(0)$-a_B corresponds the energy gap at $T=0$, a_B represents the average value of the strength of electron-phonon coupling and $k_B\Theta_B/\hbar$ corresponds to average phonon frequency.

Similarly the temperature dependence of the broadening can be written as (Lautenschlager *et al* 1987a, 1987b):

$$\Gamma(T) = \Gamma_0 + \frac{\Gamma_1}{e^{\Theta/T}-1} \tag{2.56}$$

where Γ_0 corresponds to other broadening mechanisms due to the intrinsic lifetime, electron-electron interaction, impurities, dislocations and alloy scattering. The parameter Γ_1 ($=2\ \Gamma'_1$) represents the strength of electron-phonon coupling, and $k_B\Theta$ is the relevant phonon energy. For direct transitions Γ_1 is the electron(exciton)-LO phonon (longitudinal optical phonon) coupling constant and the appropriate phonon energy is the Q=0 LO phonon energy (Lautenschlager *et al.* 1987a, 1987b).

For indirect band gap materials the situation is more complicated since there are different phonon energies involved in the electron and hole scattering processes (Lautenschlager *et al.* 1986, Yin Y. *et al.*).

Equations (2.55) and (2.56) are derived in a microscopic approach. They can be used to model the measured temperature dependence data of transition energies and the broadening parameters to obtain important information about electron-phonon interaction.

The temperature variation of $E_g(T)$ can also be described by equations involving three parameters such as the semi-empirical Varshni expression (Varshni 1967):

$$E_0(T) = E_0(0) - \alpha T^2/(\beta + T) \tag{2.57}$$

where $E_0(0)$, α, β are the Varshni parameters.

In order to obtain parameters directly related to the influence of electron-phonon coupling effects, it is necessary to eliminate the contribution of the temperature shift of E_0 due to thermal expansion from Eq. (2.57). The energy shift ΔE_{th} due to the thermal expansion can be written as:

$$\Delta E_{th} = -3a\alpha_{th}T \tag{2.58}$$

where a is the hydrostatic deformation potential and α_{th} is the linear expansion coefficient. After taking of the thermal expansion contribution, Equation (2.57) can be rewritten as:

$$E_g(T) - \Delta E_{th} = E_B(0)' - a_B' \left[1 + \frac{2}{e^{\Theta_p'/T} - 1} \right] \qquad (2.59)$$

The parameter α' of Eq. (2.59) can be related to a_B and Θ_{sp} of Eq. (2.55) by taking the high temperature limit of both expressions, yielding $\alpha' = 2a_B/(k_B\Theta_{sp})$. The parameter β' of Eq. (2.59) is directly proportion to the Debye temperature by the relation $\beta' = (3/8)\Theta_D$ (Manoogian and Woolley 1984). These relations are indeed satisfied for these parameters.

Chapter 3. MODULATION SPECTROSCOPY

3.1. Introduction

Since its inception in 1964 modulation spectroscopy has proven to be a powerful experimental technique for studying and characterizing the properties of bulk semiconductors, reduced dimensional systems (surfaces, interfaces, heterostructures, etc.), actual device structures and growth/processing. The derivative nature of modulation spectroscopy emphasizes structure localized in the photon energy region of interband (intersubband) transitions of semiconductors (semiconductor microstructures) and suppresses uninteresting background effects. Also weak features that may not have been detected in the absolute spectra are often enhanced. Because of this derivative-like nature a large number of sharp spectral features can be observed, even at room temperature. As an example of the power of modulation spectroscopy, shown in Fig. 6 is a comparison of the reflectivity (R) and electric-field modulated [electroreflectance (ER)] spectra of bulk GaAs at 300K (Pollak 1981). While the reflectivity is characterized by broad features, the ER trace has zero as a base and is dominated by a series of very sharp, derivative-like features corresponding to specific transitions in the Brillouin zone (BZ).

The ability to perform a lineshape fit is one of the great advantages of modulation spectroscopy. Since for the modulated signal the features are localized in photon energy it is possible to account for the lineshapes to yield accurate values of energies and broadening parameters of interband transitions. For example, it is possible to determine

the energies of the E_0, $E_0+\Delta_0$, E_1 and $E_1+\Delta_1$ peaks in Fig. 6 to within a few meV, even at room temperature. Thus, the effects of static external perturbations such as electric and magnetic fields, temperature, hydrostatic pressure, uniaxial stress, composition, etc. can be conveniently studied.

Research efforts in the first decade were focused on the properties of bulk semiconductors. The results have been reviewed by Cardona (Cardona 1969, 1970), Hamakawa and Nishino (Hamkawa and Nishino 1976), Aspnes (Aspnes 1980) and Pollak (Pollak 1981). One can also find valuable references in Vol. 9 of Semiconductor and Semimetals, eds. R. L. Willardson and A. C. Beer (Academic, New York 1972) and in the Proceedings of the First International Conference on Modulation Spectroscopy, published as Vol. 37 of Surface Science (1973) .

In the 1980's modulation spectroscopy enjoyed a renaissance. It was shown that the same advantages long exploited for bulk studies also were evident in the artificial semiconductor microstructures fabricated by modern thin film methods such as MBE or organometallic chemical vapor deposition (Mendez *et al.* 1981, Erman *et al.* 1984, Alibert *et al.* 1985, Glembocki *et al.* 1985a, 1985b). The important work of Glembocki *et al.* (Glembocki *et al.* 1985a, 1985b) demonstrated that a large number of intersubband transitions in a multiple quantum well could be observed at room temperature using the contactless electromodulation method of photoreflectance (PR). Thus, the rich modulated spectra from microstructures could be used to probe the "band structure" of reduced

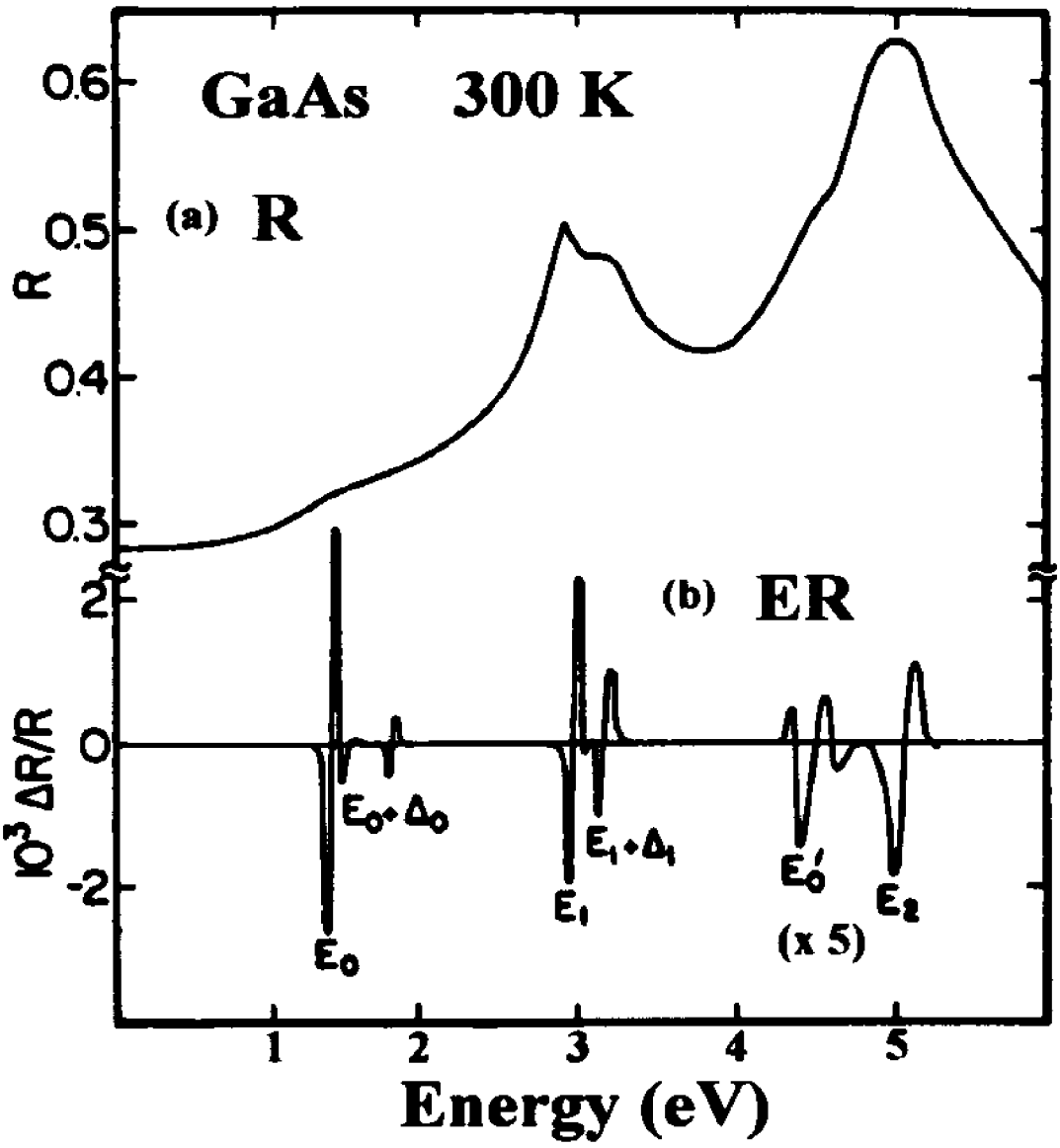

Fig. 6. Comparison of room temperature reflectivity and electric-field modulated reflectivity (electroreflectance) of GaAs (Pollak 1981).

dimensional systems just as this optical method was employed for bulk material.

These advances have stimulated a considerable amount of activity in experimental and theoretical areas as well as the development of new instrumentation, particularly contactless modes. Not only is work being carried out on the fundamental aspects of a large variety of reduced dimensional systems such as single quantum wells (SQWs), multiple quantum wells, superlattices, heterojunctions and surfaces/interfaces, but the properties of bulk material again are being revisited. The effects of various external perturbations also are being explored. The advent of the diamond anvil cell makes it possible to generate extremely high pressures.

Although not applied in this thesis, it should be pointed out that in addition to the utility of the sharp, derivative-like peaks of Fig. 6, there is also important information in other modulation variables such as phase, modulation frequency, modulation amplitude, etc. Certain types of modulation spectroscopy can be spatially (depth) selective and thus act as probes of specific regions of the sample being studied. Also, the ability to change the perturbation in a specific manner can be used to investigate the effects of that perturbation on the sample (Shen and Pollak 1990).

In this chapter the experimental techniques and the lineshape theory of modulation spectroscopy will be discussed.

3.2. Modulation techniques

The spectral response of a material can be modified directly by applying a repetitive perturbation such as electric field (electromodulation), heat pulse (thermomodulation), or stress (piezomodulation). This procedure is termed "external" modulation (Aspnes 1980). It produces sharp, derivative-like spectral peaks to allow precise measurement of the transition energies and broadening parameter. In addition, "external" modulation is an *ac* method which represents the optical response of the system to the modulating parameter. Thus, there is also important information in other modulating variables such as phase, modulation frequency, modulation amplitude, pump wavelength, etc.. For example, electromodulation can be employed as an optical impedance spectroscopy technique to gain information about trap studies or the equivalent circuit of the structure.

The change may also occur in the measuring system itself, e.g., the wavelength or polarization conditions can be modulated or the sample reflectance (transmittance) can be compared to a reference sample. This mode has been labelled "internal" modulation (Aspnes 1980).

The methods used in this thesis belongs to the category of "external" modulation. The rest of this section will be devoted to the discussion of the external modulation techniques.

Shown in Fig. 7 is a schematic drawing of the experimental arrangement for a general "external" modulated reflectance experiment (with the exception of photoreflectance or electron beam electroreflectance) (Aspnes 1980, Pollak 1993). Light from an appropriate light source (Xenon arc, halogen or tungsten lamp) passes through a monochromator (probe monochromator). The exit intensity at wavelength λ, $I_o(\lambda)$, is focused onto the sample by means of a lens (or mirror). The modulation (electric field, stress, temperature) is applied to the sample at frequency Ω_m. The reflected light is collected by a second lens (mirror) and is focussed onto an appropriate detector (photomultiplier, photodiode, etc.). For the sake of simplicity the two lenses (mirrors) are not shown. For modulated transmission the detector is placed behind the sample. In general, however, reflectance is more useful.

The light striking the detector contains two signals: the *dc* (or average value) is given by $I_o(\lambda)R(\lambda)$, where $R(\lambda)$ is the *dc* reflectance of the material while the modulated value (at frequency Ω_m) is $I_o(\lambda)\Delta R(\lambda)$, where $\Delta R(\lambda)$ is the change in reflectance produced by the modulation source. The *ac* signal from the detector, proportional to $I_o\Delta R$, is measured by a lock-in amplifier (or other signal averaging procedure). Typically $I_o\Delta R$ is 10^{-4} - 10^{-6} of I_oR. A servo mechanism is used to maintain a constant *dc* signal, therefore the *ac* output from the lock-in amplifier is proportional to the normalized signal $\Delta R/R$.

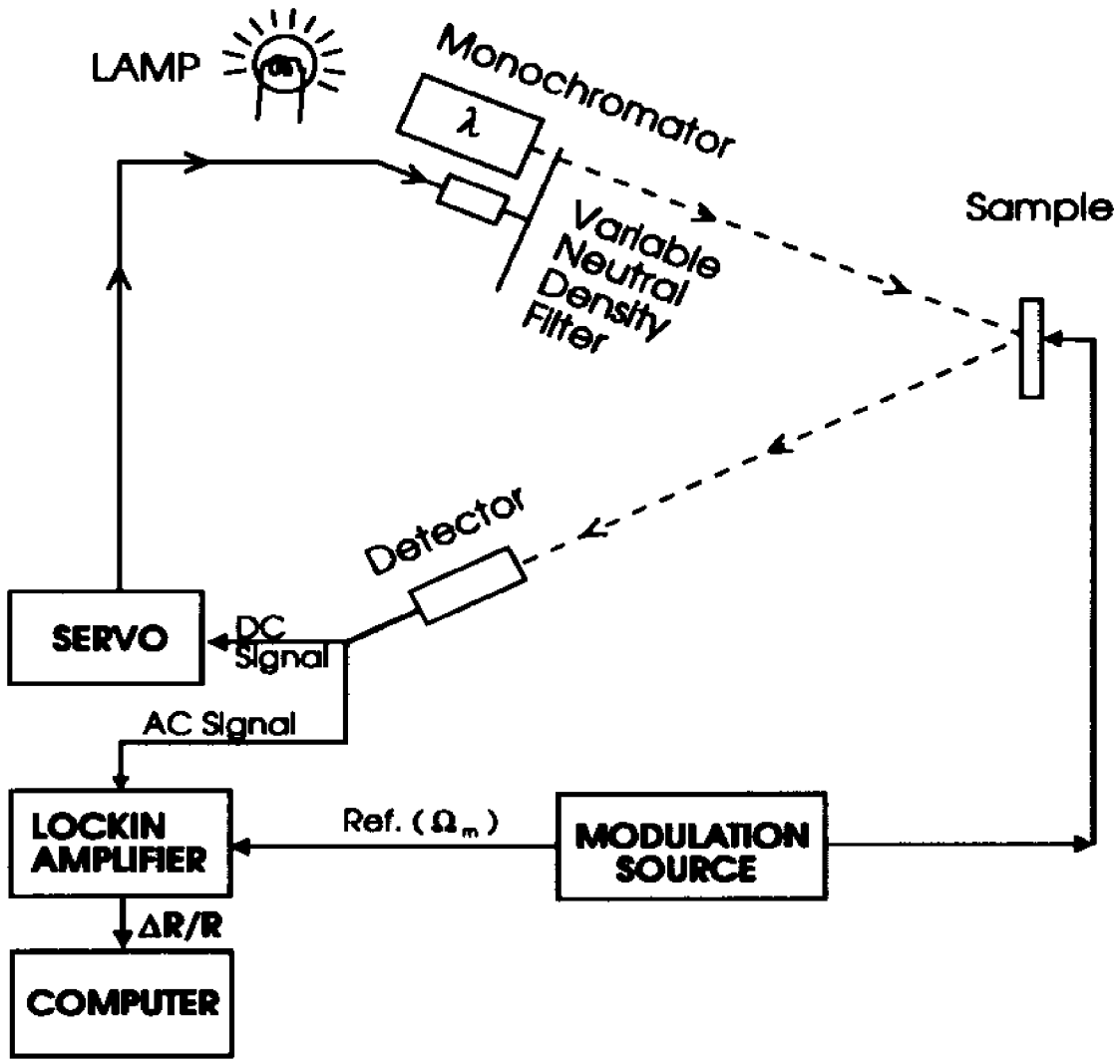

Fig. 7. Schematic representation of an "external modulation" experimental apparatus (Aspnes, 1980; Pollak, 1993).

Electromodulation (EM) can be accomplished in several ways, including contact and contactless modes. Four common contact configurations, designated as electroreflectance, can be divided into "longitudinal" and "transverse" categories (Aspnes 1980). The "longitudinal" method can be applied in the semiconductor-electrolyte,

metal-insulator-semiconductor (MIS), Schottky barrier or p-i-n configurations. In the latter the sample of interest is placed in the insulating region of a p-i-n diode (Glembocki 1990a, 1990b). The former has in the past been the most widely used form of ER because of the ease of implementation since the sample surface requires no special preparation. However, it can be used only over a limited temperature range (300K to 150K) and often offers less control over the space charge field owing to chemical passivation or dissolution effects. Electrolyte electroreflectance can be employed for depth profiling measurements with the proper choice of electrolyte and electrochemical conditions. This method also has been employed for electrochemical studies. Schottky barrier, MIS and p-i-n methods can be used at low temperatures to reduce lifetime broadening. The p-i-n configuration produces a constant electric field as opposed to the position dependent field of the other "longitudinal" modes. In the "transverse" mode two metal electrodes are evaporated on the surface of the sample and EM is produced by applying a modulated high voltage across the gap (~ 1mm). However, this technique can only be used on materials with resistivities greater than 10^8 ohm-cm (Aspnes 1980).

In temperature modulation [thermoreflectance (TR)], the sample may be mounted on a small heater attached to a heat sink and the temperature varied cyclically by passing current pulses through the heater. If the sample is properly conducting, the current can be passed through the sample directly. Alternatively, a secondary beam of light may be used to heat the sample. Generally, Ω_m for this method must be kept below 10-20Hz and hence there are often problems with the 1/f noise of the detector.

In piezoreflectance (PzR), modulation is achieved by mounting the sample on a piezoelectric transducer which varies the lattice constant of the material producing a band gap modulation. Although PzR is contactless it requires special mounting of the sample, as does TR.

Contactless electromodulation can be performed using (a) photoreflectance (Pollak and Glembocki 1988, Glembocki 1990), (b) a new approach which uses a capacitor-like arrangement (Yin X. and Pollak 1991, Yin X., *et al.* 1992a, Yin X., *et al.* 1992b, Mioc, *et al.* 1992) or (c) electron-beam electroreflectance (EBER) (Herman 1990b). The method of PR is not only contactless but requires no special mounting of the sample. It can be used in any transparent medium under a variety of conditions. It has been demonstrated that PR can be used at temperatures as high as 650°C.

Shown in Fig. 8 is the schematic representation of a PR apparatus (Shen *et al.* 1987, Pollak and Glembocki 1988). Modulation of the electric field in the sample is caused by photo-excited electron-hole pairs created by the pump source (laser or other light source) which is chopped at frequency Ω_m. Most PR experiments have utilized a mechanical chopper with maximum $\Omega_m \approx 5$ kHz. To achieve higher modulation frequencies up to about 1MHz an acousto-optic modulator can be used (Shen *et al.* 1990). The photon energy of the pump source should be above the band gap of the semiconductor being investigated. The pump creates photo-injected electron-hole pairs which modulate the built-in electric field of the semiconductor or semiconductor

microstructure under investigation. A typical pump source is a 5mW He-Ne laser (except at high temperatures where a more powerful beam must be used).

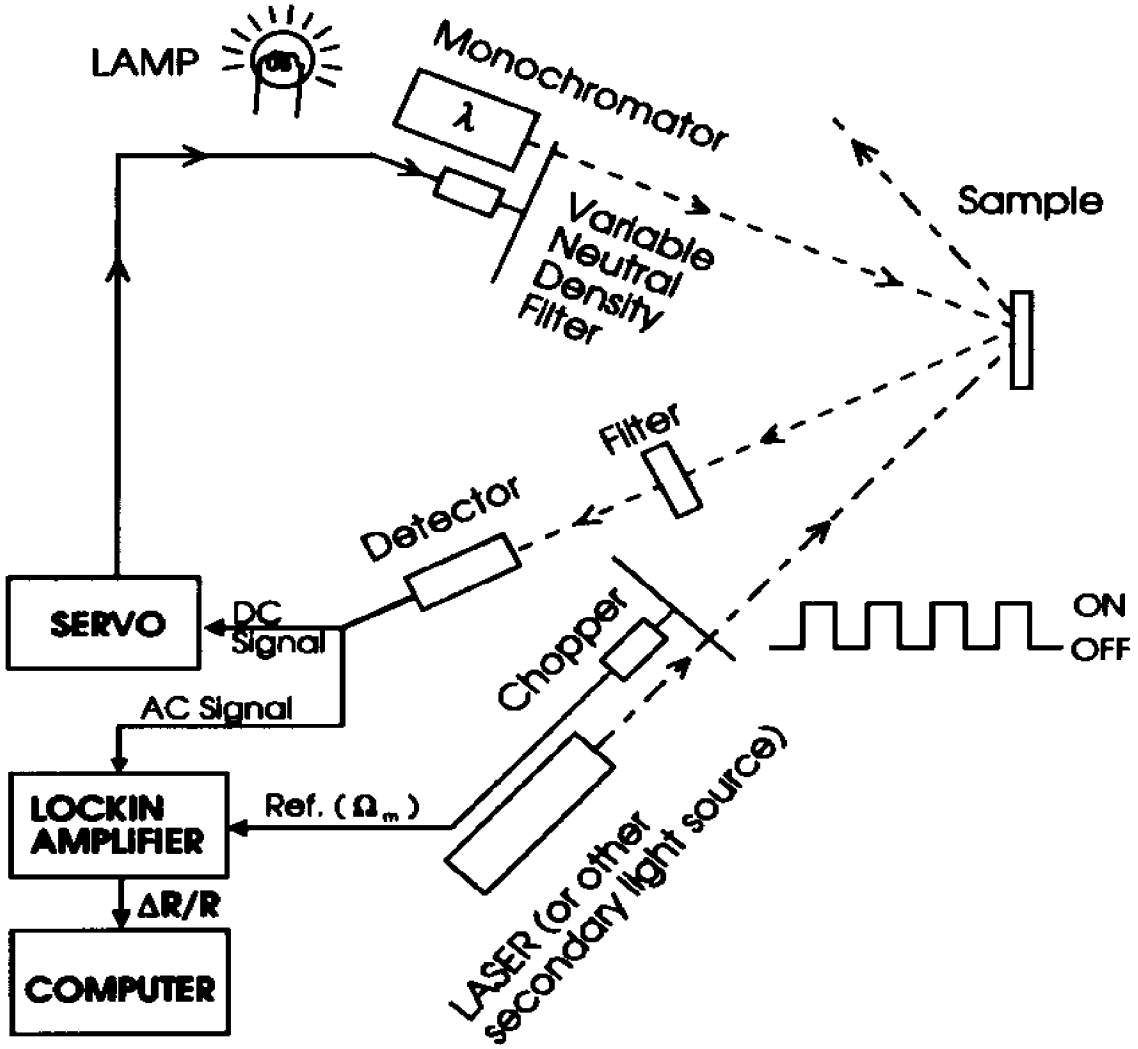

Fig. 8. Schematic representation of a photoreflectance apparatus (Shen, et al., 1987).

In Fig. 8 the normalization is performed by a variable neutral density filter (VNDF) connected to a servo mechanism. The *dc* signal from the detector, which is proportional to $I_o(\lambda)R(\lambda)$, is introduced into the servo which moves the VNDF in such a manner as to keep $I_o(\lambda)R(\lambda)$ a constant, i.e., $I_o(\lambda)R(\lambda)=C$. Under these conditions the *ac* signal $I_o(\lambda)\Delta R(\lambda)=C\ \Delta R(\lambda)/R(\lambda)$. Thus, the signal to the lock-in-amplifier is proportional to the quantity of interest, i.e., $\Delta R(\lambda)/R(\lambda)$.

A drawback of PR is the spurious modulated background signal reaching the detector because of (a) luminescence from the sample and/or (b) scattered light from the pump source. Luminescence can sometimes be a problem for measurements near the fundamental gap, particularly at low temperatures. Scattered pump light can be reduced by means of an appropriate long pass filter in front of the detector. If the overall spurious background signal is not too large in relation to $\Delta R/R$, it can be subtracted by the normalization method of Fig. 8. The spurious background signal also can be reduced or eliminated by approaches such as the use of a double monochromater (Theis *et al.* 1988), tuneable dye laser as the probe beam (Glembocki *et al.* 1987a), sweeping PR (Shen and Dutta 1990) or differential PR (Sydor *et al.* 1991).

A contactless electroreflectance (CER) method has been reported which utilizes a condenser-like system consisting of a thin, transparent, conductive coating (indium-tin-oxide or 50-60Å of a metal such as Au or Ni) on a transparent substrate (glass, quartz, etc.) which serves as one electrode (Yin X. and Pollak 1991, Yin X., *et al.* 1992a,

1992b). A second electrode consisting of a metal strip is separated from the first electrode by an insulating spacer. The sample (~ 0.5mm thick) is placed between these two capacitor plates. The dimensions of the spacer are such that there is a very thin layer (~ 0.1mm) of air (or vacuum) between the front surface of the sample and the conducting part of the first electrode. Thus, there is nothing in direct contact with the front surface of the sample. Shown in Fig. 9 is an illustration of the sample holder and electrode arrangement. The *ac* modulating (~ 1kV peak-to-peak) and *dc* bias voltages are applied between the metal strip and the transparent conductor. The probe beam is incident through the first transparent electrode. This approach can also be employed in the transmission mode by replacing the metal electrode with a second transparent electrode/substrate.

In this thesis work electromodulation and piezomodulation techniques were employed.

3.3. Lineshape considerations

Differential changes in the reflectivity are related to the perturbation of the complex dielectric function [$\epsilon(=\epsilon_1+i\epsilon_2)$] expressed as (Cardona 1969, 1970, Aspnes 1980):

$$\Delta R/R = a(\epsilon_1,\epsilon_2)\Delta\epsilon_1 + b(\epsilon_1,\epsilon_2)\Delta\epsilon_2 \qquad (3.1)$$

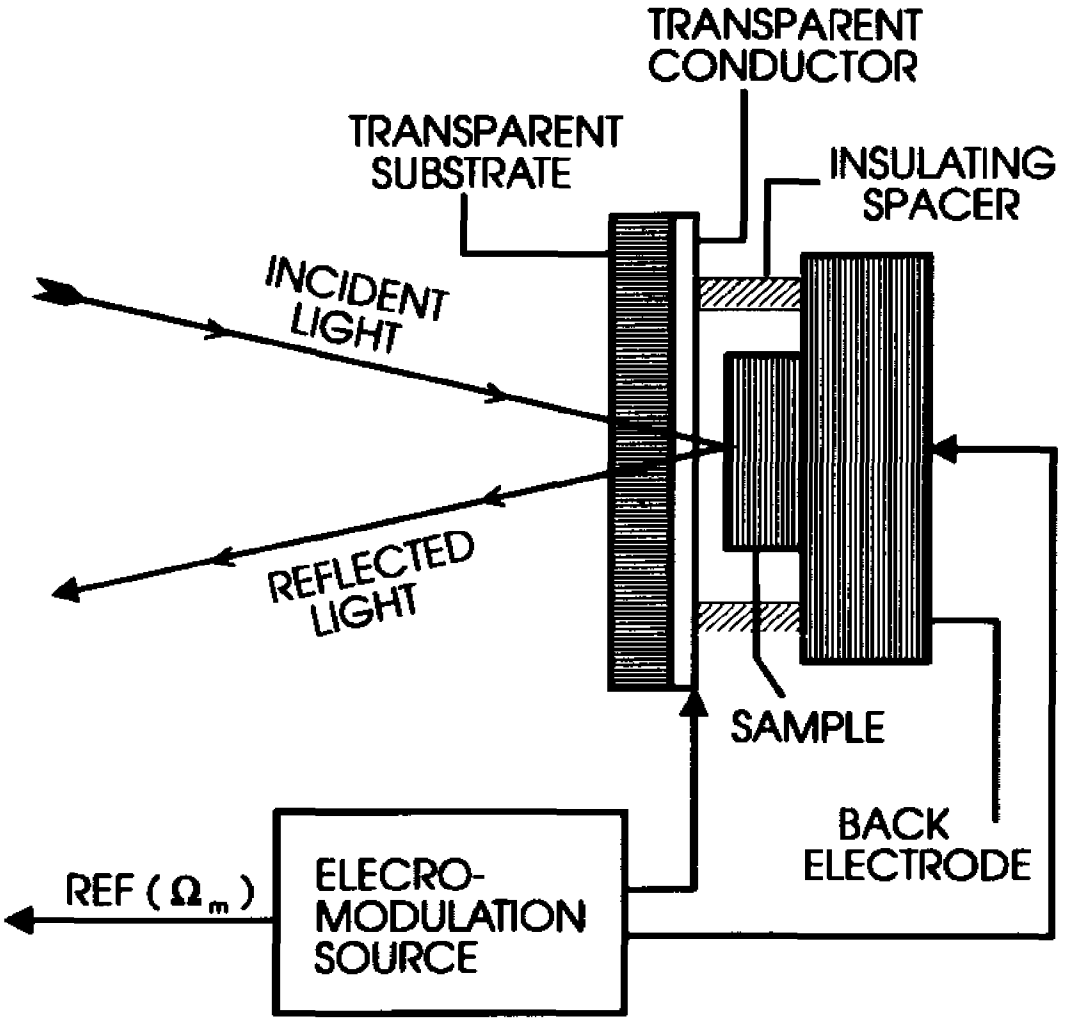

Fig. 9. Schematic view of the condenser-like arrangement used in CER experiments.

where a and b are the Seraphin coefficients, related to the unperturbed dielectric function, and $\Delta\epsilon_1$ and $\Delta\epsilon_2$ are the changes in the complex dielectric function due to the perturbation. The quantities $\Delta\epsilon_1$ and $\Delta\epsilon_2$ are related by a Kramers-Kronig inversion.

Near the fundamental gap of bulk materials $b \approx 0$ (Aspnes 1980) so that $\Delta R/R \approx a\Delta\epsilon_1$, is the only term that is important. However, in multilayer structures interference effects are important so that both $\Delta\epsilon_1$ and $\Delta\epsilon_2$ may have to be considered. The functional form of $\Delta\epsilon_1$ and $\Delta\epsilon_2$ can be calculated for a given perturbation provided that the dielectric function and critical point type are known.

3.3.1 Electromodulation

Electromodulation is the most useful and the most complex form of modulation spectroscopy. It can be classified into three categories, i.e., low-, intermediate- and high-field regime depending on the relative strengths of certain characteristic energies (Hamakawa and Nishino 1976, Aspnes 1980). In the first range $|\hbar\Theta| \leq \Gamma$, where Γ is the broadening parameter and $\hbar\Theta$ is the electro-optic energy given by:

$$(\hbar\Theta)^3 = q^2\hbar^2F^2/2\mu_\parallel \tag{3.2}$$

In Eq. (3.2) F is the field and $\mu_\parallel$ is the reduced interband mass in the direction of the field. In the intermediate-field case $|\hbar\Theta| \gtrsim \Gamma$ but $qFa_0 << E_g$, where a_0 is the lattice constant (or an appropriate periodic length in microstructures) and E_g is the band gap. In this situation the band structure is unchanged. For even higher field strength the electro-optic energy is much greater than the broadening with $qFa_0 \sim E_g$, and the Stark effects would be expected for ideal systems (see, for example, Aspnes *et al* 1972). We are not interested in such a high-field regime and it will be ingored in the following discussions.

3.3.1.A. Unbound States (Low-field regime)

For the unbound situation the case of low field modulation from flatband will be considered, i.e., no built-in *dc* field. I present below a simple physical derivation of the effects of an electric field on the dielectric function (Pollak and Glembocki 1988). The energy, $E(F)$, gained by a free particle in an electric field F can be written as

$$E(F) = \frac{q^2F^2t^2}{2\mu_{\parallel}} \tag{3.3}$$

where t is the time. If we consider an optical structure near a critical point with energy E_g, the dielectric function has the general form

$$\epsilon = \epsilon(E - E_g, \Gamma) + B \tag{3.4}$$

where E is the photon energy, and B is the featureless background.

The change in the dielectric function, $\Delta\epsilon$, induced by a modulating electric field F_{ac}, is given by:

$$\Delta\epsilon = \epsilon[E - E_g + E(F_{ac}), \Gamma] - \epsilon(E - E_g + , \Gamma) \tag{3.5}$$

where we have assumed that the electric field does not change Γ. If the field is sufficiently small so that $E(F_{ac}) \ll \Gamma$ (low field regime), Eq. (3.5) can be expanded in a Taylor's series to yield:

$$\Delta\epsilon = E(F)[(\partial/\partial E)\epsilon(E - E_g, \Gamma)] + \ldots \tag{3.6a}$$

$$=(q^2F_{ac}^2t^2/2\mu_{\parallel})[(\partial/\partial E)\epsilon(E-E_g,\Gamma)]+\ldots \tag{3.6b}$$

in quantum mechanics, the time t is also an operator:

$$t=i\hbar(\partial/\partial E) \tag{3.7}$$

so that Eq. (3.6b) becomes:

$$\Delta\epsilon=(q^2\hbar^2F_{ac}^2/2\mu_{\parallel})\left[(\partial^3/\partial E^3)\epsilon(E-E_g,\Gamma)\right] \tag{3.8a}$$

$$=(\hbar\Theta)^3\left[(\partial^3/\partial E^3)\epsilon(E-E_g,\Gamma)\right] \tag{3.8b}$$

where the electro-optic energy $\hbar\Theta$ is given by Eq. (3.2) with $F=F_{ac}$. Equation (3.8b) has all the essential features of low field EM. The quantity $\Delta\epsilon$ is proportional to F_{ac}^2 (modulating field), is inversely proportional to $\mu_{\parallel}$, and has a lineshape that is the third derivative of the unperturbed optical function (Aspnes 1980). Note also that the condition $E(F_{ac}) \ll \Gamma$ is equivalent to $\hbar\Theta \ll \Gamma$ if we take $\tau\Gamma=\hbar$, where τ is a characteristic lifetime.

A more rigorous and elegant treatment can be found in Aspnes 1980 and references therein. For the unbound situation, considering the case of low field modulation ($\hbar\Theta \leq \Gamma$) from flatband, i.e., no built-in *dc* field (Aspnes 1980, Pollak and Glembocki 1988, Glembocki, *et al.* 1992), it can be shown that:

$$\Delta\epsilon = [(\hbar\Theta)^3/E^2][(\partial^3/\partial E^3)E^2\epsilon(E-E_g,\Gamma)] \quad (3.9)$$

3.3.1.B. Bound states

As discussed above the third-derivative nature of EM for unbound states in the low-field regime is a consequence of the fact that the electric field can destroy the translational symmetry of the material (***k*** is no longer a good quantum number) and accelerate the electrons and/or holes. It can be equivalently explained in terms of the mixing of different ***k***-states near the critical point caused by the perturbing electric field.

Although modulation spectroscopy generally produces first-derivative spectra traces for bound states systems, it is possible for EM to obtain a third-derivative lineshape.

For confined systems, however, EM can yield either a third-derivative or a first derivative spectra. If energy level spacing in the bound states system is small compared to $qF_{ac}L_Z$ (L_z is the dimension of the confinement, i.e., the dimension of a quantum dots, the well width of a QW), the electric field will cause a mixing of the quantum levels. This is similar to the bulk EM picture. Therefore, a third-derivative EM lineshape is possible for certain bound systems. Microstructures such as quantum boxes which are confined in all three dimensions belong to this category.

On the other hand, if the level spacing in the bound system are large compared to qF_aL_Z, the mixing of levels will not happen. It is not possible for the perturbing electric field to accelerate the particles. Under such conditions, as will become clear later, the EM lineshape is first-derivative. In this thesis, we are only concerned about the first-derivative EM spectroscopy for bound states. I will discuss this type of bound systems in greater detail in the rest of this section.

Confined systems, such as the isolated states of quantum wells and multiple quantum wells, excitons, impurities, etc., differ significantly from the unbound states of bulk material because the particle (electron or hole) and its wave function are localized in space. Because of this confinement, the energies (in the confinement direction for microstructures) are discrete and dispersionless resulting in an infinite effective mass (in the confinement direction). An applied electric field (along the confinement direction) adds a linear potential, which tilts the confining potential, changing its shape. The electrons and holes become spatially polarized, but still remain confined. This alters both the electronic energies and the wave function overlap [intensity (I)]. Also the tilting of the potential can result in a change in lifetime Γ as a result of tunneling.

In terms of EM, the infinite mass means that Eq. (3.9) is no longer applicable since $\hbar\Theta=0$. Several authors have treated this problem in detail (Shanabrook *et al.* 1987a, 1987b, Enderlein *et al.* 1988, Pollak and Glembocki 1988, Jiang *et al* 1989, Enderlein 1990, Pollak and Shen 1990, Tang 1991, Pollak 1992, 1993, Glembocki, *et*

al. 1992). They have shown that under these conditions the change in the dielectric function induced by the modulating field, F_{ac}, is first-derivative and can be expressed as:

$$\Delta\epsilon = [(\partial\epsilon/\partial E_g)(\partial E_g/\partial F_{ac}) + (\partial\epsilon/\partial\Gamma)(\partial\Gamma/\partial F_{ac}) + (\partial\epsilon/\partial I)(\partial I/\partial F_{ac})]F_{ac} \qquad (3.10)$$

This equation can be rewritten as (Huang Y. S. *et al.* 1991a):

$$\Delta\epsilon_i = [A_E f_E^{(i)} + A_\Gamma f_\Gamma^{(i)} + A_I f_I^{(i)}](I/\Gamma)F_{ac} \qquad (i = 1,2) \qquad (3.11a)$$

with

$$A_E = (\partial E_g/\partial F_{ac}) \qquad (3.11b)$$

$$A_\Gamma = (\partial\Gamma/\partial F_{ac}) \qquad (3.11c)$$

$$A_I = (1/I)(\partial I/\partial F_{ac}) \qquad (3.11d)$$

and

$$f_E^{(i)} = (\partial\epsilon_i/\partial E_g) \qquad (3.11e)$$

$$f_\Gamma^{(i)} = (\partial\epsilon_i/\partial\Gamma) \qquad (3.11f)$$

$$f_I^{(i)} = (\partial\epsilon_i/\partial I) \qquad (3.11g)$$

3.3.2. Piezomodulation

Since the piezomodulation method does not destroy the translation symmetry of the material the lineshape will be the first-derivative expression of Eq. (3.10). However, the band gap modulation term is due not to the Stark effect, as in EM, but is created by the stress dependence of the energy gaps. Thus for PzR Eq. (3.10) is appropriate with F_{ac} replaced by the modulating stress S_{ac}.

3.3.3. Functional form of ϵ

3.3.3.A. Unbound states without final states Coulomb interaction

As remarked earlier the structures in modulation spectra are localized in photon energy. Because of this fact, we have the enormously simplifying results that for the purpose of analyzing modulation spectra it is usually entirely adequate to replace the actual complicated dispersion of the energy bands with local parabolic expansions in the neighborhood of the critical points (Aspnes 1980). If the Coulomb interaction between the electrons and holes is neglected, in the one-particle picture for the case in which the line width is primarily due to life time broadening, the local expression of the dielectric function takes a simple Lorentzian form which can be written for a one-dimensional (1D) critical point (Aspnes 1980):

$$\epsilon(E,\Gamma) = \frac{C_1}{E^2}(E-E_g+i\Gamma)^{-1/2} \qquad for\ 1D, \tag{3.12a}$$

for a two-dimensional critical point:

$$\epsilon(E,\Gamma) = \frac{C_2}{E^2}\ln(E-E_g+i\Gamma) \qquad for\ 2D, \tag{3.12b}$$

and a three-dimensional (3D) critical point:

$$\epsilon(E,\Gamma) = \frac{C_3}{E^2}(E-E_g+i\Gamma)^{1/2} \qquad for\ 3D, \tag{3.12c}$$

where the parameters C_1, C_2 abd C_3 are related to matrix element effects and can be considered constants over the vicinity of the critical point.

Given the above explicit functional form of dielectric functions, the low field electromodulation lineshape can be obtained by substituting Eq. (3.12c) in to Eq. (3.9) and the resulting expression takes a particularly simple form (Aspnes 1980):

$$\Delta R/R = (\hbar\Theta)^3 Re[Ae^{i\phi}(E-E_g+i\Gamma)^{-m}] \tag{3.13a}$$

or

$$\Delta R/R = (\hbar\Theta)^3 L(E-E_g,\Gamma) \tag{3.13b}$$

where

$$L(E-E_g,\Gamma) = Re[Ae^{i\phi}(E-E_g+i\Gamma)^{-m}] \tag{3.13c}$$

In Eqs. (3.13a) and (3.13c) A is the amplitude, ϕ is a phase angle which accounts for Eq. (3.1) and the influence of non-uniform electric fields as well as interference and electron-hole interaction effects (Hamakawa and Nishino 1976, Aspnes 1980). The lineshape factor $L(E-E_g,\Gamma)$ is independent of the modulating field in the low-field regime.

The parameter m in the lineshape factor of Eq. (3.13c) depends on critical point type. For a three dimensional M_0 critical point, such as the direct gap of GaAs, $m=2.5$. For a two-dimensional critical point $m=3$ (Aspnes 1980).

The change in dielectric functions induced by piezomodulation can be obtained by substituting the appropriate dielectric functions Eqs.(3.12a) - (3.12c) into the first-derivative expression of Eq. (3.10). It is straight forward to see that the lineshape function has the same form Eq. (3.13a) with m taking a value from that of EM for a given type critical point. For a three dimensional M_0 critical point, $m=0.5$ for PzR.

In arriving at the Lorentzian form of the dielectric function, Eqs. (3.12), the broadening of transitions has been assumed to be predominantly due to the life time effects. If the relaxation of the electron-hole pair excitation of the crystal is primarily associated with a large number of weak scattering centers and statistical inhomogeneity, the dielectric function will have a Gaussian form (Toyozawa 1958, Edwards and Gulyaev 1964, Lukes and Somaratna 1970, Garland *et al.* 1988). The general form of Gaussian dielectric function (ϵ_G) can be expressed as (Lukes and Somaratna 1970, Garland *et al.* 1988):

$$\epsilon_G(E,\Gamma) = \frac{Const}{E^2} \int_{B.Z.} dk \int_0^{\infty} ds(-i) \exp\{is[E-E_{cv}(k)] - 2s^2\Gamma^2\} \qquad (3.14)$$

where the interband transition matrix element has been considered a constant, and $E_{cv}(k)$ is the difference between the conduction band and the valence band dispersions. For low-field electromodulation the field induced change in the dielectric function is calculated by substituting Eq. (3.14) into Eq. (3.9). Similarly the stress induced change in the dielectric function in the case of piezomodulation is obtained by taking the first derivative of Eq. (3.14) with respect to the energy gap. The lineshape function is then obtained from Eq. (3.1) (Garland *et al.* 1988).

3.3.3.B. Unbound states with final states Coulomb interaction

If the Coulomb interaction between holes and electrons is important, the dielectric function will be modified (See, for example, Elliott 1957, Seraphin 1972, Aspnes 1972, Bassani *et al* 1973, Aspnes 1980). We will limit our discussions to 3D M_0 type critical points only. For a 3D M_0 critical point the absorption profile in the presence of electron-hole Coulomb interaction consists of a series of discrete lines corresponding to the bound excitonic states below the band edge, and an increasing continuum at higher energies with an enhanced step-like rise at the band edge. When broadening is ignored the energy dependence of the imaginary part of dielectric function corresponding to the unbound states, $\epsilon_{2Coulomb}$, is given by (Bassani *et al.* 1973, chapter 6):

$$\epsilon_{2Coulomb}(E,E_g) = 0 \qquad for\ E < E_g,$$

$$= \epsilon_{2F}(E,E_g)\frac{\pi\chi\exp(\pi\chi)}{\sinh(\pi\chi)} \qquad for\ E \geq E_g \tag{3.15}$$

with

$$\chi = \sqrt{\frac{R_y}{E-E_g}}$$

where R_y is the exciton binding energy and

$$\epsilon_{2F}(E,E_g) = \frac{C}{E^2}(E-E_g)^{1/2} \qquad for\ E \geq E_g \tag{3.16}$$

where C is related to matrix element effects and can be considered constant over the vicinity of the critical point. ϵ_{2F} is the imaginary part of dielectric function in the absence of electron-hole Coulomb effects, which is identical to that given by the imaginary part of Eq. (3.15) when life time broadening is not included. We see that for $\chi \ll 1$, i.e., $(E-E_g) \gg R_y$, we simply obtain $\epsilon_{2Coulomb}(E,E_g) = \epsilon_{2F}(E,E_g)$, similarly for $\chi \gg 1$, i.e., $(E-E_g) \ll R_y$, we obtain $\epsilon_{2Coulomb}(E,E_g) \approx$ constant, and thus we have a finite limit in the absorption coefficient at energies near the energy gap.

The life time broadening of $\epsilon_{2Coulomb}$ has to be taken into account by means of numerical convolution with the Lorentzian broadening response function (Cardona 1969, Aspnes 1980, Shen and Pollak 1990):

$$R_L(E,\Gamma) = \Gamma/\pi(E^2+\Gamma^2) \tag{3.17a}$$

and

$$\epsilon_{Coulomb}(E,E_g,\Gamma) = \int \epsilon_{Coulomb}(E',E_g)R_L(E',\Gamma)dE' \tag{3.17b}$$

There is no closed form for the broadened $\epsilon_{2Coulomb}$ (Rees 1967, 1968, Aspnes 1970). The real part can be obtained from a Kramers-Kronig inversion of $\epsilon_{2Coulomb}$. Displayed schematically in Fig. 10 is a comparison of the traces of $\epsilon_{2Coulomb}$ and ϵ_{2F} for a three-dimensional M_0 critical point.

Electromodulation and piezomodulation spectra lineshapes can be obtained by first calculating third- and first-derivative changes in dielectric function, respectively, and then substituting the obtained changes in dielectric function into the general lineshape function, Eq. (3.1). The calculation involves a numerical convolution and a numerical Kramers-Kronig transformation. The computing load can be greatly reduced by the use of spectral fast Fourier transform (FFT) method (see Press *et al* 1988 and references therein). King's Fourier transform approach of Kramers-Kronig inversion in optical data proves to be an extremely valuable tool (King 1977, 1978, Peiponen and Vartiainen 1991). Shown in Fig. 11 are the calculated lineshape of $\Delta\epsilon_{2Coulomb}$ and $\Delta\epsilon_{2F}$ for third-derivative spectra for a three-dimensional M_0 critical point.

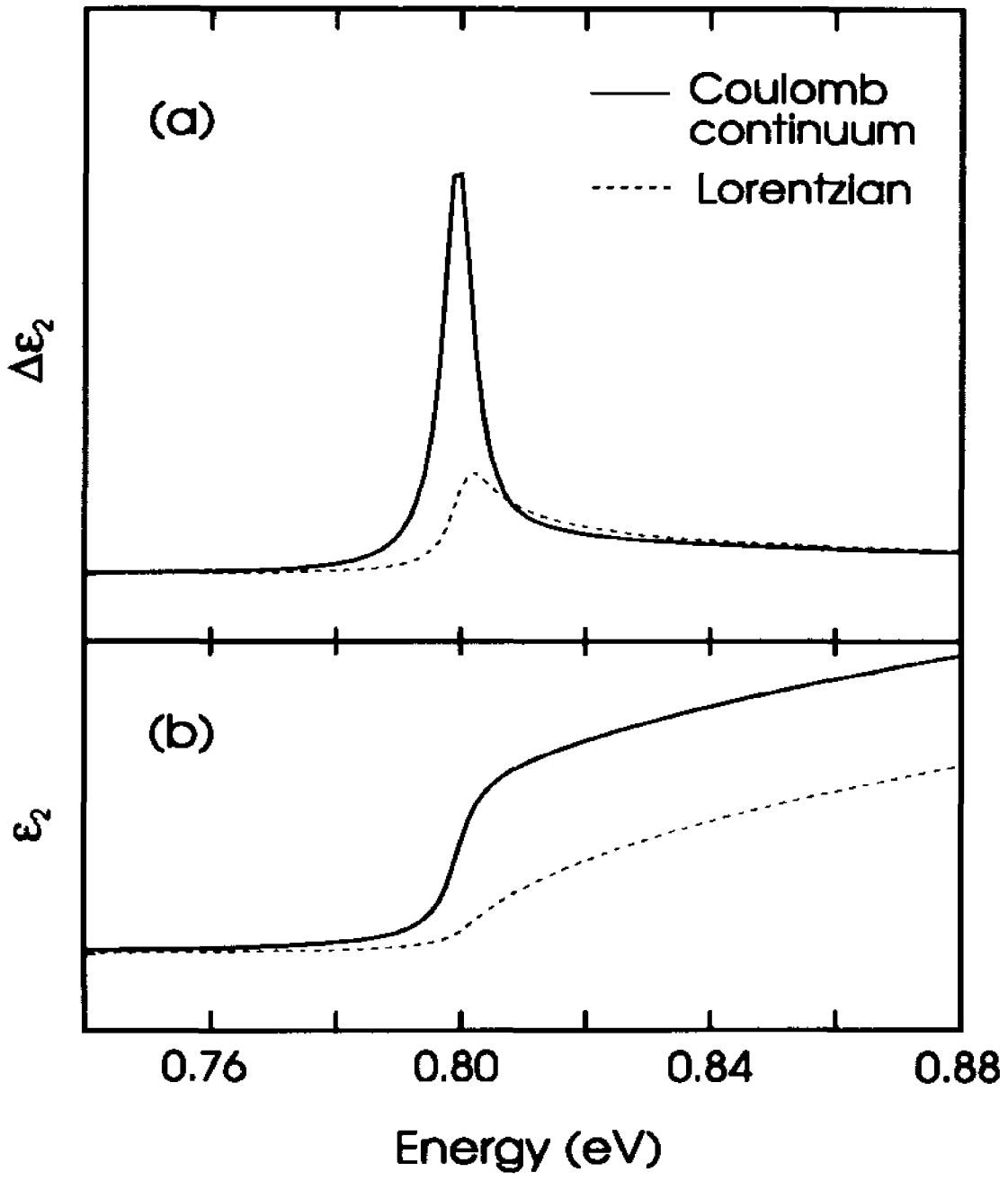

Fig. 10. Calculated $\epsilon_{2\text{Coulomb}}$ and ϵ_{2F} (b) and their first derivatives (a). The values of E_g, Γ and R_y are taken to be 0.8 eV, 3 meV and 2 meV, respectively.

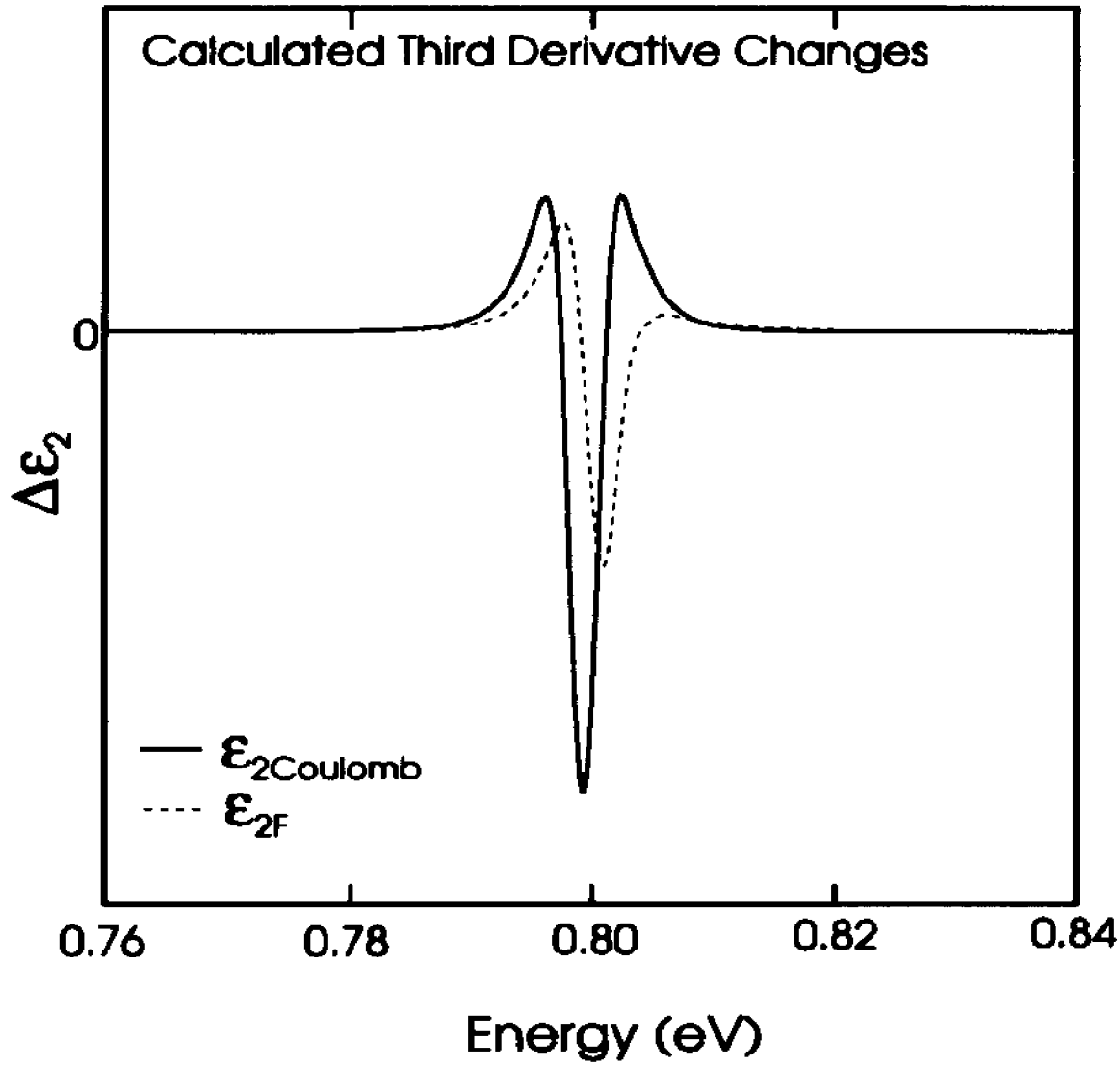

Fig. 11. Comparison of the third-derivative lineshapes of $\Delta\epsilon_{2Coulomb}$ and $\Delta\epsilon_{2F}$. The values of E_g, Γ and R_y are taken to be 0.8 eV, 3 meV and 2 meV, respectively.

3.3.3.C. Bound states

The unperturbed dielectric function for a bound states transition of Eq. (3.10) or (3.11a) will be either Lorentzian or Gaussian, depending on the broadening mechanism and/or temperature (Glembocki and Shanabrook 1987, 1992, Pollak and Glembocki 1988, Glembocki 1990b).

One extremely important case of bound states is the quantum well system. The quantum levels in quantum well structures are bound states with respect to the motion of electrons and holes along the growth direction (assumed to be the z-axis). The carriers in these states are confined in the z-direction, but free to move in the xy-plane, exhibiting a quasi two-dimensional character. The reduction in dimensionality from 3D to 2D changes the absorption profile from a square root dependence on photon energy of bulk material to a two-dimensional form which consists of a series of quantized step functions independent of photon energy. In addition, the 2D character of the system enhances exciton binding energy effects. Shown in Fig. 12 by the dot-dashed line is ϵ_2 for the 3D case of bulk material while the dashed line is the step-like 2D profile. The solid line shows schematically the influence of the excitons. The energy difference between the exciton peak and the corresponding step in the 2D absorption edge is the exciton binding energy. Because of these strong excitonic effects, in undoped QW structures, even at 300K, the absorption profile (ϵ_2) consists of sharp excitonic peaks, superimposed on a step-like two-dimensional joint density of states (2DJDS). In this case

$\Delta\epsilon$ in Eq. (3.10) or (3.11a) is the first derivative of a Lorentzian or Guassian profile, depending on the nature of the broadening mechanism of the exciton.

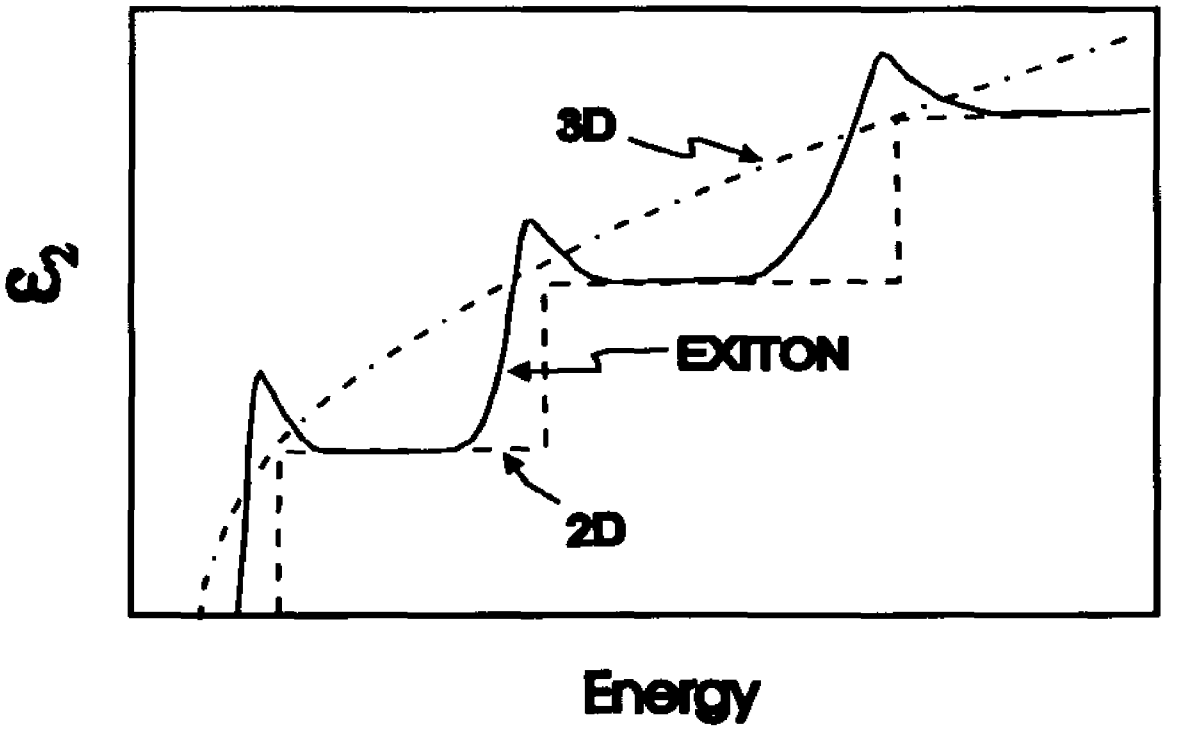

Fig. 12. Schematic representation of ϵ_2 for a three-dimensional M_0 critical point (dot-dashed), two-dimensional joint density of states (dashed) and exciton (solid).

This thesis involves the first-derivative spectroscopy of bound states systems. In the following I will discuss the first-derivative lineshapes for Lorentzian and Gaussian broadening in great detail.

The Lorentzian dielectric function can be written as (Aspnes 1980, Shanabrook and Glembocki 1989, Glembocki 1990a 1990b):

$$\epsilon = 1 + \frac{I}{E - E_g + i\Gamma} \tag{3.18a}$$

The various modulation terms of Eqs. (3.11a)-(3.11g) are given by:

$$f_E^{(1)} = (y^2 - 1)/(y^2+1)^2 \tag{3.18b}$$

$$f_E^{(2)} = -2y/(y^2+1) \tag{3.18c}$$

$$f_\Gamma^{(1)} = f_E^{(2)} \tag{3.18d}$$

$$f_\Gamma^{(2)} = -f_E^{(1)} \tag{3.18e}$$

$$f_I^{(1)} = y/(y^2+1) \tag{3.18f}$$

$$f_I^{(1)} = -1/(y^2+1) \tag{3.18g}$$

where

$$y = (E - E_g)/\Gamma \tag{3.18h}$$

The relations between the energy gap and broadening modulation terms of Eqs. (3.18d) and (3.18e) are due to the symmetry of E_g and Γ in Eq. (3.18a).

Plotted in Fig. 13 are $f_E^{(1)}$ [$= -f_\Gamma^{(2)}$], $f_E^{(2)}$ [$= f_\Gamma^{(1)}$] and $f_I^{(1)}$, $f_I^{(2)}$ as a function of y for the Lorenztian case. If intensity modulation terms are neglected there are only two independent lineshape factors. The combined spectral dependence can then be analytically expressed by Eq. (3.13c) with $m=2$ (Aspnes 1980).

If the unperturbed profile is Gaussian the situation is more complicated since E_g and Γ no longer have the same symmetrical relation as in Eq. (3.18a). The unperturbed dielectric function is obtained from Eq (3.14) and is given by (Huang Y. S. *et al.* 1991):

$$\epsilon = 1 + I(L_1 + iL_2) \tag{3.19a}$$

where

$$L_1 = -(y/\Gamma)\Phi(1, 3/2, -y^2/2) \tag{3.19b}$$

$$L_2 = -(\pi/2)^{\frac{1}{2}}(1/\Gamma)\exp(-y^2/2) \tag{3.19c}$$

where y is given by Eq. (3.18h) and Φ is the confluent hypergeometric function.

In this case the various modulation terms of Eqs. (3.11a)-(3.11g) can be written as

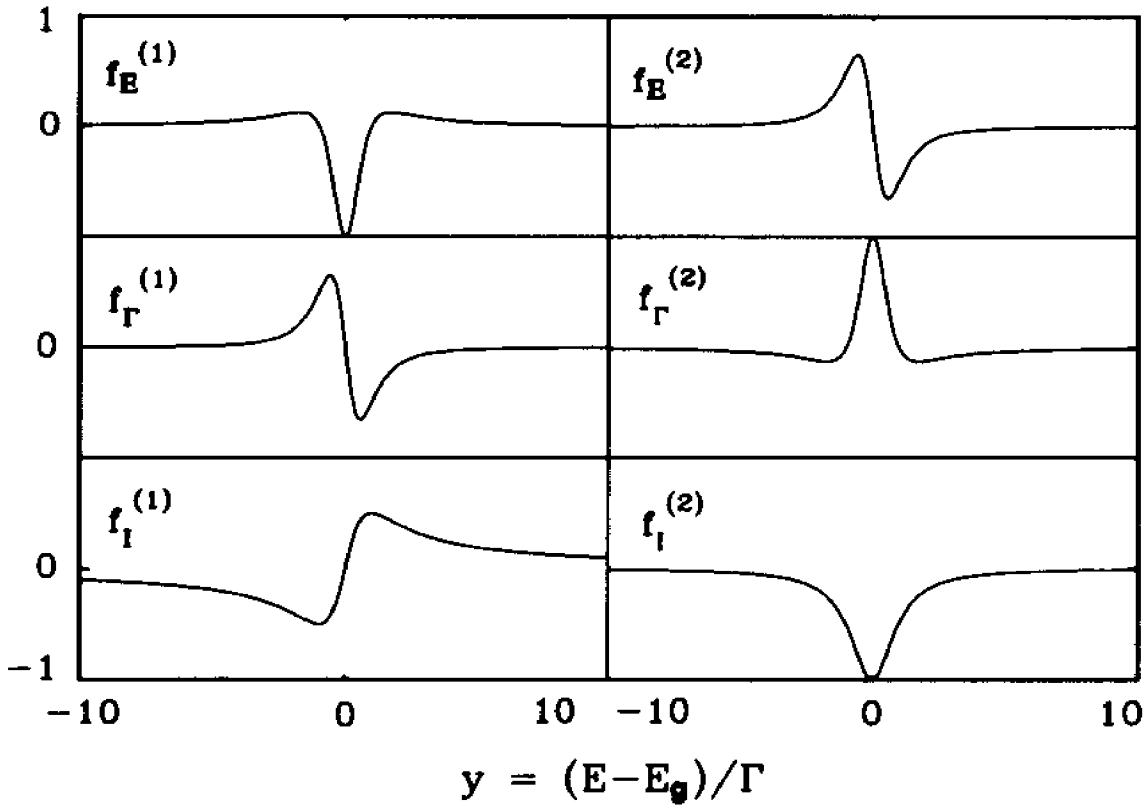

Fig. 13. Calculated lineshapes for the first derivatives of ϵ_1 and ϵ_2 of a Lorentzian dielectric function given in Eqs. (3.18b)-(3.18h).

$$f_E^{(1)} = -\Phi(1, 1/2, -y^2/2) \tag{3.20a}$$

$$f_E^{(2)} = -(\pi/2)^{\frac{1}{2}} y\, e^{(-y^2/2)} \tag{3.20b}$$

$$f_\Gamma^{(1)} = -2y\Phi(2,3/2,-y^2/2) \tag{3.20c}$$

$$f_\Gamma^{(2)} = -(\pi/2)^{\frac{1}{2}}(y^2-1)e^{(-y^2/2)} \tag{3.20d}$$

$$f_I^{(1)} = y\Phi(1,3/2,-y^2/2) \tag{3.20e}$$

$$f_I^{(2)} = -(\pi/2)^{\frac{1}{2}}e^{(-y^2/2)} \tag{3.20f}$$

In contrast to the Lorenztian situation there is not a simple, analytical relation between $f_E^{(1)}$ $[f_E^{(2)}]$ and $-f_\Gamma^{(2)}$ $[f_\Gamma^{(1)}]$.

Plotted in Fig. 14 are the various modulation terms of Eqs. (3.20a)-(3.20f). Note that although $f_E^{(1)}$ $[f_E^{(2)}]$ and $-f_\Gamma^{(2)}$ $[f_\Gamma^{(1)}]$ are not exactly the same, as in the case of the Lorenztian profile, their lineshapes look very similar, i.e., $f_E^{(1)} \approx -f_\Gamma^{(2)}$ and $f_E^{(2)} \approx f_\Gamma^{(1)}$. Therefore, for many practical applications, if $f_I^{(1)}$ and $f_I^{(2)}$ are neglected, only two lineshape profiles need to be used to fit experimental data. Hence, even for the Gaussian situation an expression similar to Eq. (3.13c) can be used, i.e.,

$$\frac{\Delta R}{R} = Re\{Ae^{i\phi}[f_E^{(1)} + if_E^{(2)}]\} \tag{3.21}$$

It should be noted that in high quality bulk materials grown by techniques such as MBE or vapor phase epitaxy (VPE) direct gap excitons may be present even at 300K (Zheng *et al.* 1988a). In such cases the first-derivative lineshape form of Eq. (3.10) will

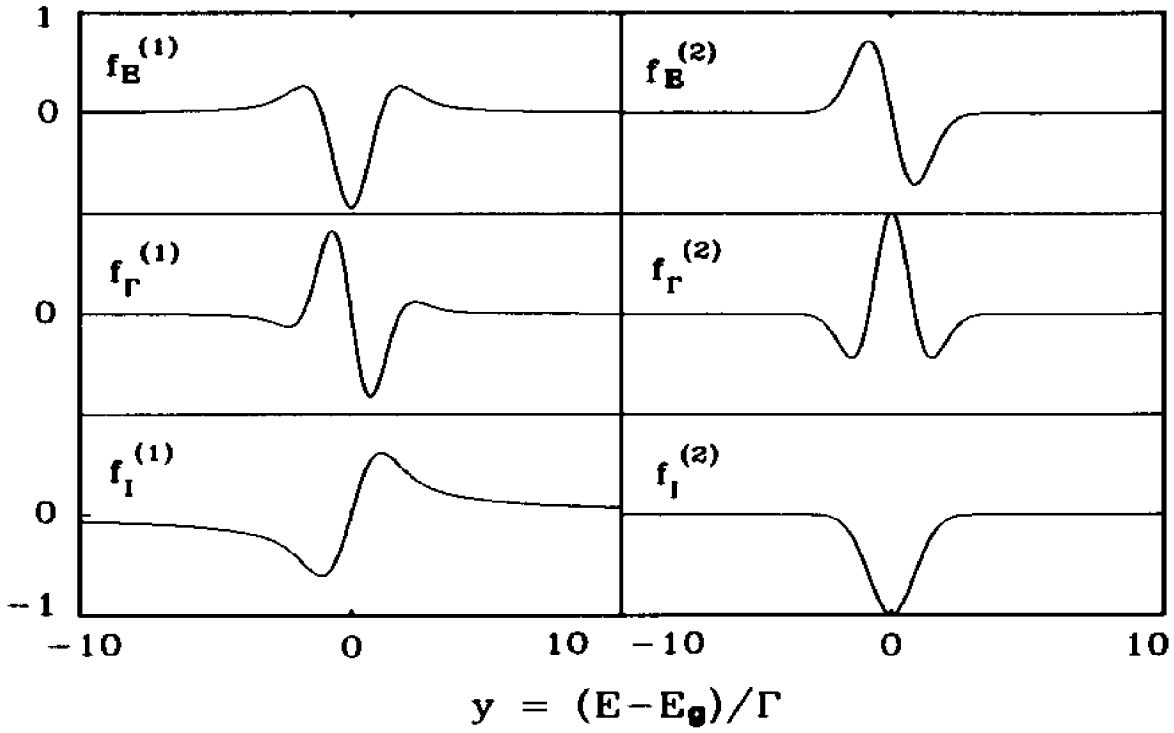

Fig. 14. Calculated lineshapes for the first derivatives of ε_1 and ε_2 of a Gaussian dielectric function given in Eqs. (3.20a)-(3.20f).

be appropriate rather than the third-derivative profile of band-to-band transitions.

3.3.4. Lineshape for screened two-dimensional exciton - 2DEG effects

As has been discussed in Section 3.3.3.C, the lineshape for quantum transitions in an undoped QW is excitonic. In modulation-doped quantum wells, however, there

exists a large density of electrons in the well channel. The presence of a sufficiently dense 2DEG (or 2D plasma) produces a screening effect which wipes out these strong excitonic resonances (Huang D. *et al.* 1988, Chemla *et al.* 1988). In addition, the large population of electrons will occupy the lower levels in the lowest subbands that are below the Fermi energy, resulting in a filling of the lower energy levels. These characteristics of 2DEG make the absorption profile of MDQW very different from those of undoped QWs. In such systems the intersubband transition absorption function will be the broadened step-like 2DJDS of Eq. (3.12b) multiplied by a Fermi level filling function. Neglecting the many-body effects, this lineshape can be expressed as (Yin Y. *et al* 1992):

$$\epsilon_2 = \sum_j I_j \; Im\{\ln[E_j(mnH) - E + i\Gamma_j]\}[1 - f_c^j(E, E_F)] \qquad (3.22a)$$

where I_j is the amplitude of the j^{th} spectral feature, *Im* denotes the imaginary part, E is the photon energy, E_F is the Fermi energy, Γ_j is the broadening parameter and $E_j(mnH)$ is the intersubband energy given by:

$$E_j(mnH) = E^c_{m,j} - E^v_{n,j}(H) \qquad (3.22b)$$

In Eq. (3.22b) $E_{m,j}^{c}$ and $E_{n,j}^{v}(H)$ are the energies of the m^{th} conduction and n^{th} heavy-hole (out-plane) valence subbands, respectively, associated with the j^{th} feature.

Similar results apply to electron-light hole transitions if there are light hole levels confined in the well. However, we will choose the electron-heavy hole system as an

example in the following discussion. The results thus obtained are general and apply to confined quantum transitions in MDQWs in the presence of a dense sheet of electrons.

The Fermi function in Eq. (3.22a) can be expressed as:

$$f_e^j = \{1 + \exp[\lambda E - \lambda E_j(mnH) - E_j(m)]/kT\}^{-1} \tag{3.23a}$$

with

$$E_j(m) = E_F - E_{mj}^c \tag{3.23b}$$

The parameter λ in Eq. (3.23a) is given by:

$$\lambda = m_h^*/(m_c^* + m_h^*) \tag{3.23c}$$

where m_c^* and m_h^* are the conduction and in-plane heavy-hole effective masses, respectively, in units of the free electron mass.

The real part of the dielectric function ϵ_1 can be obtained from the Kramers-Kronig transformation of ϵ_2 given in Eq. (3.22a). $\Delta\epsilon_1$ and $\Delta\epsilon_2$ are then obtained by taking the first derivative with respect to the appropriate parameters. The lineshape function is obtained by substituting them into Eq. (3.1), which can be written as:

$$\frac{\Delta R}{R} = Re\{I_j e^{i\phi}(\Delta\epsilon_1 + i\Delta\epsilon_2)\} \tag{3.24}$$

This first-derivative of a 2DJDS lineshape is designated as a FD2DJDS lineshape. The fitting parameters are I_j, E_j(mnH), Γ_j , ϕ_j and E_j(m).

It can be shown that for the case of a broadened step-like 2D density of electron states N_s is given by (for $KT \gg E_F$)(Yin Y. *et al.* 1992):

$$N_S = (m_e^*/\pi\hbar^2)\sum_m \int_0^\infty \{(1/2)+(1/\pi)\arctan[(E-E_m^c)/\Gamma_m]\} \times \{\exp[(E-E_F)/kT]+1\}^{-1} dE \qquad (3.25)$$

where E_m^c and Γ_m are the energy and broadening of the m^{th} electronic level, respectively, and can be deduced from transition energies [E_j(mnH)] and broadening parameters (Γ_j) obtained from the lineshape fit (Yin Y. 1992). The Fermi energy can be directly obtained from a least-square fit of the experimental data to the FD2DJDS lineshape. Using the values of E_F, Γ_m and E_m^c, the 2DEG density N_s can be obtained from the above equation.

The FD2DJDS lineshape has many important features. It is very sensitive to both the Fermi energy and temperature, in addition to the parameters such as transition energy and broadening parameter that are common to all other lineshapes discussed in Section 3.3. Shown in Fig. 15 are the calculated curves for ϵ_2 and $\Delta\epsilon_2$ (for energy gap modulation) for a single intersubband transition in a modulation-doped quantum well at 300K and 77K. The input parameters used are $E_g = 1.2$ eV, $\Gamma = 5$ meV, $E_F - E_1^c = 60$ meV, the electron and in-plane hole masses are taken to be 0.063 m_0 and 0.11 m_0,

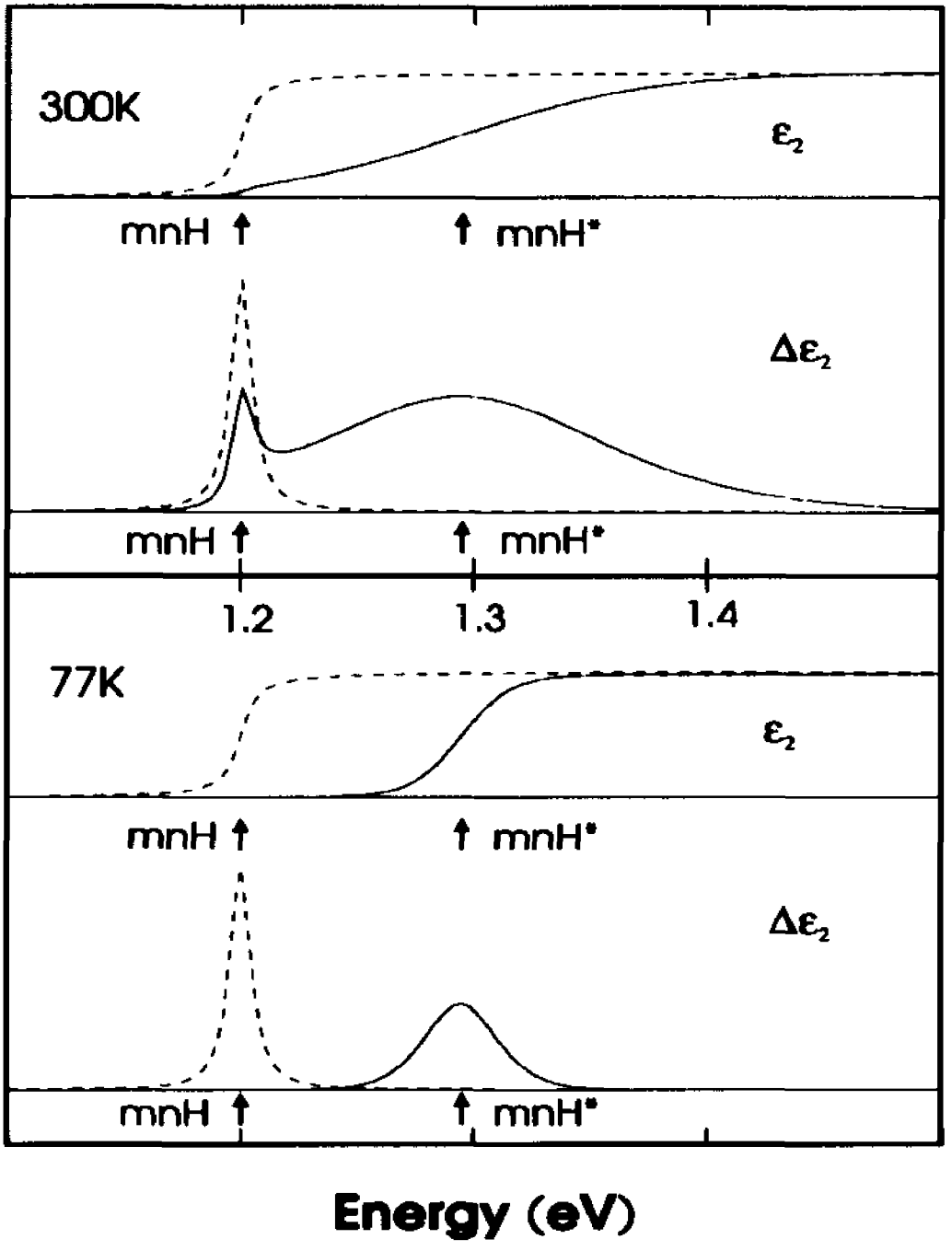

Fig. 15. The calculated ϵ_2 and $\Delta\epsilon_2$ for energy gap modulation with (solid line) and without (dashed line) Fermi level filling factor at 300K and 77K ($m=1$, $n=1$).

respectively, and the subbands involved are assumed to be the m=1 conduction band level and the n=1 heavy hole level.

It is clear from Fig. 15 that there is a big difference in the absorption profiles calculated with (solid lines) or without (dashed lines) the Fermi level filling function and the lineshape changes with temperature dramatically. Because of the band filling effects, the intensity of band edge transitions (the mnH transition indicated in Fig. 15) will be reduced (300K), or even completely wiped out (77K). This band edge signal will remain detectable if the following two conditions are satisfied: (1) The tail of $(1\text{-}f_c)$ can reach the subband edge and, (2) the overlap integral of the envelope wave functions E_m^c and the heavy hole state E_n^v(H) does not vanish.

There is also a $k \neq 0$ feature *mnH** which occurs at the Fermi wave vector (see Fig. 15). It will be observed as long as condition (2) holds. The *mnH** transition appears as a very broad feature at higher temperatures, but narrows down as the temperature decreases. However, when the temperature is low enough to have appreciable many-body effects in the 2DEG, this Fermi edge transition peak can not be accounted for by our simple one-electron model. The lineshape and properties of this peak at lower temperatures have to be understood in an approach that takes into account of the many-body interactions in the 2DEG. The study of this feature can provide important information about many-body physics and it is the subject of current research (Gumbs *et al.* 1993).

It should be pointed out that transitions involving conduction subbands above the Fermi energy will also be affected by the band filling as long as the tail of the Fermi level filling function on the higher energy side can reach them.

The great utility of this lineshape in the study of 2DEG effects will be best demonstrated in the investigation of such microstructures as modulation-doped quantum wells and high electron mobility transistors made from MDQWs, which is the subject of Chapter 4.

3.3.5. Effects of Built-in electric field on unbound states

A built-in electric field can be present in a sample due to surface/interface Fermi level pinning, space charge distribution and piezoelectric effects (Shen and Pollak 1990, Pollak 1992). The strength of such fields can easily reach the intermediate-field regime defined in Section 3.3.1. For the unbound states in bulk or thick layer (bulk-like) materials the dielectric function can exhibit Franz-Keldysh oscillations (FKO) in this case. The physical origin of this phenomenon is the photon-assisted tunnelling process (Pollak 1992). For a three-dimensional critical point the dielectric function in the presence of a uniform field F (neglecting Γ) can be written as (Aspnes 1980):

$$\epsilon(E-E_g,F) = 1 + \left[\frac{C\sqrt{\hbar\Theta}}{E^2}\right]\{G(\eta)+iF(\eta)\} + D\left(2\sqrt{E_g} - \sqrt{E_g+E}\right)/E^2 \qquad (3.26a)$$

where

$$G(\eta) = \pi\left[Ai'(\eta)Bi'(\eta) - \eta Ai(\eta)Bi(\eta)\right] + \sqrt{\eta}\, H(+\eta) \tag{3.26b}$$

$$F(\eta) = \pi\left[Ai'^{2}(\eta) - \eta Ai^{2}(\eta)\right] + \sqrt{-\eta}\, H(-\eta) \tag{3.26c}$$

with

$$\eta = (E_g - E)/\hbar\Theta \tag{3.26d}$$

The quantities $G(\eta)$ and $F(\eta)$ are referred to as electro-optic functions while $Ai(\eta)$, $Ai'(\eta)$, $Bi(\eta)$ and $Bi'(\eta)$ are Airy functions and their derivatives and $H(-\eta)$ is the unit step function (Aspnes 1980, Yin Y. *et al.* 1991). The parameters C and D are related to matrix element effects and can be considered constants over the vicinity of the critical point.

Plotted by the solid line in Fig. 16a is $\epsilon_2(E\text{-}E_g, F)$, the imaginary part of Eq. (3.26a). The dotted line is $\epsilon_2(E\text{-}E_g,0)$. It can be seen that the field produces FKO that are superimposed on top of the $(E\text{-}E_g)^{1/2}$ dependence of $\epsilon_2(E\text{-}E_g,0)$ for an three-dimensional M_0 critical point. In Fig. 16b is a plot of the expression

$$\begin{aligned}\Delta\epsilon_2(\eta) &= \Delta\epsilon_2(E - E_g, F) \\ &= \epsilon_2(E - E_g, F) - \epsilon_2(E - E_g, 0) = C\frac{\sqrt{\hbar\Theta}}{E^2}F(\eta)\end{aligned} \tag{3.27}$$

The curve in Fig. 16b shows an exponential tail for $\eta > 0$ and an oscillatory function for $\eta < 0$. The position of the n^{th} extrema (E_n) in the FKO are given by:

$$n\pi = (4/3)[(E_n - E_g)/\hbar\Theta]^{3/2} + \chi \tag{3.28}$$

where E_n is the photon energy of the n^{th} extrema and χ is an arbitrary phase factor (Aspnes 1974, Aspnes 1980). A plot of $(4/3)(E_n-E_g)^{3/2}$ vs the index number n will yield a straight line with slope $(\hbar\Theta)^{3/2}$. Therefore, the electric field, F, can be directly obtained from the period of FKO if $\mu_\parallel$ is known. Or conversely $\mu_\parallel$ can be measured if the field is known.

In the presence of Lorentzian broadening (Γ) the field-induced change in the dielectric function $\Delta\epsilon(\eta,\Gamma)$ can be obtained from a convolution integral of the unbroadened change $\Delta\epsilon(\eta,0)$ and the Lorentzian response function given by Eq.(3.17a) (Cardona 1969, Aspnes 1980, Shen and Pollak 1990). Although the exact form of $\Delta R/R$ for the intermediate-field case with broadening is quite complicated Aspnes and Studna (1973) and Aspnes (1974) have written down a relatively simple expression (for $E > E_g$):

$$\frac{\Delta R}{R} \propto \frac{1}{E^2(E-E_g)} \exp\left[-\frac{2\Gamma\sqrt{E-E_g}}{(\hbar\Theta)^{3/2}}\right] \times \cos\left[(4/3)\left(\frac{E-E_g}{\hbar\Theta}\right)^{3/2} + \chi\right] \tag{3.29}$$

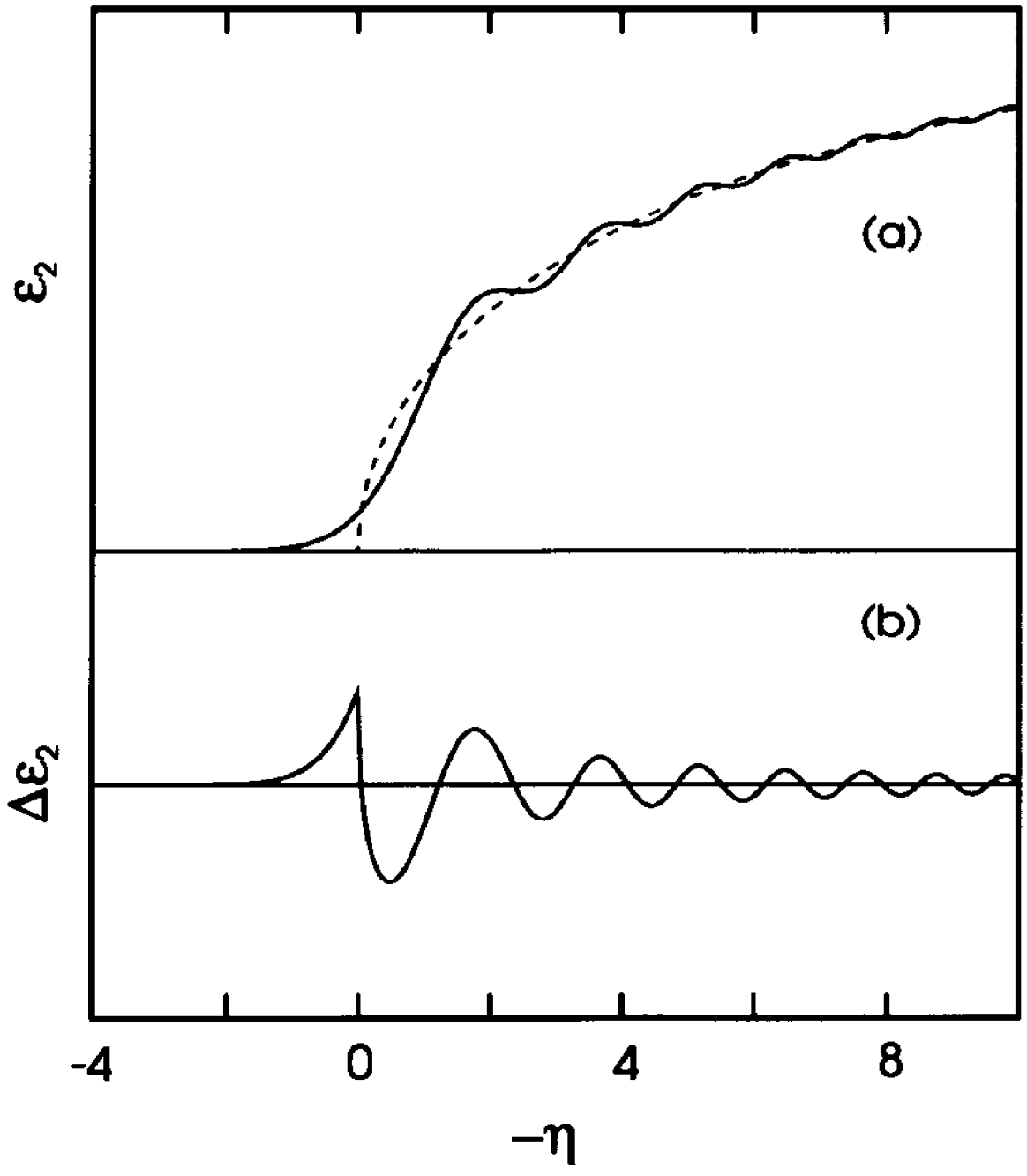

Fig. 16. The effects of electric field. (a) $\epsilon_2(E\text{-}E_g, F)$ (solid) and $\epsilon_2(E\text{-}E_g, 0)$ (dotted); (b) $\Delta\epsilon_2=\epsilon_2(E\text{-}E_g, F) - \epsilon_2(E\text{-}E_g, 0)$.

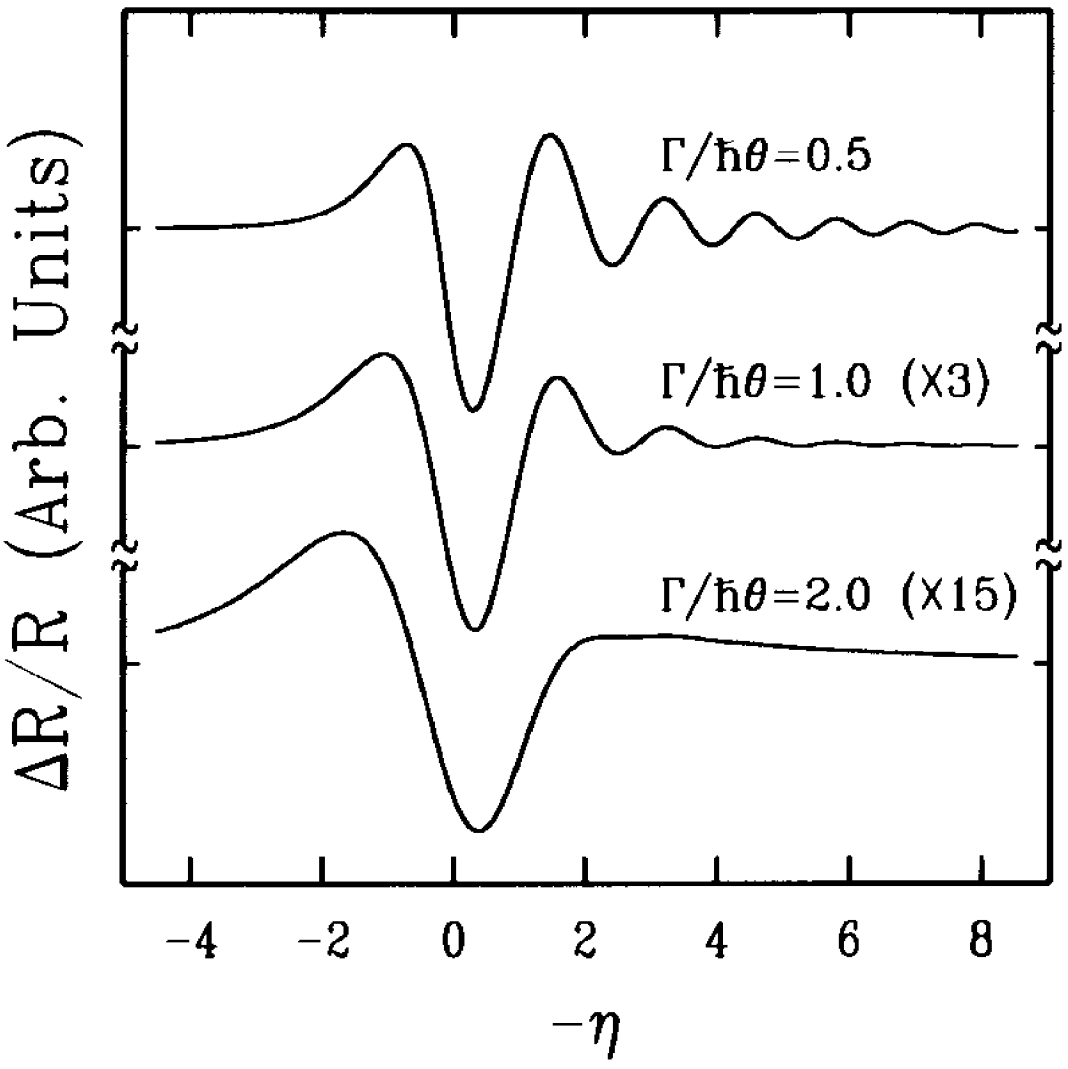

Fig. 17. The effects of broadening on FKO (see text).

To illustrate the effects of broadening in Fig. 17 Eq. (3.29) is plotted for values of the $\Gamma = 1.0$, 1.5 and 2.0 in units of $\hbar\Theta$ (Shen and Pollak 1990). For the smallest Γ it is still possible to observe eight or nine FKOs. The effects of Γ becomes quite evident above about $-\eta = 8$ in relation to the undamped case (see Fig. 16b). Only two or three

FKO can still be seen for $\Gamma=1.5$ while $\Gamma=2.0$ the FKOs are completely damped out. In this case the EM is in the third-derivative regime discussed in Sec. 3.1.1 (Aspnes 1974, Aspnes 1980).

The treatment of FKO discussed above has assumed a uniform electric field. However, in many situations this is not the case. For example, in the space-charge region (SCR) of a doped semiconductor the field is non-uniform and varies linearly with distance (z) from the surface. For non-uniform fields the effective change in the dielectric function $\Delta\epsilon$ can be expressed as (Aspnes 1980, Shen and Pollak 1990):

$$<\Delta\epsilon<\Delta\epsilon>=-2i\kappa(E)\int_0^{\infty}\exp[i2\kappa(E)\,z']\Delta\epsilon\left[E-E_g,F(z')\right]dz' \qquad (3.30)$$

where κ(E) is the complex propagation vector of the light in the solid.

Franz-Keldysh oscillations can easily be observed in EM experiments for both a uniform and a non-uniform field. For the case of EM for a non-uniform field the resultant signal comes only from a small near-surface region, where the field is almost uniform and equal to the surface (maximum) field.

For non-EM modulation experiments such as PzR (Tober *et al.* 1988, Tober *et al.* 1989) or TR, however, with one exception (Yin Y. *et al.* 1991) these field-dependent features have not been observed. In principle either thermo- or piezo-modulation (which

vary E_g), should produce a derivative-like spectrum similar to EM, which varies $\hbar\Theta$. This can be seen from Fig. 16.

While PzR, TR and EM should produce similar spectra for the uniform field case, this is not true for the non-uniform field situation. For a non-uniform field it is very difficult for non-EM methods to see FKOs. This is because for non-EM techniques Eq. (3.30) represents a weighted average over all possible field values, since these perturbations vary the dielectric function but not the width of the SCR. Since the magnitude of the field determines the period of the FKOs, this is a weighted superposition of oscillatory features of various periods. Such a superposition tends to diminish the oscillations. Shown in Fig. 18 in solid line is the result calculated from Eq. (3.30) for GaAs for a field with a linear z dependence as is the case for SCR (see, for example, Shen and Pollak 1990):

$$F(z) = F_s(1 - z/W), \tag{3.31}$$

where F_s represents the maximum field at the surface and W is the width of the SCR. Their values were taken to be 43 kV/cm and 6700 Å, respectively, which correspond to a surface Fermi-level-pinning value of 0.7 V and a net carrier concentration of 2×10^{15} cm^{-3}. The functional form of κ(E) is given in Shen and Pollak 1990. The corresponding case for a uniform field F_0 ($=F_s$) was also derived and shown as dotted line in the figure. A severe reduction in the oscillation amplitude in the linear field case can be clearly

observed from the figure. In practice, broadening will further diminish these FKOs, making them even more difficult to observe.

For a structure with a large, almost uniform field, Yin Y. *et al* (Yin Y. *et al.* 1991) have demonstrated that PzR also produces FKOs. The fact that only uniform electric fields can produce FKOs in non-EM spectra has important applications. For example, the presence of FKO in PzR spectra can be used as a test for a uniform field (Warren *et al.* 1992).

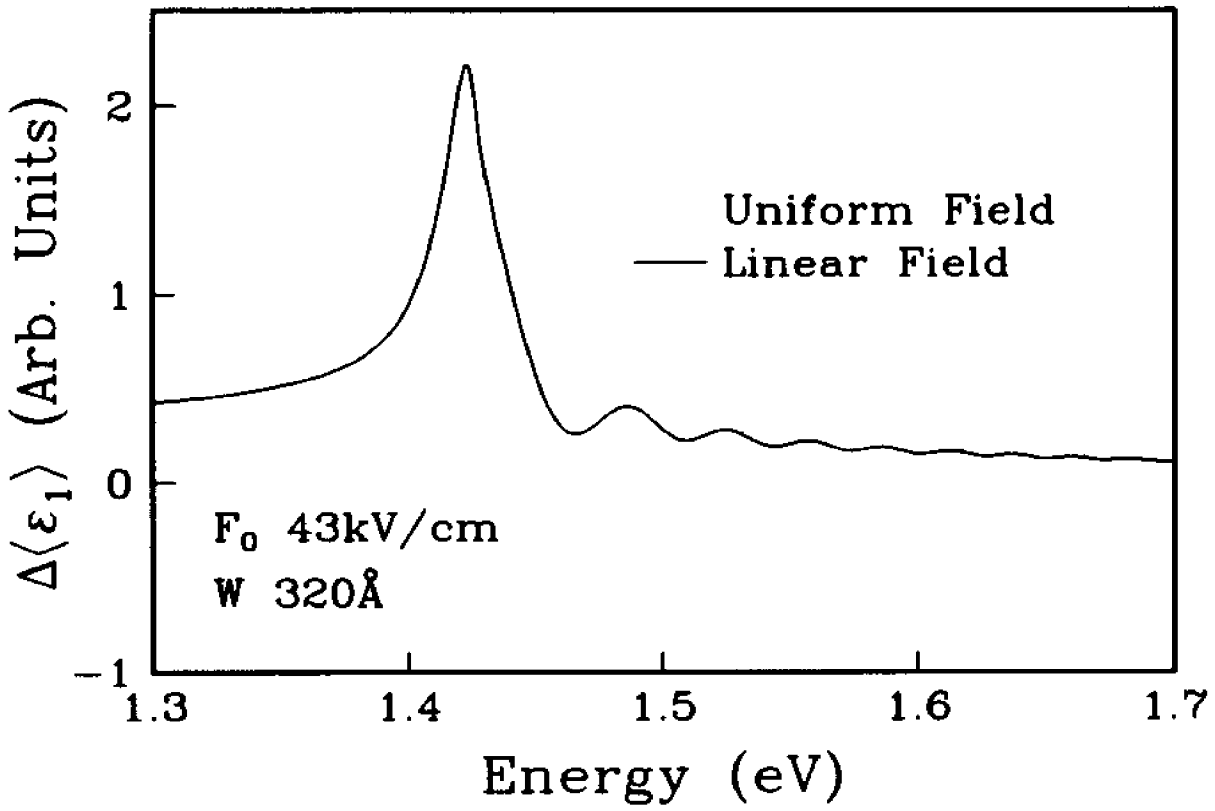

Fig. 18 Theoretical calculations of $<\Delta\epsilon_1>$ of GaAs for the case of nonuniform (solid line) and uniform (dotted line) electric fields (see text).

Chapter 4. PSEUDOMORPHIC GaAlAs/InGaAs/GaAs MODULATION-DOPED QUANTUM WELL STRUCTURES

4.1. Introduction

As has been remarked in Chapter 1, PMDQW structures are extremely important and interesting systems from both fundamental and applied point of view. The study of such systems can reveal information on the physics of many-body systems, reduced dimensionality, quantum hall effect, etc.. They can also be applied to make actual high performance devices called HEMTs that offer superior transistor noise performance compared to other solid-state amplifiers. Such devices have gained widespread acceptance as the device of choice for the majority of high performance receivers at frequencies up to 100GHz. They are also proving to be an excellent choice for power amplifiers.

Considerable effort has been directed to the study of modulation-doped heterostructures. Early studies were mainly carried out by means of transport measurements. Optical spectroscopy has recently been employed with great success in the investigation and characterization of such structures. The most frequently used optical methods are photoluminescence (PL) (see, for example, Pinczuk *et al.* 1984, Miller *et al.* 1985, Ruckenstein *et al.* 1986, Meynardier *et al.*, 1986, Delalande *et al.* 1986, 1987, Lobentanzer *et al.* 1987, Brierley 1991, Chen *et al.* 1992, Zhang and Ploog 1992, Gilperez *et al.* 1992, Fritze *et al.* 1992), photoluminescence excitation spectroscopy (PLE) (see, for example, Pinczuk *et al.* 1984, Miller *et al.* 1985, Ruckenstein *et al.* 1986, Meynardier *et al.* 1986, Delalande *et al* 1986, 1987),

magnetoluminescence (ML) (see, for example, Smith *et al.* 1984, Petrou *et al.* 1986, Meseguer *et al.* 1987, Skolnick *et al.* 1987a, 1987b, 1987c), direct absorption (see, for example, Lee *et al.* 1987, Huang D. *et al.* 1987, Chemla *et al.* 1987, Bar-Joseph *et al.* 1987, Huang D. *et al.* 1988a, Livescu *et al.* 1988), as well as modulation spectroscopy (see, for example, Snow *et al.* 1988, Tober *et al.* 1989, Herman *et al.* 1990a, Mendonca *et al.* 1990, Novellino *et al.* 1991, Sydor *et al.* 1991, 1992, Yin Y. *et al.*, 1992a, 1992b, 1993, Dimoulas *et al.* 1993).

In spite of the proven utility of modulation spectroscopy, particularly electromodulation, in studying and characterizing semiconductor microstructures (see, for example, Pollak and Glembocki 1988, Pollak 1992, Pollak and Shen 1993) it has had very limited success when first applied to the investigation of 2DEG effects. Most of the modulation spectroscopy studies of the 2DEG were performed on GaAlAs/GaAs modulation-doped heterojunctions (MDHJ). The interpretation of 2DEG has been the subject of considerable controversy (Hopfel *et al.* 1985, Pollak and Glembocki 1988, Glembocki 1990, Pan *et al* 1990, Sydor *et al* 1990, Sydor and Badakhshan 1991, Glembocki and Shanabrook 1992, Pollak 1992, Pollak and Shen 1993). In their original PR work Glembocki *et al* (1985a, 1985b) reported oscillatory features above the band gap of GaAs in a GaAs/GaAlAs MDHJ. They initially assigned these structures simply to transitions from the GaAs valence band to the quantized levels in the nearly triangular shaped potential at the interface. However, subsequent investigations have not shown clear evidence for a signature associated with the 2DEG (Sydor *et al.* 1990, Pan *et al.*

1990, Sydor and Badakhshan 1991, Glembocki and Shanabrook 1992, Pollak and Shen 1993). This is because in the GaAlAs/GaAs MDHJ systems there exist electric fields associated with E_0 of GaAs not only in the region of the 2DEG but also in other portions of the sample.

One type of 2DEG system, however, does not have the complication of the substrate signal. This is the GaAlAs/InGaAs/GaAs PMDQW system. The band alignment for indium content (x) of interest ($x \sim 0.2$) in these PMDQW systems is such that the electron-heavy hole system is a type I, while the electron-light hole system is type II (Pan *et al.* 1988, Arnaud *et al.* 1992). This is extremely advantageous for the purpose of optical investigation of the 2DEG effects since only the electrons and heavy holes are confined in the well channel. As will be discussed in Section 4.2, the InGaAs PMDQW structures also have many other advantages over the GaAlAs/GaAs MDHJs from the device application point of view. We will concentrate on the InGaAs PMDQWs in the rest of this chapter.

A conclusive evidence of the 2DEG signature in modulated spectra was not reported until the publication of our work on the electroreflectance of a $Ga_{0.78}Al_{0.22}As/In_{0.21}Ga_{0.79}As/GaAs$ pseudomorphic modulation-doped quantum well (Yin Y. *et al.*, 1992a, 1992b, 1993). Dimoulas A. *et al.* have recently reported a phototransmittance study on $Ga_{0.68}Al_{0.32}As/In_{0.15}Ga_{0.85}As/GaAs$ PMDQWs and reached an interpretation of 2DEG effects based on a model consistent with ours (Dimoulas *et al.*

1993). Such progress has established that modulation spectroscopy is just as powerful a technique in studying and characterizing 2DEG in MDQWs as it is for any other microstructures.

The derivative nature of modulation spectroscopy makes it possible to observe the effects of the 2DEG on optical transitions in the spectra over a wide temperature range, even at elevated temperatures. A variety of properties of such 2DEG systems, such as Fermi level position, sheet charge density N_s, Fermi edge singularity, indium and aluminum composition, electric field distribution in the sample, well width, etc., can be accessed by modulation spectroscopy. Also, from the application point of view, the ability to detect Fermi level position at room temperature and above and the fact that experiments can be performed in contactless ways make modulation spectroscopy an extremely useful technique for the characterization of such 2DEG device structures.

In this chapter I present a detailed study of the pseudomorphic GaAlAs/InGaAs/GaAs PMDQWs, emphasizing the 2DEG effects. The GaAlAs/InGaAs/GaAs PMDQWs structure is discussed in Section 4.2. The ER, PR and CER work on several pseudomorphic $Ga_{1-y}Al_yAs/In_xGa_{1-x}As/GaAs$ MDQWs are presented in Section 4.3, including a preliminary investigation of the feature occurring at the Fermi wave vector. Conclusions and discussions are given in Section 4.5.

4.2 Pseudomorphic GaAlAs/InGaAs/GaAs MDQW Structures

Recent advances in the growth of stable strained layer GaAlAs/InGaAs/GaAs modulation-doped quantum wells have produced HEMT structures with peak carrier velocities exceeding those of GaAlAs/GaAs alone. In addition, these pseudomorphic structures (a) overcome the problem in GaAlAs/GaAs HEMTs due to the DX center in the GaAlAs (with Al mole fraction over 15%) and (b) make it possible to achieve a large conduction band discontinuity for a given Al composition (Morkoc and Unlu 1987, Schaff *et al.* 1990). Thus in the GaAlAs/InGaAs/GaAs system, large 2DEG carrier concentrations can be achieved while maintaining high electron mobilities, alleviating difficulties inherent in the GaAlAs/GaAs approach. These structures hold promise for device performance up to 400 GHz.

Typical pseudomorphic modulation-doped GaAlAs/InGaAs/GaAs quantum well structures can be either δ-doped or step-doped. Usually a contact layer of doped GaAs of ~ 100Å is grown on top of the structure. Immediately after the contact layer there is the wide-gape barrier GaAlAs layer of several hundred angstroms. Doping is usually achieved by uniformly doping the entire layer (step-doped) or by placing a planar doped sheet in the end near the InGaAs well channel. A spacer layer of undoped GaAlAs layer is placed between the doped GaAlAs layer and the undoped InGaAs channel. The other side of the InGaAs channel is bounded by the GaAs barrier. The undoped spacer layer is of great importance. It prevents the doping impurity from diffusing into the well to cause the unwanted scattering of the conduction electrons. Its thickness is a very

important device parameter. Too thick a spacer layer will degrade the charge transfer effects, whereas if it is too thin the electrons in the well will undergo scattering by the Coulomb field of the doping ions, which in turn will result in a reduced mobility. Typical spacer layer thickness is about 30 ~ 50 Å. At thermal equilibrium the electrons in the doped wide-gap GaAlAs portion is transferred into the coherent grown undoped well channel, forming a nearly ideal 2DEG in the InGaAs channel.

An additional advantage of the GaAlAs/InGaAs/GaAs PMDQWs is that these structures are best suitable for optical studies of the electronic properties of the two-dimensional electron gas systems as compared to the GaAlAs/GaAs MDHJs. The energies of the transitions carrying the signatures of the 2DEG are lower than that of the GaAs substrate, hence are clear from the complication of the substrate signal. This makes it possible to correctly identify and precisely analyze the properties of the 2DEG.

4.3. Modulation spectroscopy study of GaAlAs/InGaAs/GaAs PMDQWs

In this section we present the ER and PR study of several GaAlAs/InGaAs/GaAs MDQWs. The effects of the two-dimensional electron gas on the optical properties of several δ-doped or step-doped GaAlAs/InGaAs/GaAs pseudomorphic modulation-doped quantum wells have been observed in the modulation spectroscopy traces over a wide range of temperatures. The lineshapes of the features from the InGaAs channel where a high density two-dimensional electron gas is present can be accounted for on the basis of the first derivative of the 2DJDS multiplied by a Fermi level filling factor, i.e., the

FD2DJDS lineshape discussed in Section 4.4. The Fermi level position relative the conduction subbands can be obtained from a detailed lineshape fit, from which the sheet charge density, N_s, can be evaluated using Eq. (3.25).

4.3.1. Study of a δ-doped GaAlAs/InGaAs/GaAs PMDQW of 150Å well width

We have performed a detailed ER and PR study of a pseudomorphic $Al_{0.22}Ga_{0.78}As/In_{0.21}Ga_{0.79}As/GaAs$ modulation doped quantum well structure in the temperature range $79K<T<304K$ (Yin Y. *et al.* 1992a, 1992b). We have detected several features associated with the InGaAs MDQW portion of the sample, which exhibit an unusual modulation spectroscopy line shape. We have been able to account for these spectral features based on a two dimensional density of states, due to the screening of the excitons by the 2DEG (Huang D. *et al.* 1988a, Chemla *et al.* 1988a, 1988b, Liveseu *et al.* 1988) and a Fermi level filling factor. From the details of the lineshape fit to the InGaAs features we can extract the Fermi level position and hence the density of the 2DEG. By comparing the experimentally obtained energies of the InGaAs intersubband transitions with a theoretical model we can also obtain other important materials parameters such as the MDQW width (L_z), In composition and built-in electric field. The GaAlAs signal also yields the Al composition, and the FKOs above the GaAs and GaAlAs direct gap (E_0) give accurate measure of the electric fields that exist in their respective portions of sample.

The structure employed in this study was fabricated by MBE at TRW and is similar to profiles used for both low noise (Tan *et al.* 1990) and power applications (Streit *et al.* 1991) at 94 GHz. Grown on top of an undoped (001) GaAs substrate were 500 Å not-intentionally doped (NID) GaAs, 1000 Å $Al_{0.22}Ga_{0.78}As$, five periods of GaAs (50 Å)/$Al_{0.22}Ga_{0.78}As$ (100 Å) MQW, 3000 Å NID GaAs buffer, 150 Å $In_{0.21}Ga_{0.79}As$ 2DEG channel, 30 Å NID $Al_{0.22}Ga_{0.78}As$ spacer, a sheet planar Si doping (5×10^{12} cm^{-2}) layer, 500 Å NID $Al_{0.22}Ga_{0.78}As$, and finally 50 Å NID GaAs cap layer. Sheet electron densities of $N_s=2.3\times10^{12}cm^{-2}$ at 77 K and $N_s=2.5\times10^{12}cm^{-2}$ at 300 K were determined from Hall measurements assuming unity Hall coefficient. For the ER measurements the sample had a semitransparent ($\sim$50 Å) Au electrode on top of the GaAs cap and a thick Au electrode on the back surface.

Shown in Fig. 19 are the ER and PR spectra at 304 K. Three distinctive portions are well resolved in the energy domain. The features labeled A, B, and C below 1.4 eV are from the InGaAs MDQW. The structure between 1.40 and 1.45 eV is from the GaAs portion of the sample. The peaks at about 1.50 eV and 1.65 eV are from the GaAlAs cap layer (and possibly some contribution from the spin-orbit split peak of GaAs). We shall focus our attention on the InGaAs portion of the spectrum, which was related to the 2DEG channel. Note that in the PR spectrum the high energy side of peak A is more pronounced in relation to the ER trace.

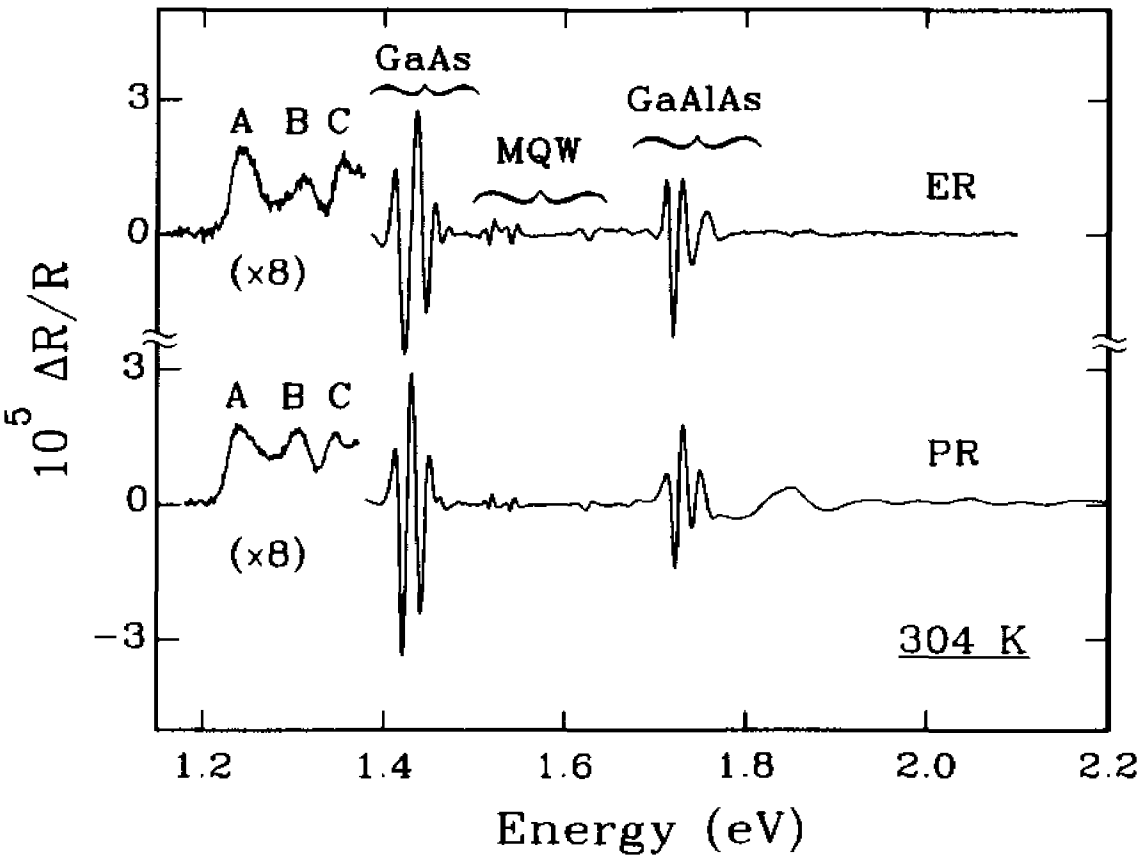

Fig. 19 ER and PR spectra from a $Al_{0.22}Ga_{0.78}As/In_{0.21}Ga_{0.79}As/GaAs$ pseudomorphic HEMT structure at 304 K.

Displayed by the solid lines in Fig. 20 are the A, B, and C features of the InGaAs PR spectrum at 304 K and the ER traces at 304, 238, 148, and 79 K. The lineshapes are unusual for modulation spectroscopy from a quantum well system. Such spectra generally exhibit sharp, derivative like features (i.e, positive and negative lobes) associated with excitons, even at 300 K (see, for example, Pollak 1991 and references therein). In addition, these lineshapes are symmetric (see Section 3.3.3.C). The traces of Fig. 20 lie on only one side of the baseline. Also, the peak A is asymmetric on the

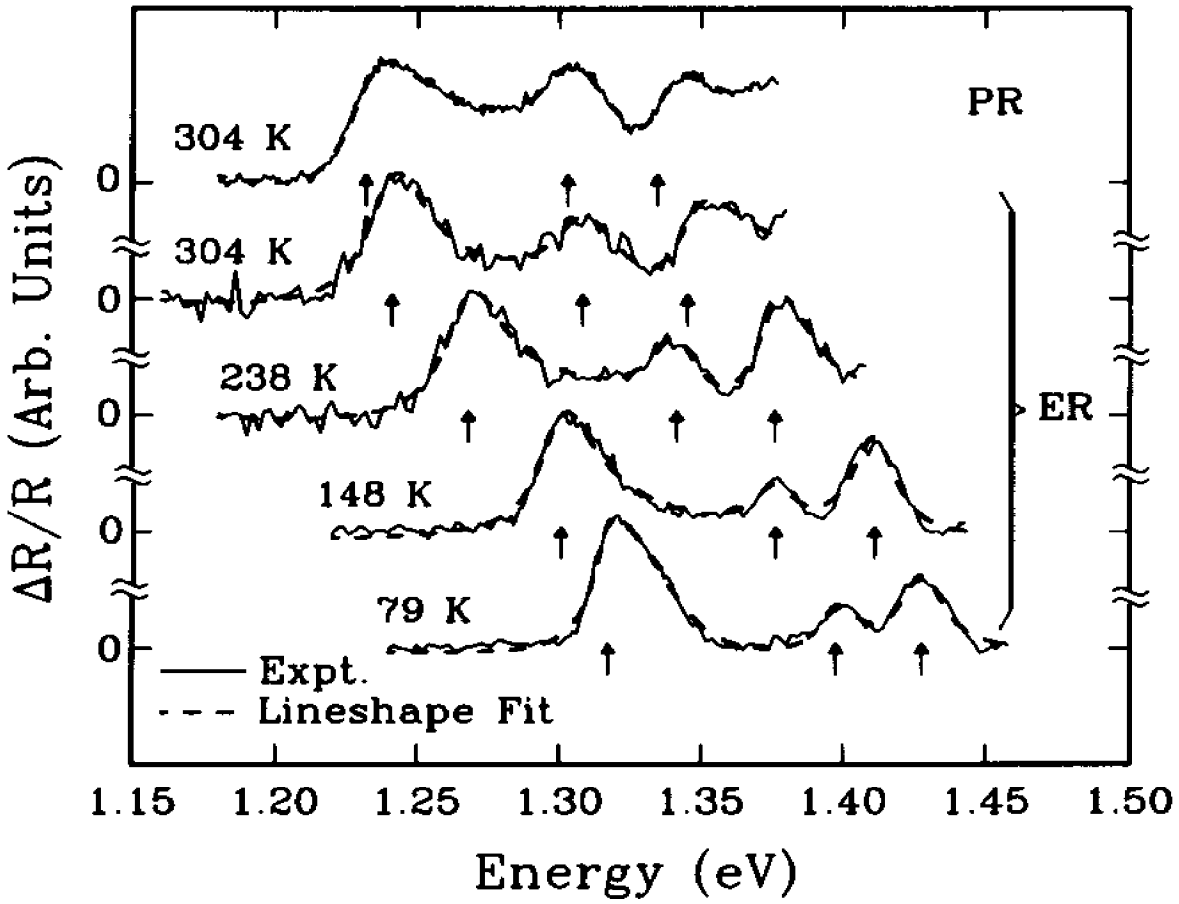

Fig. 20 Experimental PR (304 K) and ER (304, 238, 148, and 79 K) spectra below E_0(GaAs) from an InGaAs HEMT structure.

high energy side, an effect which becomes more pronounced as the temperature is increased. These characteristics are the manifestations of the FD2DJDS of the screened excitons including the Fermi level filling factor ($1-f_e$) discussed in Section 3.3.4. The excitonic features are quenched by the large density of electrons. We are probing directly the 2DJDS. The asymmetric property is due to the Fermi level filling factor. To the lowest order approximation, the modulation of the dielectric function can be considered predominantly due to the periodic Stark shift in the bound subband energy

levels caused by the modulating field F_{ac}, i.e., energy gap modulation [see Eq. (3.10)]. This assumption is justified by the good agreement between the results from the lineshape fits and those from Hall measurements and theoretical calculations.

The dashed lines in Fig. 20 are least squares fits to FD2DJDS lineshape with energy gap modulation. The obtained intersubband energies are indicated by arrows. The asymmetry of the feature A is due to the Fermi filling factor and makes it possible to determine E_F-E_A^c. We find E_F-E_A^c = +(5±2), -(6±3), -(10±5), and -(20±15) meV at 79, 148, 238, and 304 K, respectively. The error bars are larger at the higher temperatures because of the increased thermal broadening. The peaks B and C are relatively symmetric since E_B^c-E_F and E_C^c-E_F are larger than k_BT and hence relatively insensitive to the Fermi filling factor.

In order to identify the origins of the A, B, and C features, we have performed a self consistent Schodinger-Poisson theoretical calculation (see Section 2.1.4), including electric field effects, of the intersubband energies and intensities (wavefunction overlap) at 79 K (Ando *et al*, 1982, Stern 1986, Bastard G. 1988). We assumed midgap Fermi level pinning for the free surface of the GaAlAs and GaAs buffer/MQW interface (Shen *et al*, 1990b), a planar doping density of 5×10^{12} cm^{-2} from growth, an In composition of 21%, L_z=150 Å and a background doping level of 1×10^{14} cm^{-3}. Exchange terms were neglected because of the carrier concentrations involved ($N_s \approx 2.5\times10^{12}$ cm^{-2}) (Ando *et al.* 1982). Details of this calculation can be found in Qiang 1993.

Listed in Table I are the theoretical results as well as the experimental values. It can be seen that there is very good agreement between experiment and theory for both energies and intensities, if we identify the spectral features A, B, and C with transitions 21H, 32H, and 42H, respectively. Zone center ($k=0$) transitions which involve the first electron subband are not allowed since E_F lies far enough above this level. Also the asymmetric potential profile confines the ground state subband electrons and holes in spatially different regions, thus greatly reducing their transition oscillator strengths. We will show later that a weak signature of these transitions may still be found under suitable conditions. The overall agreement is very good.

Based on this calculation and the experimental results we can determine the position of E_F relative to the electron ground state of the system. We find from Table I a value of E_2^c-E_1^c=70 meV. Since E_F-E_2^c= +(5±2) meV at 79 K and -(20±15) meV at 304 K we conclude that E_F-E_1^c=(75±2) meV and (50±15) meV at these two temperatures.

The 2D density of electron states N_s can be obtained from Eq. (3.25) of Chapter 3. From the data above and Eq. (3.25) we find that $N_s=(2.2\pm0.2)\times10^{12}$ cm^{-2} at 79K and $(1.9\pm0.5)\times10^{12}$ cm^{-2} at 304 K, in good agreement with the Hall values (2.3×10^{12} cm^{-2} at 77 K and 2.5×10^{12} cm^{-2} at 300 K). The decrease in E_F as the temperature is increased is consistent with the temperature dependence of the Fermi energy in a 2D system (Ando *et al.* 1982).

Table I Various transition energies and the associated intensities (overlap integral) from a self-consistent calculation on a HEMT structure, as well as the experimental values at 79 K.

Transition	Energy (eV)		Intensity[a] (arb. unit)	
	Expt.	Calc.	Expt.	Calc.
11H		1.247[b]		0.11
12H		1.275[b]		0.24
13H		1.305[b]		0.32
21H	1.317 (A)	1.317	1.0	1.00
22H		1.345		0.09
23H		1.375		0.01
31H		1.377		0.21
32H	1.398 (B)	1.405	0.3	0.34
41H		1.406		0.06
42H	1.428 (C)	1.434	0.5	0.43

a. Intensities are normalized to the 11H transition.
b. Not allowed at $\mathbf{k}=\mathbf{0}$ due to the Fermi level position.

We now turn our attention to the PR data at 304 K in Fig. 20. From the line shape fit of the feature A (21H) we find that E_F-E_A^c=-(6±3) meV. Thus, the Fermi energy, and hence N_s, is larger than that of the corresponding ER measurement [-(20±15) meV]. This is evident from the enhanced high energy tail in the PR trace compared to the ER peak. This effect is due to the presence of photoexcited carriers created by the pump beam (Chemla *et al.* 1988a, 1988b, Liveseu *et al.* 1988). Note also that the energy positions of the A, B, and C features in the PR data are red shifted by about 10 meV from the corresponding ER peaks. This is consistent with the large N_s

which increases the electric field in the MDQW. The differences in the high energy component of the A structure (and also peak positions) between the PR and ER spectra can be reduced significantly by decreasing the pump light intensity by means of neutral density filters.

The GaAlAs feature in the PR spectrum of Fig. 19 exhibits pronounced Franz-Keldysh oscillations (FKO). These FKO are due to the large, almost uniform electric field in this portion of the sample caused by the difference in the Fermi level at the surface and in the Si δ-doping layer. From the FKO we find a field of 1.65 x 10^5 V/cm which is consistent with a midgap surface Fermi level (Shen *et al.* 1990). Also from the position of the GaAlAs peaks (1.746 eV) we can determine the Al composition to be 22% (Kuech *et al.* 1987).

To summarize we have performed a detailed ER and PR study of a GaAlAs/InGaAs/GaAs pseudomorphic modulation-doped quantum well structure. The features associated with the InGaAs PMDQW exhibit an unusual traces which can be accounted for on the basis of a two-dimensional density of states (screened excitons) and a Fermi level filling factor. From a detailed lineshape fit, particularly to the high energy side of the lowest lying feature at 79K, we have been able to deduce the Fermi energy and hence N_s. The latter is in good agreement with a Hall effect measurement. The general trends of E_F with temperature and light intensity are consistent with the properties of a 2DEG. Comparison of the obtained intersubband energies with a theoretical calculation also makes it possible to deduce other important parameters such as L_z, In composition and built-in field.

4.3.2. Study of three step-doped GaAlAs/InGaAs/GaAs PMDQWs of 100 Å well widths

We have also done a detailed PR study at 300K of three step-doped $Ga_{1-y}Al_yAs/In_xGa_{1-x}As/GaAs$ pseudomorphic MDQWs with nominal y=0.2, x=0.2 (samples #1 and #2) or x=0.16 (sample #3) and L_z=100 Å (Yin Y. *et al* 1993). The structures employed in this study were fabricated by MBE on undoped (001) GaAs substrates. On top of this was grown a buffer layer consisting of 4000 Å of NID GaAs, 300 Å of NID GaAlAs, 500 Å of NID GaAs, 100 Å of NID InGaAs which formed the MDQW, 20 Å of NID GaAlAs spacer, 200 Å and 125 Å of GaAlAs doped with Si at levels of 4.5 x 10^{18} cm^{-3} and 2 x 10^{17} cm^{-3}, respectively, and a 100 Å GaAs cap with 6 x 10^{18} cm^{-3} Si doping. From the growth conditions nominal values of y=0.2, x=0.2 (samples #1 and #2) or 0.16 (sample #3) and L_z = 100 Å were deduced. Sample #1 amd #2 were grown to the same target specifications but at different times. This structure is shown schematically in Fig. 21. Sheet electron densities at 77K and 300K were determined for the three samples from Hall measurements, with the n^+ -GaAs cap in place, assuming unity Hall coefficient. These values are listed in Table II. There was some variation in N_s among the three materials, as will be discussed below. The PR measurements were made at room temperature. The pump beam was the 6328 Å line of a HeNe laser chopped at 200 Hz. The pump beam power density on the sample was 1000 $\mu W/cm^2$.

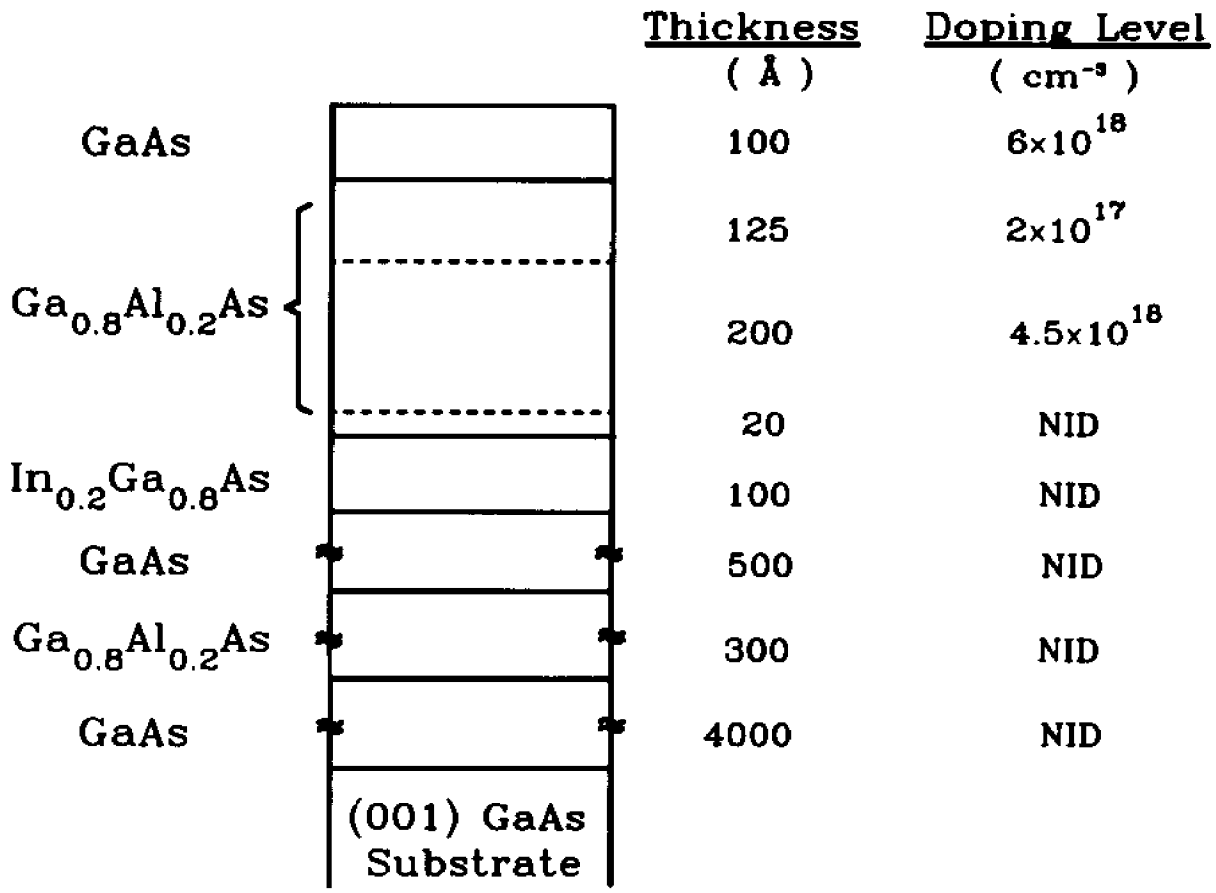

Fig. 21. Schematic representation of the step-doped GaAsAs/InGaAs/GaAs PMDQW structures used in the experiments of Section 4.3.2 and 4.3.3.

Table II. Experimental values of the sheet density, N_s, and mobility at 300 K and 77 K for the three step-doped GaAlAs/InGaAs/GaAs PMDQWs.

Sample	300 K		77 K	
	N_s (10^{12} cm^{-2})	Mobility (cm^{2}s^{-1}V^{-1})	N_s (10^{12} cm^{-2})	Mobility (cm^{2}s^{-1}V^{-1})
#1	1.60 ± 0.1	5580	1.90 ± 0.1	19000
#2	1.77 ± 0.1	4490	2.00 ± 0.1	13600
#3	1.68 ± 0.1	4680	1.75 ± 0.1	18400

Shown in Fig. 22 by the solid lines are the PR spectra at 300K of samples #1,#2 and #3. The features below 1.4 eV are from the InGaAs MDQW. Also indicated are the optical signals arising from the GaAs and GaAlAs portions of the samples. We shall first focus our attention on the InGaAs region of the spectra and return to the other traces later.

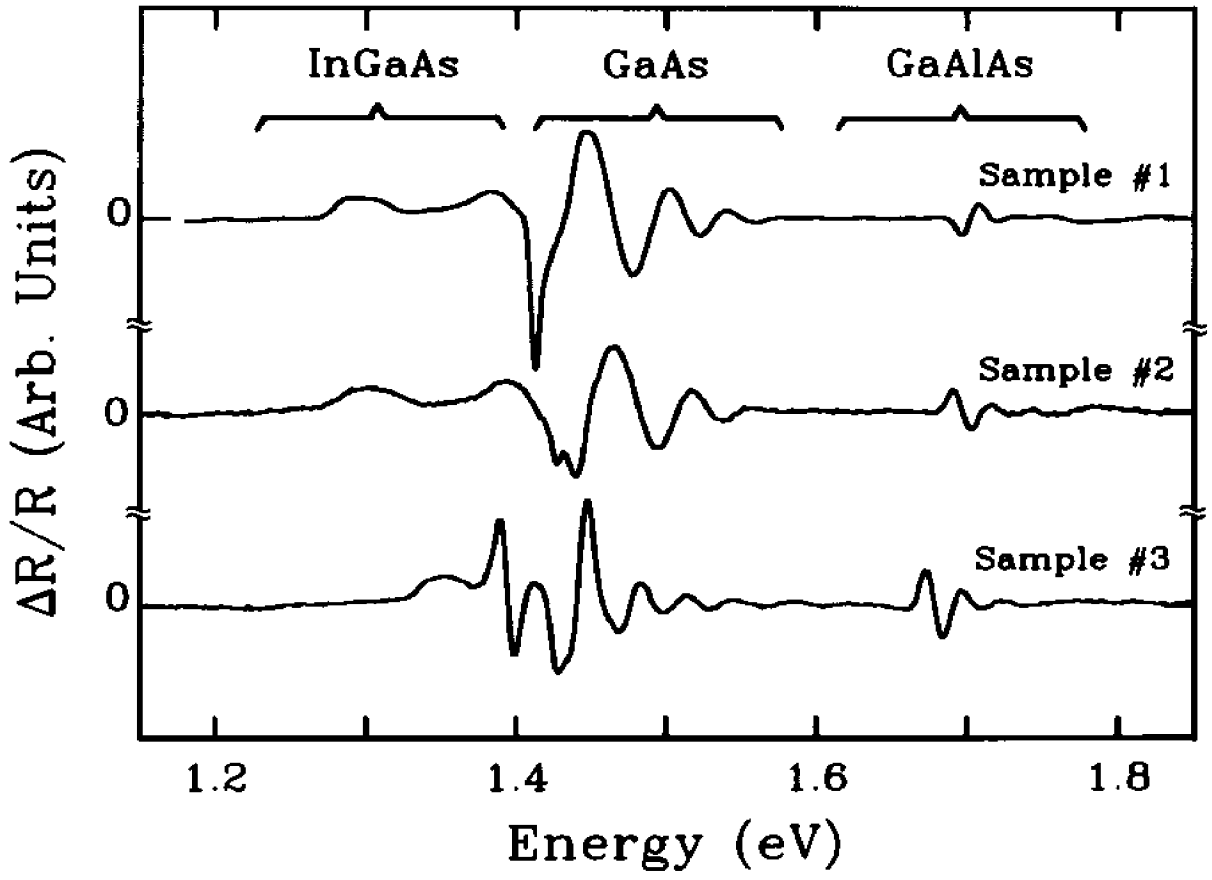

Fig. 22. Room temperature PR spectra of InGaAs MDQW structure sample #1, #2 and #3.

Displayed by the solid lines in Fig. 23 are PR spectra originating in the InGaAs MDQW section of the samples. The dashed lines are least-squares fits to the FD2DJDS

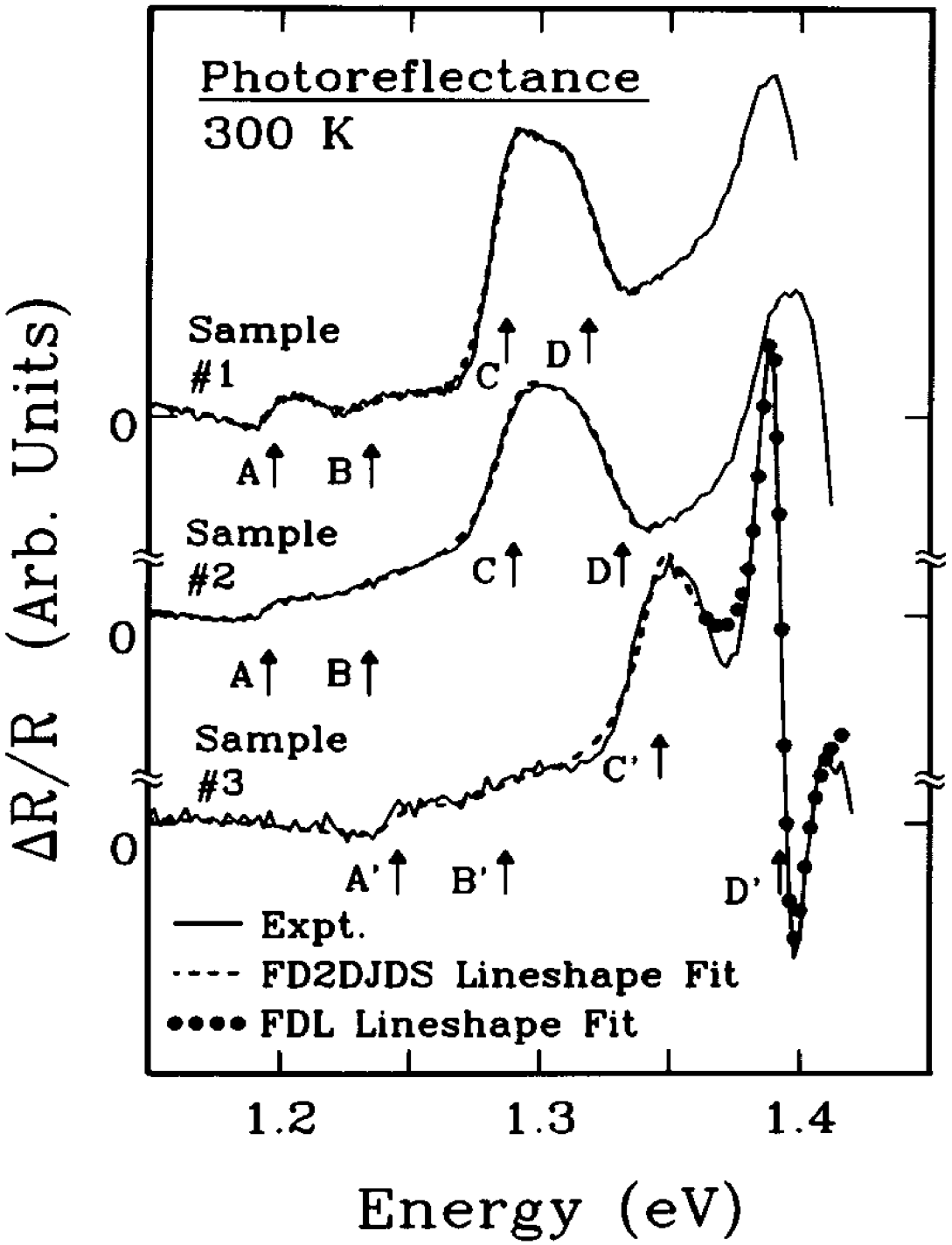

Fig. 23. Solid lines are the experimental PR spectra from the InGaAs MDQW region of the samples. The dashed and dotted lines are least squares fits to appropriate lineshape functions (see text).

lineshape. The obtained intersubband transition energies, $E_{g,j}$ for j=A,B,C and D (except for sample #3 with j = A', B' and C') are indicated by arrows and also are listed in Table III. The sharp, high energy "S" shaped structure of sample #3 (labelled D') has been fit with FDLL function (dotted line). The obtained intersubband energy also is indicated by an arrow and is presented in Table III.

As we shall demonstrate below these features for samples #1 and #2 correspond to mnH = 11H (j=A), 12H(j=B), 21H(j=C) and 22H(j=D). The situation for sample #3 is more complex. The background on which these resonances are superimposed is due to the Fermi filling factor, $(1-f_c^j)$. The fit to this background makes it possible to evaluate $E_F-E_A^c$ = 62 meV, 71 meV and 56 meV for samples #1, #2 and #3, respectively.

We have performed theoretical calculations using the self-consistent Schrödinger-Poisson method for these structures. The results are listed in Table III. For all calculations we used a well width L_z = 100Å taken from the growth condition and a background doping level of 1 x 10^{14} cm^{-3} for the NID region. The other parameters, i.e., x and y, are indicated in Table III. The In composition was taken to be the intended growth value while the Al content was deduced from the energy position of the GaAlAs peak (see Fig. 22). The $In_xGa_{1-x}As$ band gap and InGaAs/GaAs band offset were taken from Pan *et al* 1988, the out-plane masses from Zhan *et al* 1991, the deformation potentials were a linear interpolation between those of GaAs and InAs (Pollak 1990).

For samples #1 and #2 the overall agreement is very good if we identify feature A with 11H, etc. For sample #3 the feature A′ and C′ can be correlated with 11H and 21H, respectively. We shall return to the question of the nature of B′ and D′ below.

Also based on this calculation we can determine the position of E_F relative to the electron ground state (m=1) of the system. Since m=1 for the feature A, we can

Table III Experimental and theoretical values of various intersubband transition energies from the InGaAs MDQW region of three $Al_yGa_{1-y}As/In_xGa_{1-x}As/GaAs$ HEMTs.

Sample	Intersubband Characteristics				$N_s(10^{12}$ cm$^{-2})$	
	Spec-tral Feature	Expt. (eV)	Theory (eV)	Transition	PR Expt.	Hall Measure-ment
1	A	1.198	1.203[a]	11H[a]	1.90±0.20[a]	1.90±0.1[e]
	B	1.235	1.238[a]	12H[a]		1.60±0.1[f]
	C	1.287	1.307[a]	21H[a]		
	D	1.319	1.341[a]	22H[a]		
2	A	1.196	1.204[b]	11H[b]	2.15±0.25[b]	2.00±0.1[e]
	B	1.234	1.239[b]	12H[b]		1.77±0.1[f]
	C	1.292	1.307[b]	21H[b]		
	D	1.332	1.342[b]	22H[b]		
3	A'	1.246	1.246[c]	11H[c]	1.85±0.20[c]	1.75±0.1[e]
	B'	1.287	------	(12H)[c,d]		1.68±0.1[f]
	C'	1.346	1.341[c]	21H[c]		
	D'	1.393	------	(22H)[c,d]		

a. y=0.195, x=0.2.
b. y=0.185, x=0.2.
c. y=0.175, x=0.16.
d. The 2H valence level is unbound.
e. 77K.
f. 300K.

determine that E_F-E_A^c=E_F-E_1^c. Hence, from the above mentioned fitted results we conclude that E_F-E_1^c= +62 meV, +71 meV and +56 meV for samples #1, #2 and #3, respectively. The quantity E_2^c-E_1^c($\approx$ 100 meV) can be obtained from the separation between 21H and 11H(see Table III). Thus the Fermi level lies between the m=1 and m=2 conduction subbands.

From Eq. (3.25) and the values of E_F and E_m^c discussed above we have calculated the numbers for N_s for the three samples listed in Table III. Values for Γ_m were taken from the lineshape fits in Fig. 23. There is very good agreement between the PR analysis of N_s and the 77K Hall measurements, which also are displayed in Table III. For completeness we also list in Table III the N_s values from the 300K Hall determinations.

We now return to the question of sample #3. Because of the lower In content of this sample in relation to the other two materials the 2H valence level becomes unbound and hence m2H transitions should be very weak in a one electron picture. However, experimentally we still see in Fig. 23 evidence for the contribution of 12H (feature B') and a very strong resonance (D') which appears to correspond to 22H. The fact that the D' structure has a lineshape of FDLL strongly suggests that its origin is an unscreened exciton. Clearly further work needs to be done with regard to this peak.

Both the GaAs and GaAlAs features in the PR spectra of Fig. 22 exhibit pronounced FKOs. The electric fields (in units of 10^4 V/cm) deduced from the GaAs FKOs are 4.7, 5.3 and 3.1 while from the GaAlAs FKOs we find 1.6, 1.8 and 1.8 for samples #1,#2 and #3, respectively.

Also from the position of the GaAlAs peaks of 1.695 eV, 1.689 eV and 1.672 eV (see Fig. 22) we can evaluate the Al compositions (Kuech *et al*, 1987) to be 19%,18.5% and 17.5% for samples #1,#2, and #3 , respectively. These values are in reasonably good agreement with the intended numbers.

From the self-consistent Schrödinger-Poisson calculation we also can determine the built-in electric fields in the GaAs and GaAlAs portions of the sample. Based on midgap Fermi level pinning at the 500Å NID GaAs/300Å NID GaAlAs interface we determine a field of about 7.6 x 10^4 V/cm in the 500Å GaAs region. This is somewhat larger than the fields deduced from the FKOs. This observation suggests that the pinning level is less than midgap and is about 0.30-0.35 eV below the conduction band.

The FKOs associated with the GaAlAs signal originate in the 300Å NID GaAlAs portion next to the 4000 Å NID GaAs buffer. If we assume that the Fermi level at the 300 Å NID GaAlAs/ 4000 Å NID GaAs buffer interface is not pinned near midgap but is about 0.30-0.35 eV above the valence band, a uniform field of approximately 2 x 10^4 V/cm will be present in this region of the sample. This number is close to our

experimental values. The GaAlAs layers above the InGaAs channel are all fairly heavily doped and the field in this space charge region is about 2 x 10^5 V/cm, about an order of magnitude larger than our experimental values. The FKOs from this region are probably not observable because of the high doping levels (H. Shen and F. Pollak 1990).

The 11H and 12H ($\mathbf{k}=\mathbf{0}$) transitions can be observed at room temperature in the PR spectra (see Fig. 23) from the 100Å wide PMDQWs even when the Fermi level is some 60 meV above the m=1 ground state conduction electron subband. In contrast, these transitions are not seen in the ER or PR spectra from the 150Å wide PMDQW structure studied in Section 4.5.1, although the Fermi position relative the ground state conduction subband is about the same. This phenomenon can be understood as follows. The well width plays a very important role. In the latter case where the well is 150Å wide, the electrons and holes are spatially pulled away from each other by the electric field, enough to make the transition matrix element (overlap integral of the ground state electron subband wave function and n=1 heavy hole subband level wave function) significantly smaller. The already small oscillator strength is further attenuated by the Fermi level filling function. Thus the 11H and 12H signals are effectively wiped out. The relatively small 100Å well width in the former case, on the other hand, keeps confined electrons and heavy holes in the same spatial region. Although the electric filed does cause a reduction of their wave function overlap, it is not enough to diminish it completely since they are located within the 100Å thick layer. Therefore when the thermal broadening of the Fermi distribution function is enough to reach the m=1

electron subband edge, the 11H transition will still survive. As we will see in the following section, the 11H transition will be wiped out when temperature is lowered.

4.3.3. Transitions occurring at the Fermi edge

One of the most important issues of fundamental interests about the two-dimensional electron gas is the many-body correlation (see, for example, Ruckenstein and Schmitt-Rink 1987, Hawrylak 1990, 1991, Mueller *et al.* 1991). Such many-electron - one-hole interactions in the presence of the Fermi sea was initially considered by Mahan for bulk semiconductors in the framework of the final-state electron-hole scattering (Mahan 1967a). He showed that in spite of the static screening by the equilibrium electrons, an exciton-like effect still survives at moderate electron densities and there is a bound state slightly below the Fermi level (recently called Mahan exciton). This bound state results from the sharpness of the Fermi surface and the Pauli exclusion principle's restriction on the electron's scattering. Later theories included the dynamic response of the Fermi sea to the creation of the photohole, as well as the exchange effect due to the increased carrier density to show how the bound state eventually becomes unbound and merges with continuum (Mahan 1967b, Nozieres and De Dominicis 1969). In optical absorption, a divergence of the optical oscillator strength appears at the threshold energy (the Fermi level) giving rise to the term Fermi-edge singularity (FES), which persists into the high density limit and follows a power-law divergence (Mahan 1967b, Nozieres and De Dominicis 1969). It is a many-electron excitonic feature actually composed of two compensating processes, the scattering of electrons by the hole (vertex corrections)

and the strong renormalization of the hole (self-energy effects). For the 2DEG in a modulation-doped quantum well, the reduced dimensionality diminishes the efficiency of the long-range Coulomb screening as compared to the 3D case (Chemla 1988a), which suggests that this type of phenomena will persist above the 3D limit and will be easier to detect.

The FES feature has been observed in luminescence spectra from an InGaAs/InP modulation doped quantum well (Skolnick *et al.* 1987a, 1987c, 1987b), absorption spectra (see, for example, Lee *et al.* 1987, Huang D. 1987, Livescu *et al.* 1988), and photoluminescence excitation spectra (see, for example, Delalande *et al.* 1986, 1987). However, no observation of optical transitions of any nature occuring near the Fermi edge has been reported in modulation spectroscopy. As a derivative method, modulation spectroscopy has higher sensitivity than any of the previously mentioned experiments. Its experiments can also be performed in a contactless manner, and over a wide temperature range. All these advantages make modulation spectroscopy an extremely valuable tool in the optical investigations of the Fermi edge. As we will see in the following we indeed observed a feature in CER spectra that is due to the vertical transitions occurring at the Fermi edge. Although it is not the FES feature, it is the first observation of an optical feature occurring at the Fermi edge using modulation spectroscopy method and it does carry rich information about the many-body effects of a 2D interacting electron gas(Gumbs *et al.* 1993).

In this section we present a CER study of a 100 Å pseudomorphic GaAlAs/InGaAs/GaAs PMDQW structure (sample #1 in Section 4.3.2) as a function of temperature ($17K < T < 351K$). Contactless electroreflectance has the advantage over ER in that it requires no contact on sample, thus the original conditions of the sample are maintained. It also has an advantage over PR since it does not have the pump beam related problems, such as photo-excited carriers, and luminescence background (Yin X. and F. H. Pollak 1991). Because of the derivative-like nature of this method we have been able to observe a feature occurring at the Fermi edge ($k=k_F$) at temperatures as high as 152 K (down to 17K). Above 152 K the trace from the InGaAs portion of the sample can be accounted for on the basis of one electron theory, i.e., the derivative of a broadened step-like two-dimensional density of states (screened exciton) times a Fermi level filling factor, which is the FD2DJDS discussed in Section 4.3 and successfully applied in the previous investigation of 2DEG systems in this chapter. A detailed FD2DJDS lineshape fit makes it possible to (a) evaluate the Fermi energy, E_F (even at elevated temperatures) and hence the 2DEG density, N_s and (b) several intersubband transition energies. By comparing these experimental energies with a theoretical self-consistent Schrödinger-Poisson calculation we also can evaluate other important parameters of the PMDQW such as built-in field, well width and In composition. The values of N_s obtained from the CER are in good agreement with a Hall effect measurement (see Section 4.3.2).

The CER apparatus is described in literature (Yin X. and Pollak, 1991, also see Section 3.2). The modulation voltage used in the measurement was 200 Hz 180 Vrms sine wave. The results are shown in Fig. 24.

Shown by the solid lines in the figure are the CER spectra at 351K, 300K, 152K, 80K and 17K, respectively. For convenience we have taken the zero of energy to be 21H, since the energies of the transitions change considerably with temperature. Above about 150K the lineshape which consists of peaks riding on a background, can be fit by a FD2DJDS lineshape (Dashed line for 351K). The peaks are due to $\mathbf{k}=\mathbf{0}$ two-dimensional density of states intersubband transitions (mnH), while the background is related to the Fermi level filling factor. The obtained mnH energies are denoted by arrows. The identification of the various transitions was determined by comparison with a self-consistent theoretical Schrödinger-Poisson calculation.

For the doping level used in this sample E_F lies between the first and second conduction states. At elevated temperatures transitions (at $k = 0$) to the first conduction level, i.e., 11H and 12H are only seen because of the significant thermal broadening of the Fermi distribution. Note that as the temperature is lowered (a) the 11H and 12H resonances are no longer observed, (b) transitions to the second electron state, i.e., 21H and 22H, are still prominent, and evolve to very narrow and sharp peaks below 80K, (c) the background is reduced and (d) at 152 K and lower temperatures, a new feature, labeled as 12H* in the figure, is seen above 22H. It is also seen to have very little

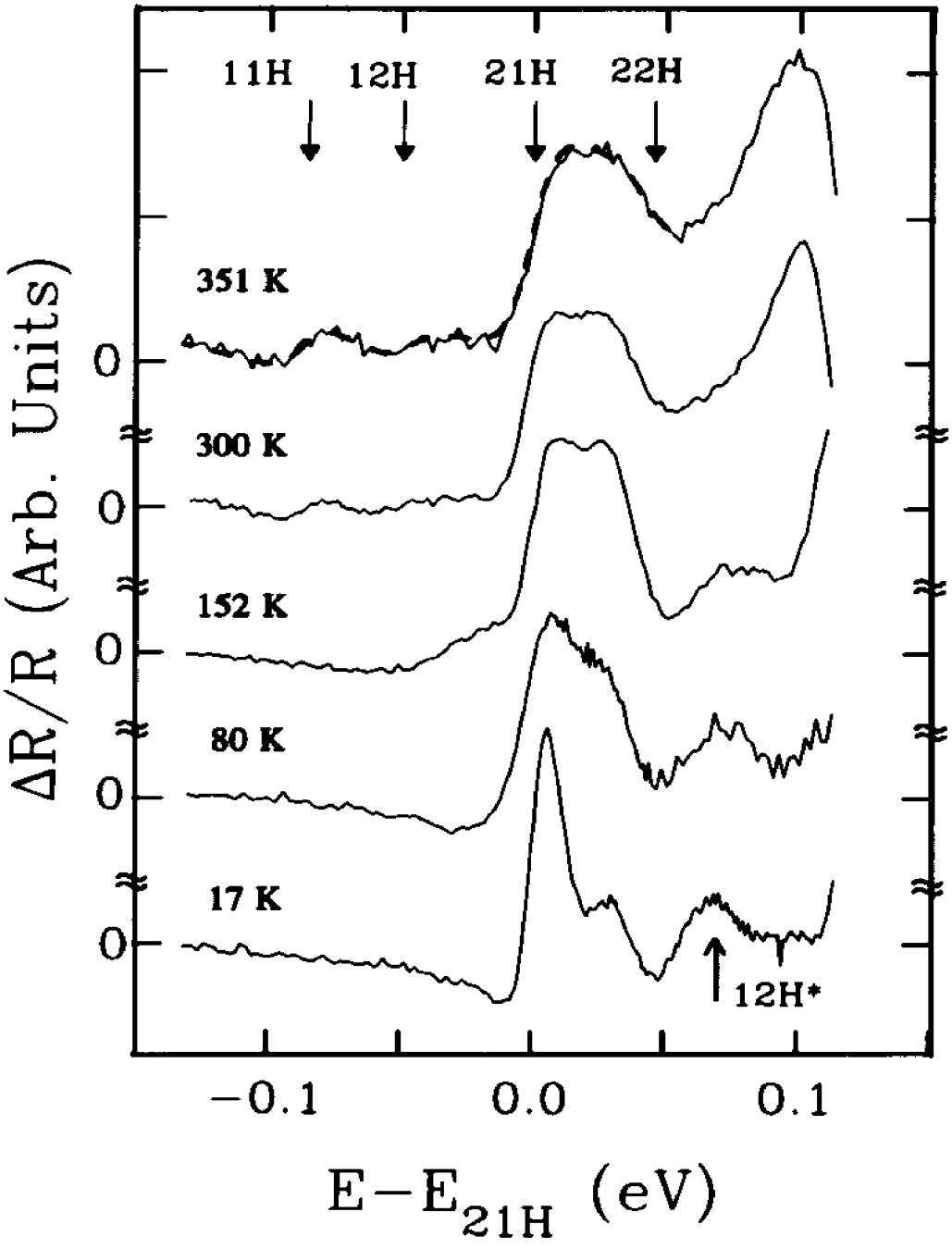

Fig. 24. Contactless electroreflectance spectra from a 100Å wide PMDQW at 351K, 300K, 152K, 80K and 17K. The energy has been normalized relative to that of 21H transition.

temperature dependence in this temperature range in relation to 21H and 22H ($\mathbf{k}=0$) transitions.

The first three observations (a)-(c) can be understood on the basis of one-electron picture and the Fermi-Dirac statistics. As the temperature decreases, the thermal broadening of the Fermi distribution function is narrowed. For example, at 100K the thermal energy is only 8.5 meV. Since the $m=1$ ground state electron subband lies about 60 meV below the Fermi level, the probability for the subband edge states to participate in a direct absorption of a photon is practically zero. The transitions involving $m=1$ subband edge ($\mathbf{k}=0$) are therefore prohibited. This explains (a). The $m=2$ electron subband lies some 30 meV above the Fermi level. At lower temperatures the tail of the Fermi distribution function will not be able to reach it. The band filling effects now will not affect the $m=2$ electron subband. There is evidence that the direct screening effect of the 2DEG is also weaker for the higher lying levels (see, for example, Huang D. *et al.*, 1988a). Therefore it is possible for transitions involving the $m=2$ subband to recover their excitonic character to some extent at low enough temperatures. That is why we have observation (b).

Observation (c) can be understood as follows. In the FD2DJDS lineshape function implied is a feature associated with the first derivative of the Femri level filling function ($1-f_e$) (see Section 3.3.4), which is due to the transitions at $\boldsymbol{k}=\boldsymbol{k}_F$. The width of this feature is linearly dependent on temperature (to be discussed in more detail later).

It appears as a background at higher temperatures (e.g. 300K and above) since the thermal broadening is very large. At low temperatures the thermal broadening of $(1-f_e)$ is small and this feature should become a well resolved peak. This prediction is only partially correct: We indeed observe a peak 12H* (see Fig. 24) at low temperatures [observation (d)], but its lineshape and temperature dependence at low temperatures can not be accounted for in terms of our FD2DJDS based on the one-particle model.

We now consider the 12H* feature in greater detail. The position of the 12H* peak is at 12H ($\mathbf{k}=\mathbf{0}$) energy plus the Moss-Burstein shift. If we associate this feature with the transition at the Fermi edge, i.e. the $\mathbf{k}=\mathbf{k}_f$ transition from the n=2 heavy hole subband to the m=1 electron subband in the one-electron picture, its higher temperature behavior can be understood. It appears as a background around room temperature (see Fig. 24). When temperature is lowered to $\sim$150K, it becomes a well defined feature. The temperature dependence of the linewidth of the 12H* peak is smaller than those of 21H and 22H, which sharpen considerably between 152 and 17K. These characteristics, which the one-electron model fails to account for, can only be understood in terms of the many-body correlation effects of the 2DEG. At low temperatures the edge of the Fermi sea is very sharp. The 2DEG is in its degenerate quantum mechanical limit. Many-body interactions are now becoming important and will exhibit their effects on the optical transitions - the Fermi edge singularity. It is a phenomenon of one-hole many-electron correlation in the presence of the Fermi sea of electrons (see, for example, S. Schmitt-Rink *et al.* 1983, Livescu *et al* 1988, Chen W. *et al* 1992). Because the derivative-like

nature of the modulation spectroscopy, we can observe the 12H* feature occurring at the Fermi edgy greatly influenced by the many-body effects at a temperature as high as 152 K. Notice that at this temperature, the thermal broadening of the Fermi distribution function is too large to produce a feature that well defined. It is the many-body effects enhancement that helps to sharpen it up. Also at very low temperatures the width of the 12H* feature is significantly greater than the thermal energy and its lineshape and broadening have very little temperature dependence below 80K in relation to the 21H and 22H transitions. This is because that the 12H* feature originates predominately from many-body correlation enhanced transitions at the Fermi edge at these temperatures. Its broadening is not governed by the electron-phonon interactions as in the case for 21H and 22H (see Section 2.3).

In principle we should also see a peak for the 11H*. Because the position of 11H* and that of the strong features 21H and 22H are almost degenerate, the 11H* peak is not clearly resolved.

Both theoretical and experimental efforts are now underway to understand the strong many-body effects on 12H* feature (Gumbs *et al.* 1993). A first-principle theorectical calculation has shown that many-body effects are a factor at all temperatures although they are most pronounced for $T \leq 152$ K (Gumbs *et al.* 1993). Efforts are also directed to the development of an appropriate derivative lineshape for the features occurring at the Fermi edge. The detailed lineshape analysis of this Fermi edge feature

should allow us to extract a lot of information, such as the position of E_F and the many-body correlation effects at low temperatures. These investigations are very important for the understanding of the fundamental properties of 2DEG.

4.4. Conclusions

We have investigated the two-dimensional electron gas effects in a number of GaAlAs/InGaAs/GaAs modulation-doped quantum well structures with modulation spectroscopy. We have, for the first time, positively identified the 2DEG signature in modulation spectroscopic traces from GaAlAs/InGaAs/GaAs PMDQW structures and proposed the proper lineshape. The great utility of modulation spectroscopy has also allowed us to study the 2DEG effects over a wide temperature range.

Transitions occurring at the Fermi edge have been observed in an 100Å-wide well width sample at temperatures up to 152 K. At higher temperatures it evolves into a broad background. The Fermi edge peak in modulation spectroscopy has less temperature dependence than the $\mathbf{k}=\mathbf{0}$ intersubband transitions over the same temperature range. This is due to the strong many-body effects on this feature. The Fermi edge feature can not be fitted by the FD2DJDS lineshape based on one-electron model. The proper lineshpae function is the subject of current research.

Chapter 5. PHOTOREFLECTANCE STUDY OF STRAINED (001) $Si_{1-x}Ge_x$/Si LAYERS

Using photoreflectance, which yields a third-derivative spectroscopy in bulk material, we have measured the Ge composition dependence of the E_1 and "E_0'" (will be defined later in this section) transition energies at 300K in a series of strained $Si_{1-x}Ge_x$/Si layers ($0 < x < 0.23$). Auger profiling was employed for an accurate evaluation of x in the near-surface region corresponding to the penetration depth of the light (about 100 Å). In our strained samples the energy of the E_1 peak is essentially the same as in unstrained material, in agreement with deformation potential theory. The "E_0'" feature, which exhibits only a very weak variation with Ge content, may also contain a strain-shifted $E_1+\Delta_1$ component. The PR work will be compared with a recent spectral ellipsometry study on similar samples in which third-derivative spectra were obtained by numerical differentiation. Our results have enriched the understanding of the properties of Si-rich strained thin SiGe alloy films grown on silicon substrate.

5.1. Introduction

Thin layers of $Si_{1-x}Ge_x$ deposited on silicon substrates are of considerable interest for the fabrication of advanced electronic devices (see, for example, Pearsall 1989b) such as heterojunction bipolar transistors, modulation doped field effect transistors and internal photoemission heterojunctions. In order to aid in the development of these structures and devices it is important to have convenient and non-destructive techniques to characterize important parameters such as alloy composition and material quality. Optical methods

such as photoreflectance (Pollak and Shen 1989a, 1989b), spectral ellipsometry (Humlicek *et al.* 1989, Raccanelli *et al.* 1992; Ferrieu *et al.* 1992, Pickering *et al.* 1993) and Raman scattering (Chang *et al.* 1988) are well suited for this purpose.

In this chapter we describe a PR study of a number of thin strained layers of (001) $Si_{1-x}Ge_x/Si$ ($0 \leq x \leq 0.23$). We have observed the Ge composition dependence of the E_1 and "E_0'" optical features (Kline *et al.* 1968, Humlicek *et al.* 1989; Ferrieu *et al.* 1992, Pickering *et al.* 1993) which appear in the photon energy range 2.6−3.6 eV. In this spectral region the penetration depth of the light is only about 100 Å so that these measurements are very sensitive to the near-surface composition and quality of the samples. The germanium content was evaluated by high resolution x-ray diffraction (HRXRD) and Auger profilometry (AP). In our strained samples the energy of E_1 is essentially the same as in unstrained material (Kline *et al.* 1968, Humlicek *et al.* 1989, Pickering *et al.* 1993), in agreement with deformation potential theory (Pollak 1990, Pickering *et al.* 1993). A parallel study on the same set of samples using spectral ellipsometry also has been performed by the CNET-Meylan group (Ferrieu *et al.* 1992). In this work the third derivative of the complex dielectric function ϵ was obtained by numerical means. Our results will be compared with this investigation.

5.2. Experimental details

The $Si_{1-x}Ge_x$ layers were grown epitaxially on (001) Czochralski silicon wafers by rapid thermal chemical vapor deposition (RTCVD) at 800 °C (Dutartre *et al.* 1991).

Table IV lists some characteristics of the samples. Columns 1 and 5 give the nominal composition and the thickness of the layers. It should be noted that the latter do not exceed the critical values known for each x (Pearsall 1989b). The lattice constant in the orientation perpendicular to the layers was directly determined form HRXRD patterns, in the samples with values of near 0.15, in order to calibrate directly the film composition. The $x=0.15$ samples served as a reference for determining the absolute Ge content profile in the film, from the ratio of intensities of the LMM(Ge) and KLL(Si) Auger lines. The Auger profile and the direct measurements of the milled crater depths were used for determining the actual thickness of the films.

The PR measurements were taken in the photon energy range $2.6-3.6$ eV using an apparatus that has been described in the section 2.1 of chapter 3 (Pollak and Shen 1989a, 1989b). The pump beam was the 633-nm line of a 3 mW HeNe laser chopped at about 200 Hz.

5.3. Experimental results

Shown in Figs. 25(a) and 25(b) are the Auger profile of two samples of nominal composition/thickness of 0.15/800Å and 0.17/400Å, respectively. We are interested in establishing the mean Ge content within about 100Å from the surface, i.e., the penetration depth of light. Both Auger profiles show a well-marked plateau up to a depth of about 600Å and 350Å, respectively. Similar results were obtained for layers thicker than about 200Å (corresponding to $x=0.2$), thus yielding the composition profile. For

Table IV. Characteristics of the $Si_{1-x}Ge_x/Si$ samples used in this study. Also listed are the energies and broadening parameters of the E_1 and "E_0'" features from the fit to the PR data.

Sample	Ge Composition			Film Thickness (Å)	E_0'/Γ (eV)	E_1/Γ (eV)
	Nominal	Auger Profiling Near Surface/Interface	HRXRD			
1	0	0 / 0		na	3.320/0.07	3.406/0.14
2	0.035	0.035/0.035		1200	3.333/0.09	3.387/0.15
3	0.035	0.035/0.035		1200	3.328/0.08	3.382/0.13
4	0.065	0.065/0.065	0.069	1200	3.308/0.14	3.341/0.15
5	0.065	0.065/0.065		3100	3.312/0.10	3.359/0.12
6	0.095	0.095/0.095		1200	3.304/0.15	3.232/0.13
7	0.12	0.120/0.120	0.123	2900	3.319/0.15	3.205/0.12
8	0.15		0.147	2400	3.290/0.15	3.156/0.12
9	0.15		0.156	1600	3.292/0.12	3.150/0.13
10	0.15	0.157/0.143	0.155	800	3.302/0.15	3.154/0.11
11	0.17	0.199/0.167	0.168	400	3.261/0.17	3.078/0.13
12	0.20	0.225/0.150	0.188	200	3.289/0.17	2.999/0.14

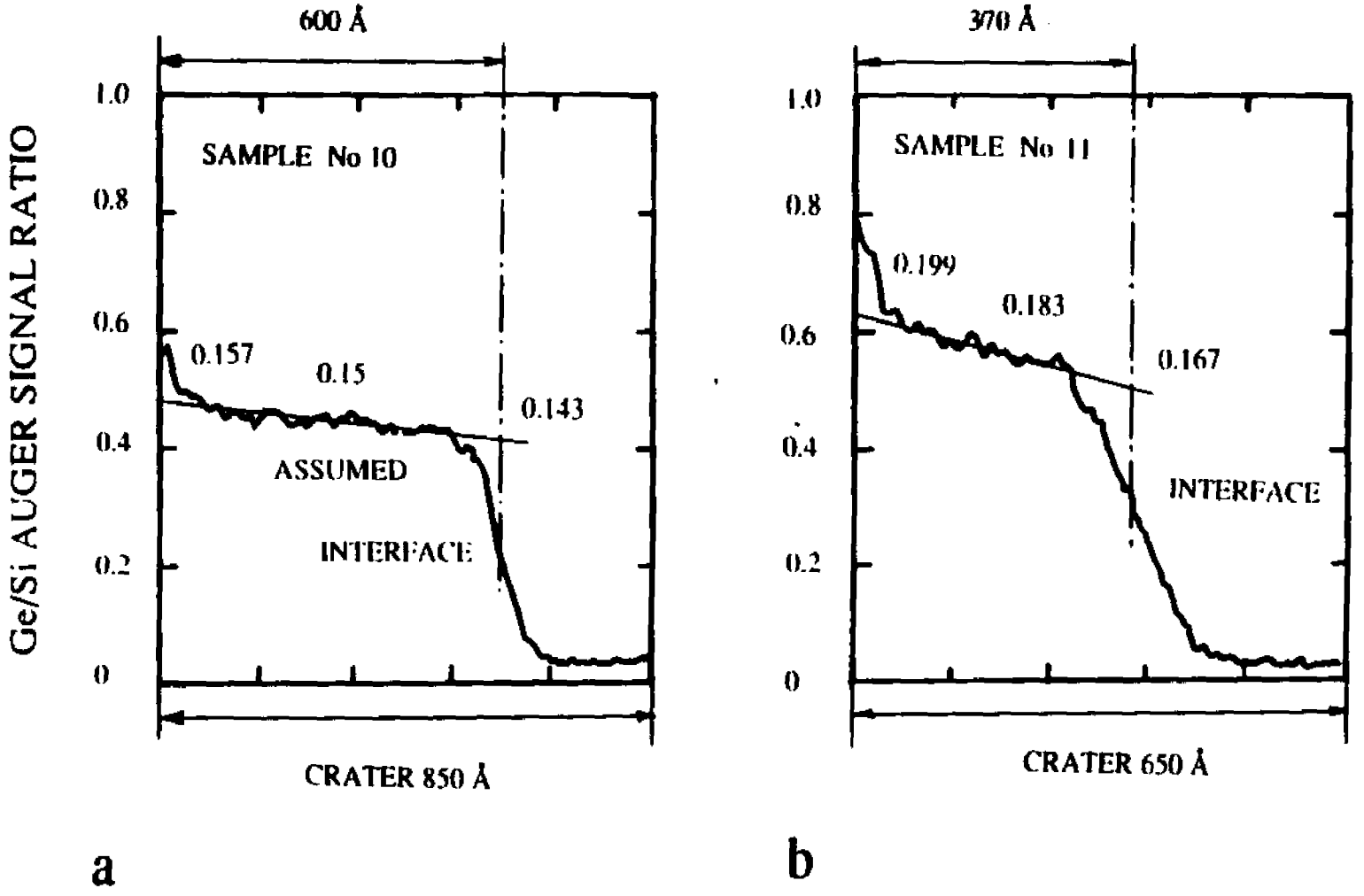

Fig. 25. Auger profile of samples #10 and #11 in Table IV.

thinner samples the Auger profile could not be interpreted in terms of the composition. For the sample of Fig. 25(a) the mean value of x, taken over the entire film thickness, was equated to that measured by HRXRD, i.e., $x=0.15$. From this and Fig. 25(a) we deduce a value of $x=0.157$ in the 100 Å near-surface region. For the material of Fig. 25(b) this procedure yielded $x=0.199$ in the relevant region. Subsequently, the mean values of x in the near-surface layer in the other samples were evaluated. These numbers are listed in Table IV. Also tabulated in this table are the nominal Ge concentrations deduced from the growth conditions as well as the Ge concentrations at the near surface region and interface. In this procedure we have disregarded the increase of the Ge Auger line intensity recorded at the very surface of the samples. It is very likely that this effect is due to a residue of Ge compounds residing at the surface after the RTCVD. A study involving surface etching is presently engaged in order to check this hypothesis and to verify directly the presence of the composition gradients in the samples.

Shown by the solid lines in Fig. 26 are the PR spectra at 300K of a number of different $Si_{1-x}Ge_x$ samples ($0<x<0.225$) in the photon energy range 2.6−3.6 eV. While the first three traces appear to be a singlet, a well-developed doublet structure develops for $x>0.095$.

The normalized changes in reflectivity $\Delta R/R$ for unbound states due to EM produce third-derivative spectroscopy (see Chapter 3). Equation (3.13C) is used to fit the data. Two oscillators were used in the fit. The resulting best fits are displayed by

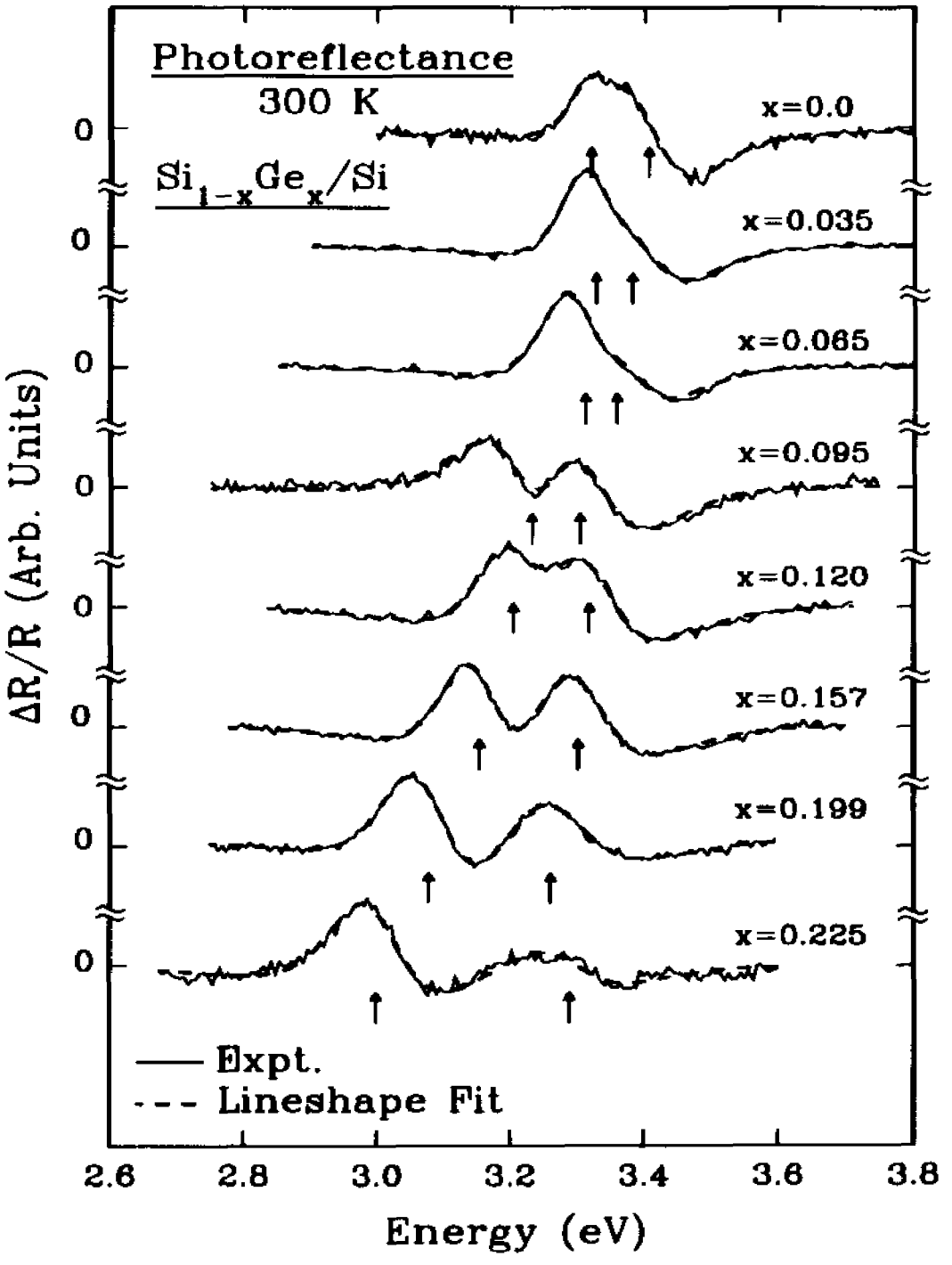

Fig. 26. Photoreflectance spectra (solid lines) at 300K of a series of SiGe/Si samples. The dashed lines are least-squares fits.

the dashed lines in Fig. 26 with the transitions energies indicated by arrows. The obtained transition energies and broadening parameters of the two features are also listed in Table IV.

5.4. Discussion

The optical spectra in $Si_{1-x}Ge_x$ ($0<x<0.23$) in the region around 3.4 eV contains three possible resonances, E_1, $E_1+\Delta_1$ and E_o' (Kline *et al.* 1968, Humlicek *et al.* 1989, Ferrieu *et al.* 1992, Pickering *et al.* 1993). The former two are due to two-dimensional critical points (m=3) along the $<111>$ directions [Λ_3-Λ_1 (L_3-L_1)] of the Brilloun zone while the latter is related to transitions near the Γ-point and has a three-dimensional nature (m=2.5) (see Section 3.3). The appropriate exponents were used in the above fits. For the end-point silicon E_o' occurs below E_1 and the energy of Δ_1 is small (about 0.03 eV) so that $E_1+\Delta_1$ is not resolved (Kline *et al.* 1968, Humlicek J. *et al.* 1989, Ferrieu *et al.* 1992). In unstrained samples E_1 undergoes a red shift as the Ge content is increased while E_o' is almost stationary (Kline *et al.* 1968). At $x\approx0.1$ these levels cross so that for higher germanium content E_1 appears below E_o'.

Plotted in Fig. 27 (strained system) are the dependences on the germanium concentration of the two spectral features, which we designate as E_1 and "E_o'". The reason for employing the latter notation is explained below. Representative error bars are shown. For both x=0.035 and 0.065 we have measured two samples while for x=0.157 three materials were evaluated. The obtained energies for a given Ge composition are almost equal for the different samples (see Table IV). For convenience

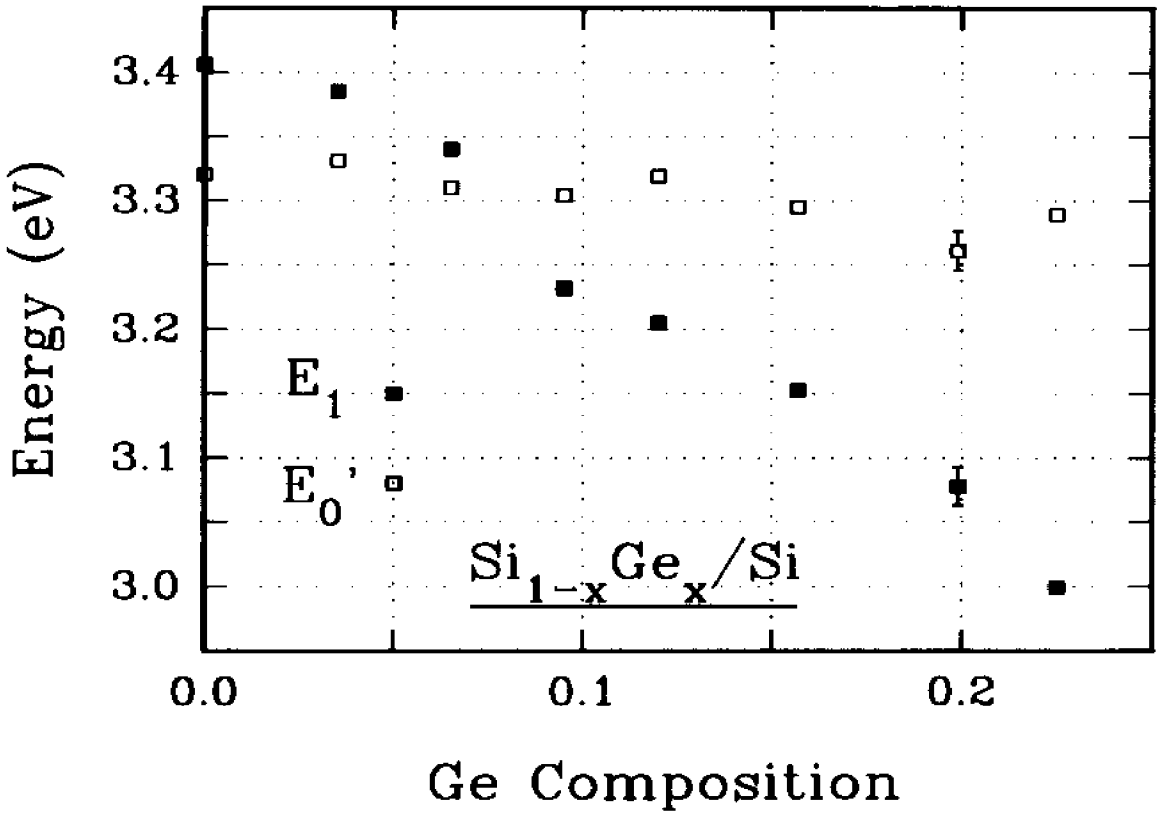

Fig. 27. Composition dependence of the E_1 (Solid squares) and "E_0'" (open squares) optical features of the $Si_{1-x}Ge_x/Si$ samples.

the average of the appropriate measurements is shown in Fig. 27 for x=0.035, 0.065 and 0.157.

The presence of the strain can affect the energies and amplitudes of E_1, $E_1+\Delta_1$ and E_0' in relation to the unstrained material values (see Section 2.3 of Chapter 2). The changes in transition energies of E_1, $E_1+\Delta_1$ due to a (001) biaxial strain ε are given by Eqs. (2.40). The energy of E_1 is approximately the same in the two systems since there is a cancellation of the hydrostatic ($\delta E_{H,A}$) and shear ($\delta E_{S,A}$) components of the strain

(Pollak 1990, Pickering *et al.* 1993). For $E_1+\Delta_1$ there is a strain induced blue shifted because of the addition of the two terms. Using deformation potentials (Pollak 1990) and elastic constants (Brantley 1973) interpolated between Si and Ge, the Δ_1 splitting would be expected to be increased to ~ 0.15 eV for the strain of ε=-0.008 caused by the lattice mismatch at x=0.2. Since E_0' has only a small strain dependence (Pollak and Rubloff 1972) these two transitions, *i.e.* $E_1+\Delta_1$ and E_0', are essentially degenerate in the strained material. This can be easily seen in Fig. 27. Hence we introduced the notation "E_0'" to label the higher lying feature which may contain contributions from both E_0' and $E_1+\Delta_1$ transitions. The built-in stress also shifts oscillator strength from $E_1+\Delta_1$ to E_1 so that the former is a factor of 3 smaller than the latter (Pollak and Rubloff 1972 Pollak 1990, Pickering *et al.* 1993). Thus, it may not be possible to resolve the $E_1+\Delta_1$ contribution to the "E_0'" peak. Measurements at 77K also show only a doublet, *i.e.*, E_1 and "E_0'" (Yin Y. *et al*, to be published). Any possible $E_1+\Delta_1$ contribution to "E_0'" could be determined by the application for a large external uniaxial stress along [100] (Pollak and Rubloff 1972).

Our results are somewhat different from those of Ferrieu F. *et al.* (1992). These researchers report values for E_1 for strained material which are significantly red shifted in relation to unstrained samples. We found E_1 (strained) to be approximately the same as E_1 (unstrained) (Humlicek *et al.* 1989), in agreement with deformation potential theory calculation and the results of Pickering *et al.* (1993). The discrepancies between our results and those reported by Ferrieu *et al.* (1992) are probably due to the fact that

we have used the actual germanium concentrations within the penetration depth of the light (~ 100Å).

Reflectivity measurements on unstrained $Si_{1-x}Ge_x$ material reported a break in the composition dependence of E_1 at $x \approx 0.2$, where E_1 and E_0' cross (Tauc and Abraham 1961). This behavior was interpreted as a change in the conduction band structure due to the cross-over of the relevant conduction levels. Note from Fig. 27 that there appears to be a discontinuity in the E_1 curve where E_1 and "E_0'" intersect ($x \approx 0.05$) for this strained layer system. No such discontinuity has been observed in Refs. Kline J. S. *et al.* 1968 and Humlicek *et al.* 1989.

5.5. Conclusions

Using the PR method we have evaluated the germanium composition dependence of the E_1 and "E_0'" optical features in a series of strained $Si_{1-x}Ge_x$/Si layers ($0 < x < 0.23$) fabricated by RTCVD. Using AP accurate values of x were evaluated in the region of the light penetration (~ 100Å). We found values of E_1 (strained) to be approximately the same as E_1 (unstrained), in agreement with a deformation potential theory calculation. Thus we have established an accurate calibration curve for $0 < x < 0.23$ that can be used to determine the Ge content of such films. Our results are somewhat different from those reported by Ferrieu *et al.* (1992), probably due to our evaluation of x in the relevant near surface region.

Chapter 6. STRAINED Si-Ge MICROSTRUCTURES GROWN ON (001) Ge

Short-period strained Si-Ge microstructures fabricated on (001) Ge have been investigated by PzR, PR and Schottky barrier electroreflectance (SBER) at 77K. In addition to bulk Ge these samples consisted of Ge quantum wells sandwiched between ordered short-period strained Si-Ge superlattice regions. No evidence for pseudodirect transitions in the Si-Ge SLs was found by any of the above measurements although quantum transitions in the Ge QWs were observed in PzR. The PR and SBER spectra measured to date derive from the bulk-like Ge regions of the sample, in contrast to previously published data on similar samples.

6.1. Introduction

The possibility of achieving pseudodirect optical transitions in the Si-Ge system through artificially ordered structures has recently received considerable experimental and theoretical attention (see, for example, Pearsall *et al.* 1989a, 1990a, People and Jackson 1990). Studies of valence-band offset and the well-known nature of the uniaxial strain in Si and Ge have established that the conduction-band edge in these structures is formed from (100)-oriented Si states. Pseudomorphic, strained-layer epitaxy of a Si-Ge superlattice (SL) on a (001) Ge substrate creates a tensile, biaxial strain (in-plane), which results in a compression along the SL growth axis. Under these conditions of strain, the conduction-band edge lies along the SL axis, and it will be mixed by the SL potential with zone-center states. This effect raises the possibility that the SL might be a

direct-gap material. Such novel properties and the capability to have interesting electronic and optical characteristics while being compatible with existing Si processing technology of these strained-layer Si-Ge superlattices have also been of great applied interest (See, for example, Peasall 1990a). Pearsall *et al.* have reported features in the SBER spectra at 40K of such samples which have been attributed to new optical transitions at energies theoretically predicted for SL-induced direct optical transitions at the center of the Brillouin zone (Pearsall *et al.* 1989c; 1989d; Pearsall 1990b). However, the interpretation of these results are complicated by the presence of FKOs whose origins were not clearly understood (Pearsall *et al.* 1989c; 1989d; Pearsall 1990b).

In this chapter we report a modulation spectroscopy study of short-period strained Si-Ge microstructures grown on (001) Ge using PzR, PR and SBER at 77K. In addition to bulk Ge (substrate/buffer) these samples consisted of Ge QWs which formed spacer layers between the ordered short-period strained Si-Ge SL regions. No evidence for pseudodirect transitions in the Si-Ge SLs was found by any of the above measurements. The PzR signals are due to quantum confined transitions in the Ge QWs (Yin Y. *et al.* 1991b, 1992c). The PR and SBER spectra are dominated by FKOs. We have found that the SBER spectra measured to date derive from the bulk-like Ge regions of these samples, in contrast to the interpretation of previously published SBER data on similar samples (Pearsall *et al.* 1989c, 1989d, Pearsall 1990b).

6.2. Experimental details

The samples used in this study were grown by MBE (Pearsall *et al.* 1989c; Bean 1984) on (001) Ge substrates at 450 °C. One category had a unit cell consisting of three monolayers (ML) of Si and seven ML of Ge (Si_3Ge_7), while the other had a unit cell of four ML of Si and six ML of Ge (Si_4Ge_6). The samples alternated one of the above ordered unit cells, repeated 5 times, with pure Ge spacer regions of various thicknesses ranging from 29 to 143 ML. We designate such configurations as $(Si_mGe_n)_5Ge_N$, where N denotes the number of ML's of the Ge spacer. This overall pattern was repeated either 10 or 20 times. This structure is illustrated in Fig. 28. Two of the samples were from the same wafers used in Pearsall *et al.* 1989c, Pearsall *et al.* 1989d and Pearsall 1990b. The periodic structure parameters were determined using high-resolution x-ray diffraction (Vandenberg J. M. *et al.* 1987).

We have performed transmission electron microscopy (TEM) and electron diffraction measurements both on pieces of the newer samples as well as on pieces of the older samples upon which SBER measurements were previously performed. The newer samples showed excellent planarity of all the interfaces with a structure in good agreement with the nominal layer spacing. In particular, the ordered short period Si-Ge regions showed excellent definition, equal to or superior to earlier TEM measurements on the older samples. Reexamination of the older samples suggested that some degradation may have occurred. As will be discussed in detail below the samples measured in our SBER study show features identical to those reported by Pearsall *et al.*

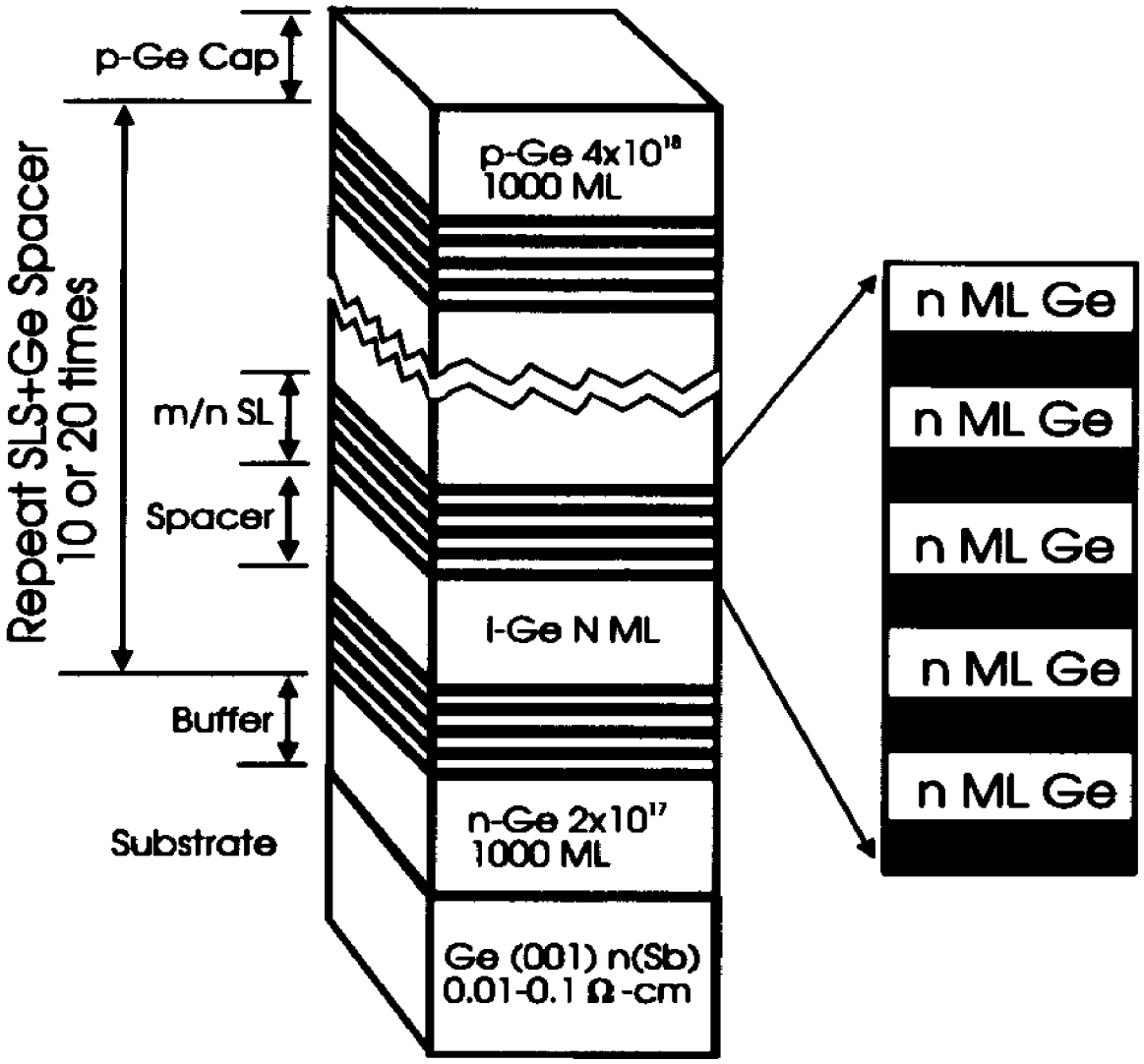

Fig. 28. The schematic sketch of the $(Si_mGe_n)/Ge_N$ structure.

(Pearsall *et al.* 1989c, 1989d, Pearsall 1990b). Any degradation which may have occurred in the original samples has no influence on the observed SBER spectra.

Stress modulation was achieved by mounting the samples on a 0.15-cm-thick zirconate-titanate piezoelectric transducer driven by a 500-V peak-to-peak sinusoidal wave at 1 kHz (Yin Y. *et al* 1991a). The PR spectra were obtained using the 633-nm line of a HeNe laser chopped at 200 Hz as the pump (Pollak and Glembocki 1988). A semitransparent gold film of ~ 50 Å was deposited on to the surface of the sample to achieve a Schottky contact for the SBER measurements. Typical modulation *ac* voltage for SBER is 0.4 Volt peak-to-peak square wave at 200 Hz.

6.3. Experimental results

6.3.1. Piezoreflectance

Shown by the solid lines in Fig. 29 are the PzR spectra at 77 K of the (001) Ge substrate and four $(Si_mGe_n)_5Ge_N$ SL's with m/n/N=3/7/143, 3/7/29, 4/6/126, and 4/6/78. The dotted lines are least-squares fits to a first-derivative Gaussian lineshape (FDGL) function which yields the transition energies denoted by the arrows. The sharp peak at 0.875 eV in the Ge substrate spectrum corresponds to the lowest direct gap (E_0) of this material while the weaker structure at 1.175 eV is due to the spin-orbit split component ($E_0+\Delta_0$). The 3/7/143 and 4/6/126 samples, which were derived from the same wafers used by Pearsall *et al.*(1989c, 1989d, 1990b), exhibit two well-resolved peaks just above the structure at 0.875 eV (which originates in the Ge substrate). The 3/7/29 and 4/6/78 materials also have doublets which are well separated from E_0. With decreasing N the doublets undergo a blueshift and the separation between the components increases. Except for the sample with the narrowest Ge spacer other spectra exhibit a number of

features above the doublet. The dotted lines are least squares fits to a FDGL, which is appropriate for PzR at 77 K (Pollak and Glembocki 1988). The obtained energies of the various peaks are denoted by arrows and also are listed in Table V.

The origin of the PzR peaks can be understood from the band diagram for the whole structure $(Si_mGe_n)_5Ge_N$, a point previously emphasized for similar structures grown in (001) Si substrates (Hybersten and Schluter 1988). Self-consistent local-density functional calculations have been performed for components of the full structure, e.g., the pure Ge, the Si_mGe_n, SL or an alloy. These calculations[a] yield the necessary band extrema as well as band offsets. The eigenvalues from such calculations require self-energy corrections for both the bulk band gaps (Hybertsen and Louie 1986, Godby *et al.* 1988) as well as the valence-band offset (Zhang *et al.* 1988; Hybertsen 1988). These have been included approximately[b]. The band diagram shown in Fig. 30 for either a Si_4Ge_6 SL (solid lines) or the corresponding alloy (dotted lines), alternating with Ge, are a result of the above procedure. The solid lines denote ordered Si_4Ge_6 portions, while the dotted lines show the corresponding alloy case. The dashed lines indicate indirect conduction-band minima. Only one Γ and Δ derived band extrema are shown.

---

[a]). The present calculations are done using norm conserving pseudopotentials and a planewave basis set including basis functions up to a kinetic energy of 11 Ry. Details may be found in Hybertsen M. S. and M. Schulter, 1987, Phys. Rev. **B36**, 9683.

[b]). The self energy correction to the valence band offset is estimated by interpolating results for bulk Si and Ge from Zhu X. and S.G. Louie, 1991, Phys. Rev. **B43**, 14142. The conduction band energies reported here are taken from experiment where possible. For the Si_4Ge_6, the appropriate correction is interpolated from bulk results using the calculated relative Si and Ge character in a given state.

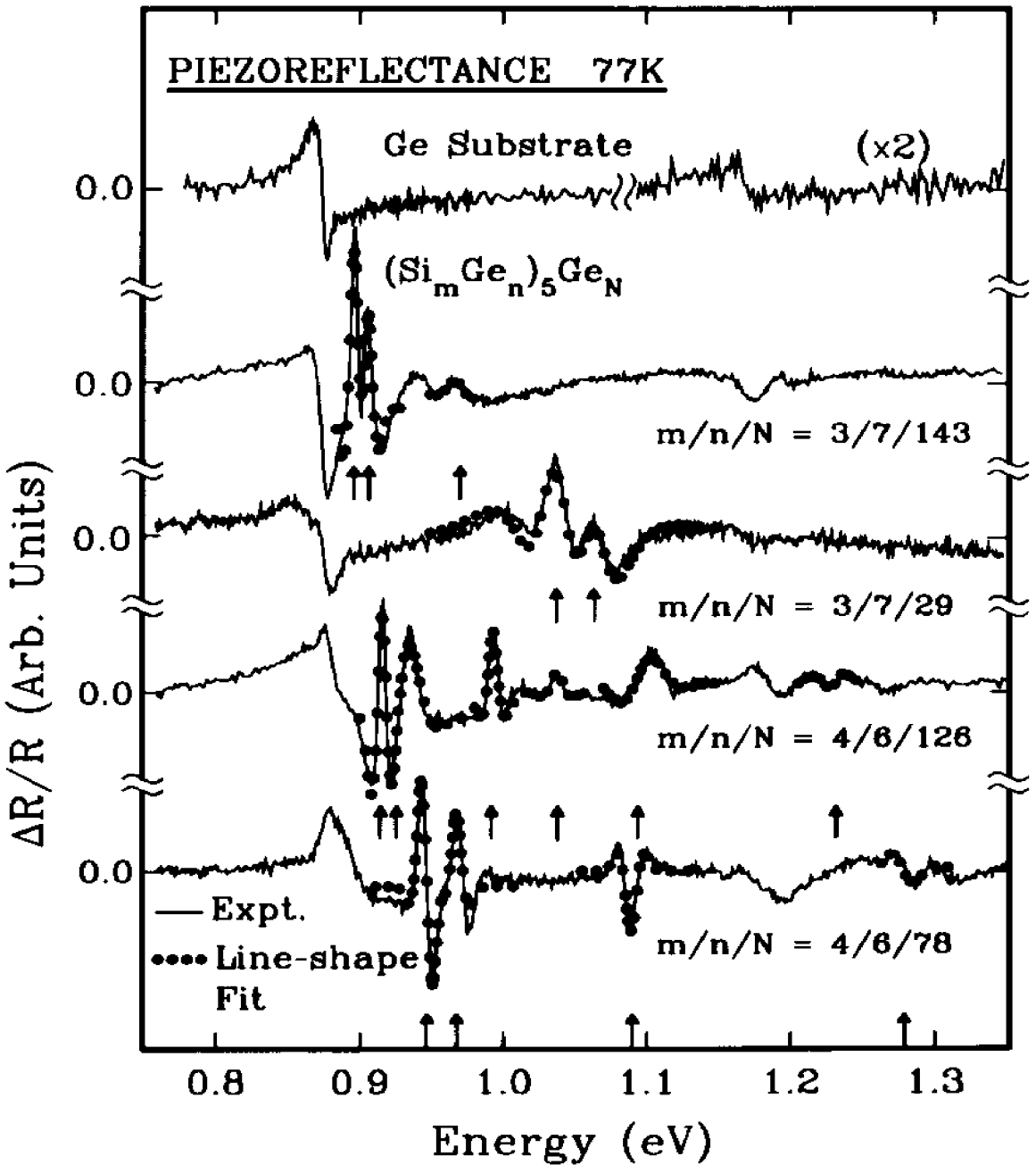

Fig. 29. Piezoreflectance spectra at 77K of the (001) Ge substrate and four $(Si_mGe_n)_5Ge_N$ SL's with m/n/N=3/7/143, 3/7/29, 4/6/126, and 4/6/78 (see text).

Energy separations are in eV.

Table V. Experimental and theoretical values of the transitions in short period $(Si_3Ge_7)_5$ and $(Si_4Ge_6)_5$ superlattices with different Ge spacer thicknesses.

Superlattice	Experiment Ge spacer (ML)	Energy (ev)	Theory Energy (ev)	Origin
$(Si_3Ge_7)_5$	143[a]	0.898	0.898	11H
		0.908	0.905	11L
		0.972	0.96	22H
			0.99	22L
			1.06	33H
			1.13	33L
	29	1.039	1.07	11H
		1.065	1.10	11L
$(Si_4Ge_6)_5$	126	0.915	0.902	11H
		0.926	0.912	11L
		0.992	0.99	22H
		1.038	1.02	22L
		1.094	1.11	33H
		1.231	1.20	33L
	78	0.947	0.93	11H
		0.967	0.95	11L
		1.090	1.10	22H
			1.17	22L
		1.278	1.39	33H

[a]Same samples as Pearsall *et al.* 1989c, Pearsall 1990b.

Several salient features in Fig. 30 should be noted. First, in the present tetragonal symmetry (i.e., due to the strain), the relevant quantum number for the valence-band states is M_j only. There are two $M_j = 1/2$ states in the Si-Ge region which

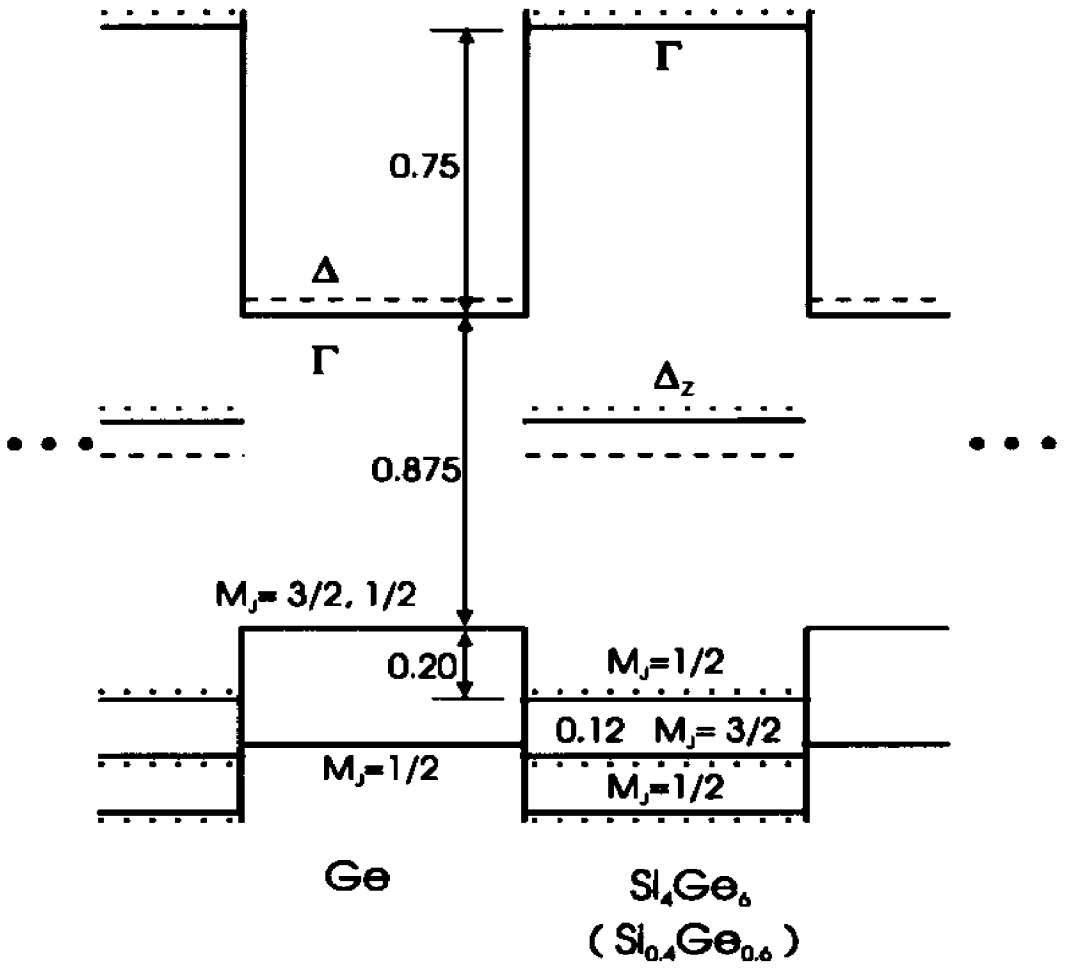

Fig. 30 Caculated band diagram for a superlattice alternating Ge spacer sections and the Si-Ge regions (see text).

couple to the light-hole and splitoff states in the Ge. The $M_j=3/2$ state couples to the heavy-hole state in the Ge. Second, the lowest conduction bands in the ordered Si_4Ge_6 region are formed from zone-folded Δ_z states which are slightly split by the superlattice order. Only the second one couples to the s-like conduction-band state, but weakly as indicated by the small oscillator strength for direct transitions from the valence-band

states. Note that while holes are confined in the Ge region, the lowest energy electrons are confined in the Si-Ge portion. This corresponds to the lowest optical transition. Third, the s-like Ge conduction-band states are confined by the corresponding states in the Si-Ge regions. These will give rise to strong dipole allowed transitions from the heavy- and light-holes confined in the Ge. Such transitions will dominate the observed optical response in the energy region immediately above the direct gap of the Ge (0.875 eV at 77 K). Fourth, the SL order has only a small influence on the band diagram. Therefore, the Si_3Ge_7 case was treated using an alloy approximation.

For direct comparison to experiment we have calculated the various subband energies using the envelope function method (Bastard 1981) and the band diagram of Fig. 30. In the Ge region we have used electron (e), light-hole (LH), and heavy-hole (HH) masses (in units of the free-electron mass) of $m^*_e=0.038$, $m^*_{LH}=0.046$, and $m^*_{HH}=0.22$ (Landolt-Börnstein 1982), taken from experiment. In the Si_4Ge_6 region the masses along the z axis have been calculated to be $m^*_e=0.07$, $m^*_{v1}=0.09$, and $m^*_{v2}=0.24$, where v_1 and v_2 refer to the ground state $M_j=1/2$ and the $M_j=3/2$ valence states, respectively (see Fig. 30). Nonparabolicity effects have not been included. For the purposes of the subband calculation there is some ambiguity about the Ge well width since one of the Ge regions is contiguous to the Ge_N spacer. For the small N cases, or for higher subbands, this uncertainty of n ML of Ge in the well width alters the calculated confinement energies by as much as ~ 50 meV, although the LH-HH splitting is much less affected. Therefore, the values reported represent an average. The final transition energies are the

calculated confinement energies plus the measured bulk Ge transition energy of 0.875 eV taken from Fig. 29. The energies listed in Table V are "symmetry-allowed" confined transitions [mmH(L)] between the m^{th} conduction to m^{th} valence subband of heavy (H-) or light (L-) hole character. There is a distinct blueshift of all the features with decreasing N. Overall there is a very good agreement between experiment and theory. Thus, we can identify the various features in the PzR spectra with transitions in the quantum wells formed by the Ge spacer regions.

Pearsall *et al.* reported electroreflectance results at 40K on $(Si_mGe_n)_5Ge_N$ SLs on (001) Ge with m/n/N of 3/7/143 and 4/6/126. However, the spectra are complicated by strong FKOs above E_0 and $E_0+\Delta_0$ of Ge. Thus, there is considerable ambiguity concerning the interpretation of features near E_0 and $E_0+\Delta_0$ as being due to SL-induced direct optical transitions. Also since these samples had a large N any features due to the Ge quantum well could also be masked by the FKO. Recently Menczigar *et al.*(1990) have published photoreflectance results as a function of temperature on Si_mGe_n SLs grown on (001) Ge with m/n = 2/6, 3/9, 4/12. The authors interpret features in the 0.9-1.2 eV range for the 2/6 sample as being due to SL induced direct interband transitions. However, their results also exhibit complex oscillating features above E_0 and $E_0+\Delta_0$ which complicates the analysis of the data.

6.3.2. Photoreflectance

The PR spectra at 77 K from samples 3/7/29 and 4/6/126 are shown in Fig. 31

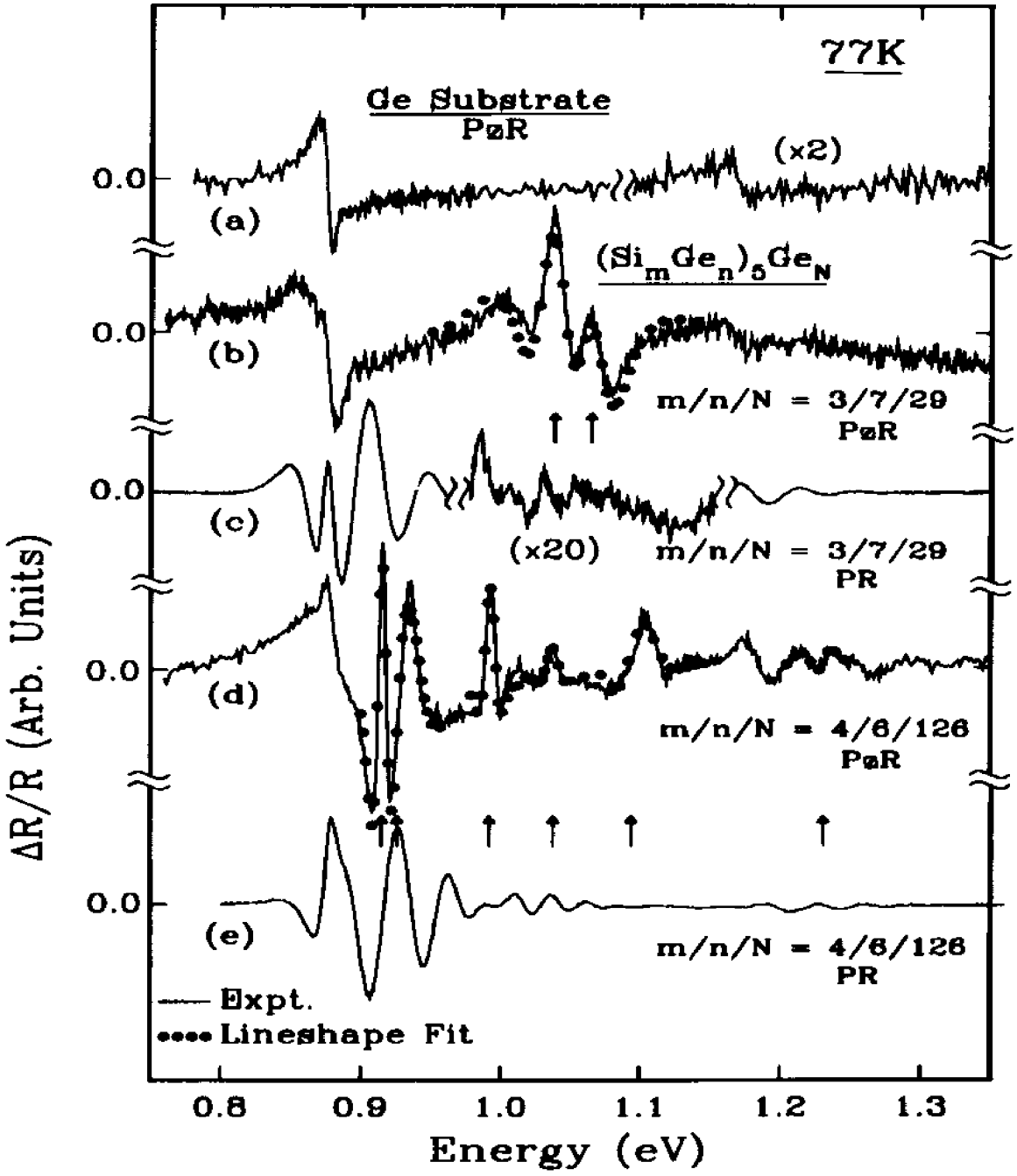

Fig. 31. Comparison of PR and PzR spectra at 77K of the $(Si_3Ge_7)_5Ge_{29}$ and the $(Si_4Ge_6)_5Ge_{126}$ samples. The PzR spectrum of (001) Ge substrate is also included.

together with the PzR spectra at 77 K (Yin Y. *et al.* 1991b). Also included in the figure is PzR spectrum at 77 K from the Ge(001) substrate material. Displayed in Fig. 31(a) is the experimental PzR spectrum of a Ge(001) substrate, Fig. 31(b) is the PzR spectrum of a $(Si_3Ge_7)_5Ge_{29}$ structure, Fig. 31(c) the PR data for the $(Si_3Ge_7)_5Ge$ Sample, Fig. 31(d) the experimental PzR spectrum for a $(Si_4Ge_6)_5Ge_{126}$ sample and Fig. 31(e) the PR data for the $(Si_4Ge_6)_5Ge_{126}$ structure. The dotted curves are least-squares fits of the FDGL function to the PzR data (see Section 6.3.1). The obtained transitions energies are indicated by arrows (see Section 6.3.1).

The PR spectrum exhibits strong FKO above E_0 and $E_0+\Delta_0$. In Figs. 31(d) and 31(e), we display the corresponding spectra for the 4/6/126 sample, also used in Pearsall *et al.* 1989c, 1989d, Pearsall T. P. 1990b. The PR data again contains a large number of FKO similar to the spectra reported by Pearsall *et al.*(Pearsall *et al.* 1989c, 1989d, Pearsall 1990b).

6.3.3. Schottky barrier electroreflectance

We also have performed SBER measurements at 77K on these samples over a wide range of both forward (+) and reverse (−) bias (V_B). Shown by the solid lines in Fig. 32 are the SBER spectra of the 3/7/143 sample (same as Pearsall's Fig. 1 in Pearsall 1990b) for representative V_B. The spectra can be divided into two regimes below and above E_0 as indicated by the dashed line. These signals are very similar to those reported for bulk semiconductors (Bhattacharya *et al.* 1988). Below 0.89 eV the SBER

traces display the so-called "lineshape rotation" effect due to non-uniform fields (Bhattacharya *et al.* 1988). Note that there is a continuous phase change with applied bias in our spectra. Above E_o the spectra exhibit Franz-Keldysh oscillations (FKO) whose period is increasing with larger bias voltage (Bhattacharya *et al.* 1988). We found that the electric field deduced from the FKOs scales as $(V_B)^{1/2}$. For comparison purposes we also have plotted the -1.0 eV and -2.0 V SBER traces of Pearsall's Fig. 1 of Pearsall 1990b by the dashed lines. The solid and dotted lines for -1.0 V are quite similar. For the dotted data there is a red shift of the spectrum for -2.0 V in relation to -1.0 V.

The $(V_B)^{1/2}$ dependence of the field deduced from FKO and the "lineshape rotation" phenomenon with increasing *dc* bias voltage are characteristic of the SCRs in bulk material (Bhattacharya *et al.* 1988, Shen and Pollak 1990, 1993). The former is straight forward since in a fully depleted SCR the field is proportional to the square root of the electric potential (see for example, Bhattacharya *et al.* 1988), and the field deduced from FKOs in EM spectra measures the maximum field in the SCR (see Section 3.3.5). But the latter is not as obvious (Pollak and Shen 1993). Possible mechanisms of how such a "lineshape rotation" is produced include (a) exciton interference effects in a portion of the SCR where the electric fields are low enough not to quench the exciton, application of V_B changes the position of this region in relation to the front of the sample thus altering the phase (Aspnes and Sudna 1973, Siberstein and Pollak 1980, Bhattacharya *et al.* 1987a, 1987b, 1988, Bottka *et al.* 1988); (b) multilayer reflection of

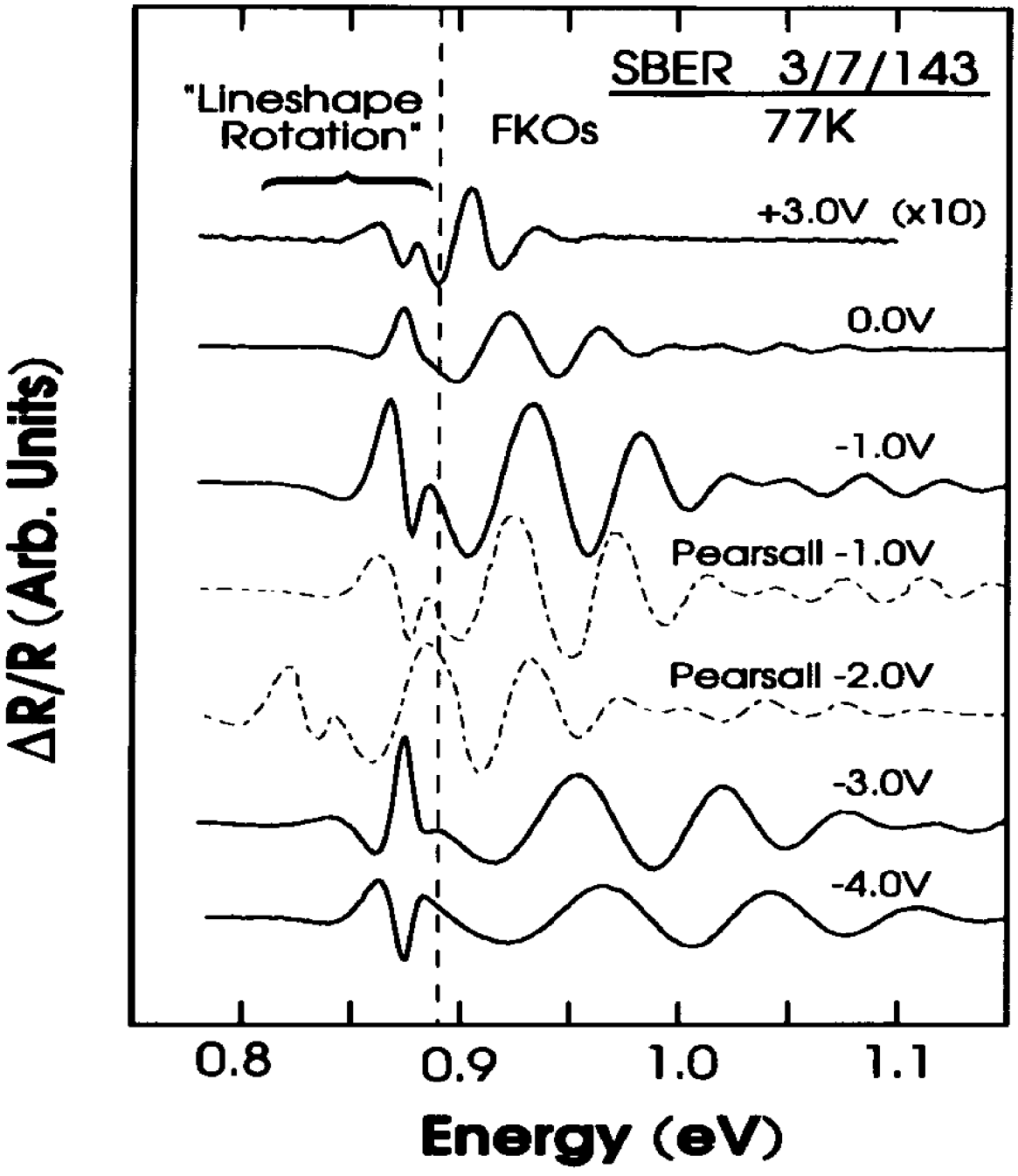

Fig. 32. Schottky barrier electroreflectance at 77 K as a function of V_B for sample 3/7/143 (solid lines). Also shown are spectra from Pearsall T. P. 1990b (dashed lines).

the inhomogeneous field (slab configuration) in the SCR (Batchelor and Hammnett 1990, Batchelor *et al* 1990). This question has been the subject of considerable investigation (Behn and Roppischer 1988, Shen and Pollak 1990, Jackson and Seebauer 1991). However, the basic physics behind it is the interference effect, whether the mechanism is excitonic or field inhomogeneity, or both. The "lineshape rotation" acts as a kind of Fabry-Perot interferometer from which it is possible to obtain information about the change in width of the SCR (Aspnes and Studna 1973, Silberstein and Pollak 1980, Bicelli 1987, Bottka *et al.* 1988). It is a well established fact that the bias dependent "lineshape rotation" of ER spectra originates from SCRs of bulk material.

For our SBER measurements the presence of the "lineshape rotation" feature and the fact that the measured electric field scales as $(V_B)^{1/2}$ shows that the SBER signals are originating from a bulk space charge region, not the uniform field of the insulating region of the PIN structure. For the latter there should be no "lineshape rotation" and the electric field would be proportional to V_B. The fact that there is a continuous change in both the phase of the "lineshape rotation" feature and the FKOs is a clear indication that the increase in bias is being manifested as a change in electric field, not current. Another important aspect of our measurements is the signal at large forward bias (+3.0 V). This spectra exhibits only the "lineshape rotation" feature and a remnant of the FKOs associated with the direct gap of bulk Ge. There is no evidence for features from the SL region. Pearsall *et al.* did not perform measurements at large $+V_B$ (Pearsall *et al.* 1989c, 1989d, Pearsall 1990b).

Pearsall's data also exhibits the "lineshape rotation" feature, as shown by the dotted lines in Fig. 32 (Peasall 1990b). In relation to -1.0 V the -2.0 V dashed data exhibits a red shift but almost no changes in the "lineshape rotation" or period of the FKO. This indicates that the increase in V_B is being manifest as a current and not a field. Thus, the red shift is probably due to heating and not a quantum confined Stark effect as claimed by Peasall (Pearsall 1990b).

At -1.0 V both solid and dotted spectra exhibit a large feature around 0.94 eV, which Pearsall has attributed to a $(Si_mGe_n)_5$ SL transition (Pearsall *et al.* 1989c, 1989d, Pearsall 1990b). Note however that this feature is not stationary but blue shifts with increased bias, i.e., it is a FKO.

Pearsall has recently reported differential optical absorption spectroscopy in Si-Ge/Si and Si-Ge/Ge SLs, the latter being a $(Si_3Ge_7)Ge_N$ sample (Pearsall 1992). For this material a differential absorption edge starting at about 1.65 microns (0.75 eV) was interpreted as evidence for a pseudodirect SL transition. This feature is only 25 meV below the LA-phonon assisted indirect gap of bulk Ge (0.775 eV). If this sample is the same as Refs. Pearsall 1990b, Pearsall *et al.* 1989c, Pearsall *et al.* 1989d the bulk Ge signal in this region could originate in the doped buffer/cap ($n \sim 10^{17}-10^{18}$ cm^{-3}). Thus the absorption onset below 0.775 eV might be due to either impurity or electric field related effects.

6.4. Summary and discussions

We have investigated $(Si_mGe_n)Ge_N$ microstructures by PzR, PR and SBER. The features observed in PzR are due to quantum transitions in the Ge_N QWs. Comparison between experiment and theory yields information about band offsets. PR and PzR data are dominated by FKOs. These FKOs originate in the bulk-like Ge regions of the samples. No evidence for pseudodirect transitions in the Si-Ge SLs in these samples was observed by any of the experimental methods employed.

In a recent comment about our PzR work (Yin Y. *et al.*, 1991b, see also Section 6.3.1) Pearsall (Pearsall 1993) raised his point that we did not observe the pseudo-direct transitions from the short period superlattice regions of 3/7/143 sample (Pearsall *et al.* 1989c), which they claimed to have seen in their SBER spectra, because of (a) sample degradation; (b) sensitivity of PzR in relation to SBER to optical transitions in a superlattice. He also commented about the theoretical point about the oscillator strengths of pseudodirect transitions. I want to give a brief reply to these questions as follows.

We have performed TEM and electron diffraction measurements on all samples used in our investigations. The newer samples showed excellent planarity of all the interfaces with a structure in good agreement with nominal layer spacing. In particular the ordered short period Si-Ge regions showed excellent definition, equal to or superior to earlier TEM measurements on the older samples. Reexamination of the older samples suggested some degradation may have occurred. However, as have been seen in Section

6.3.3, we have been able to obtain SBER spectra similar (or identical) to those of Pearsall *et al.* 1989c from the same sample in which they claimed to have seen the pseudodirect transitions (Pearsall *et al.* 1989c, Pearsall 1990b). Any degradation which may have occurred in the original samples has no influence on the observed ER spectra.

The PzR technique has proven to be just as sensitive as ER for superlattice and quantum well samples. In particular, PzR signal from single quantum wells as thin as 50 Å has been reported (Allegre *et al.* 1990). The acoustic field generated in the PzR method has a long wavelength (~ 100 cm) which implies that the active entire $(Si_mGe_n)_N$ region of the sample is being uniformly modulated. Given the structure of the samples described in Section 6.2, each Ge_N spacer is surrounded by a $(Si_mGe_n)_N$ ordered superlattice region. Therefore, the acoustic modulation is the same in both. This also rules out any spurious electric field effects in PzR due to differential stress variations in band offsets at internal interfaces. Clearly the PzR method is equally sensitive to modulated optical transitions in the Ge spacer regions and the ordered Si-Ge regions.

The oscillator strength for pseudodirect transitions in Si-Ge ordered suplattices obtained from theoretical calculations depends on the details of the period, internal structure and strain. For the structure in the present samples, e.g. 4/6 or 3/7 on Ge(001), the oscillator strength is about 100-1000 times smaller than that of a standard dipole allowed transition (Schmid *et al.* 1990, 1991), i.e., the direct gap in bulk Ge. This is most vividly illustrated in Fig. 14b of Schmid *et al.* 1991 where Schmid *et al.*

showed the calculated optical response (ϵ_2) for (Si_4Ge_6) on Ge(001). The region corresponding to pseudodirect transitions near 1 eV is 1000 times weaker than the direct threshold near 2 eV. This implies that the optical transitions derived from the $(Si_mGe_n)_N$ regions of the sample will be about 100 times weaker than the fully allowed quantum well transitions in the Ge_N regions of the sample.

The efforts to find a direct band gap group IV material from Si-Ge short period superlattices continue to expand. All kinds of structural configration, strain pattern in the superlattice, choice of substrate material (Si or Ge) have been used. With the advances in growth technology and with proper design of structural and strain parameters, we hope that our dream of having a group IV direct gap semiconductor will eventually come true.

Chapter 7. SUMMARY AND CONCLUSIONS

In this thesis we have investigated four types of very important strained-layer semiconductor microstructures with PR, PzR and CER modulation spectroscopy techniques. The strained-layer structures used in this work are GaAlAs/InGaAs/GaAs PMDQW structures, strained SiGe Si-rich alloy films grown on (001) Si substrate, strained-layer Si-Ge microstructures grown on (001) Ge and Ge/SiGe quantum wells grown on (001) Ge.

We have demonstrated that modulation spectroscopy is an extremely powerful tool for investigating semiconductor microstructures. Since there are a variety of modulation techniques available, it is possible to choose the one that is most suitable for a particular experiment. The great progress we have made in this thesis work is partially due to our proper choice of modulation techniques for each project.

For the first time we positively identified the 2DEG signature in modulation spectroscopy traces originating from the quantum transitions in modulation-doped quantum wells with high electron sheet densities. A modulation spectroscopy lineshape function for the intersubband transitions in a MDQW with 2DEG has been proposed. This lineshape allows us to extract the Fermi level position relative to the electron subband in addition to the intersubband transition energies and broadening, which in turn yields the sheet electron density present in the well channel.

We have observed for the first time an optical feature in the CER spectra which originates from the transitions occurring at the Fermi edge in an 100Å-wide well width sample at temperatures up to 152 K. At higher temperatures it evolves into a broad background. The Fermi edge peak in modulation spectroscopy has less temperature dependence than the $\mathbf{k}=\mathbf{0}$ intersubband transitions over the same temperature range. This is due to the strong many-body effects on this feature. The Fermi edge feature can not be fitted by the FD2DJDS lineshape based on one-electron model. The proper lineshpae function is the subject of current research.

We have measured the Ge composition dependence of the E_1 and "E_0'" (will be defined later in this section) transition energies at 300K in a series of strained $Si_{1-x}Ge_x/Si$ layers ($0<x<0.23$) using photoreflectance. Auger profiling was employed for an accurate evaluation of x in the near-surface region corresponding to the penetration depth of the light (about 100 Å). In our strained samples the energy of the E_1 peak is essentially the same as in unstrained material, in agreement with deformation potential theory. The "E_0'" feature, which exhibits only a very weak variation with Ge content, may also contain a strain-shifted $E_1+\Delta_1$ component. These results have enriched the understanding of the properties of Si-rich strained thin SiGe alloy films grown on silicon substrate.

We have investigated a number of short-period strained Si-Ge microstructures fabricated on (001) Ge using PzR, PR and Schottky barrier electroreflectance (SBER)

at 77K. In addition to bulk Ge these samples consisted of Ge quantum wells sandwiched between ordered short-period strained Si-Ge superlattice regions. No evidence for pseudodirect transitions in the Si-Ge SLs was found by any of the above measurements although quantum transitions in the Ge QWs were observed in PzR. The PR and SBER spectra measured to date derive from the bulk-like Ge regions of the sample, in contrast to previously published data on similar samples.

We have also made an attempt to understand the Coulomb enhancement of critical point transitions by considering the corresponding modulation spectroscopy lineshapes. It has been shown from a theoretical point of view that the final state Coulomb interaction between electrons and holes can produce profound modification in both the first- and third-derivative Lorentzian lineshape for bulk materials. Preliminary PR, ER and PzR data from Ge substrate agree with our theoretical results and it is the subject of current investigation.

PUBLICATIONS

1. **Y. Yin**, D. Yan, F. H. Pollak, M. S. Hybertsen, J. M. Vandenberg, and J. C. Bean, "Temperature Dependence of the Fundamental Direct Transitions of Bulk Ge and two Ge/SiGe Multiple Quantum Well Structures", submitted to Phys. Rev..

2. F. H. Pollak, H. Qiang, D. Yan, **Y. Yin**, and W. Krystek, "Characterization/qualification of Semiconductor Device Structures Using Modulation Spectroscopy", to be published in the Journal of Metals (1994).

3. H. Qiang, D. Yan, **Y. Yin**, and F. H. Pollak, "Characterization of Semiconductor Device Structures by Modulation Spectroscopy", Proc. SPIE. 2141, 58 (1994).

4. H. Qiang, D. Yan, **Y. Yin**, F. H. Pollak, G. Gumbs, D. Huang, and T. F. Noble, "Two Dimensional Electron Gas Effects in the Electromodulation Spectra from a Pseudomorphic GaAlAs/InGaAs/GaAs Modulation-doped Quantum Well Structures", to be published in J. Luminescence (1994).

5. H. Qiang, D. Yan, **Y. Yin** and F. H. Pollak,"Modulation Spectroscopy Characterization of Semiconductor Device Structures" to be published in Asia-Pacific Engineering Journal, Part A: Electrical Engineering (1994)

6. F.H. Pollak, H. Qiang, D. Yan, **Y. Yin** and J.B. Woodall, "Contactless Electromodulatoin for the Characterization of Semiconductor Surfaces/Interfaces", Control of Semiconductor Interfaces; Proc. of the First International Symposium of Semiconductor Interfaces, Karuiza-wa, Japan, eds. I. Ohdomari, M. Oshima and A. Hiraki (Elsevier, Amsterdam, 1994) p. 307.

7. H. Qiang, D. Yan, **Y. Yin**, and F. H. Pollak, "Modulation Spectroscopy Characterization of Semiconductor Heterostructures", Mat. Res. Soc. Symp. Proc. **326**, 513 (1994).

8. F.H. Pollak, H. Qiang, D. Yan, **Y. Yin** and V.T. Boccio, "Better Device Yields with Modulation Spectroscopy", The Photonics Design and Applications Handbook (Laurin Publishing, Pittsfield, MA, 1994) p. 36.

9. G. Gumbs, D. Huang, **Y. Yin**, H. Qiang, D. Yan, F. H. Pollak and T. F. Noble, "Many--Body Effects in the Electromodulation Spectra of Modulation-doped Quantum Wells: Theory and Experiment", Phys. Rev. **B48**, 18328 (1993) (*Rapid Communication*).

10. F.H. Pollak, H. Qiang, D. Yan, **Y. Yin** and V.T. Boccio, "Better Device

Yields with Modulation Spectroscopy", Photonics Spectra Magazine, Vol. 27, Issue 8, August 1993, p. 78.

11. **Y. Yin**, H. Qiang, D. Yan, F.H. Pollak and T. Noble, "Room Temperature Photoreflectance Characterization of Pseudomophic GaAlAs/InGaAs/GaAs High Electron Mobility Transistor Structures including the Two-Dimensional Electron Gas Density", Semiconductor Science and Technology, **8**, 1599 (1993).

12. J. H. Chen, W.S. Chi, Y.S. Huang, **Y. Yin**, F.H. Pollak, C.D. Pettit and J.M. Woodal, "Photomodulation Study of Partially Strained $In_xGa_{1-x}As$ Layers", Semiconductor Science and Technology, **8**, 1420 (1993).

13. **Y. Yin**, F. H. Pollak, P. Auvray, D. Dutartre, R. Pantel and J. A. Chroboczk, "Photoreflectance Study of Strained (001) $Si_{1-x}Ge_x$/Si Layers", Thin Solid Films, **222**, 85 (1992).

14. **Y. Yin**, H. Qiang, F. H. Pollak, D. C. Streit and M. Wojtowicz, "Two-Dimensional Electron Gas Effects in the Electromodulation Spectra of a Pseudomorphic $Ga_{0.78}Al_{0.22}As/In_{0.21}Ga_{0.79}As$/GaAs Modulation-doped Quantum Well Structure", Appl. Phys. Lett. **61**, 1579 (1992).

15. **Y. Yin**, H. Qiang, F. H. Pollak, D. C. Streit and M. Wojtowicz, "Electromodulation Spectroscopy of a Pseudomorphic $Ga_{0.78}Al_{0.22}As/In_{0.21}Ga_{0.79}As$/GaAs Modulation-doped Quantum Well Structure: Two-dimensional Electron Gas Effects", to be published in Proceedings of the Society of Photo-Optical Instrumentation Engineers (SPIE, Somerset, New Jersey), Volume **1675**, (1992).

16. **Y. Yin**, D. Yan, F. H. Pollak, M. S. Hybertsen, J. M. Vandenberg and J. C. Bean, "Piezoreflectance of Strained Si/Ge Superlattices Grown on Ge(001)", Surface Science, **267**, 99 (1992).

17. **Y. Yin**, D. Yan, F. H. Pollak, M. S. Hybertsen, J. M. Vandenberg, and J. C. Bean, "Piezoreflectance Study of Short-period Strained Si-Ge Superlattices Grown no (001) Ge", Phys. Rev. **B44**, 5955 (1991) (*Rapid Communication*).

18. **Y. Yin**, D. Yan, F. H. Pollak, G. D. Pettit and J. M. Woodall, "Observation of Franz-Keldysh Oscillations in the Stress-modulated Spectra of (001) n-type GaAs", Phys. Rev. **B43**, 12138 (1991) (*Rapid Communication*).

19. J. Marcano, Y. Darici, H. Min, **Y. Yin** and P.A. Montano, "LEED Study of 1 Monolayer Fe Deposited on Cu(110)", Surface Science, **217**, 1 (1989).

20. V. Franco and **Y. Yin**, "Elastic Collisions between Light Nuclei and the Phase

Variation of the Nucleon-nucleon Scattering Amplitude", Phys. Rev. **C34**, 608 (1986).

21. V. Franco and **Y. Yin**, "Elastic Scattering of _ Particles and the Phase of the Nucleon-nucleon Scattering Amplitude", Phys. Rev. Lett. **55**, 1059 (1985).

22. **Y. Yin**, Z. Tan and K. Chen, "Method for Calculating the Complete Expansion of the Glauber Amplitude for Nucleus-nucleus Scattering", Nuclear Physics, **A440**, 685 (1985).

23. **Y. Yin**, Z. Tan and K. Chen, "High Energy Nucleus-Nucleus Elastic Scattering", PHYSICA ENERGIAE FORTIS ET PHYSICA NUCLEARIS, **9**, 569, (1985).

BIBLIOGRAPHY

Alibert C., S. Gaillard, J. A. Brum, G. Bastard, P. Frijlink and M. Erman, 1985, Solid State Comm. **53**, 457.

Allegre J., J. Calayud, B. Gil, N. Mathieu, H. Tuffigo, G. Lentz, N. Magnea and H. Mariette, 1990, Phys. Rev. **B41**, 8195.

Allen, P. B. and V. Heine, 1976, J. Phys. **C9**, 2305.

Allen, P. B. and M. Cardona, 1981, Phys. Rev. **B23**, 1495.

Allen, P. B. and M. Cardona, 1983, Phys. Rev. **B27**, 4760.

Altarelli, M., 1986, in Heterojunctions and Semiconductor Superlattices, G. Allan, G. Bastard, N. Boccara, M. Lannoo, M. Voos (Springer, Berlin, 1986) p. 12.

Ando T., A. G. Fowler, and F. Stern, 1982, Rev. Mod. Phys. **54**, 437.

Antoncik E., 1955, Czeck. J. Phys. **5**, 449.

Arnaud G., J. Allègre, P. Lefebvre and H. Mathieu, 1992, Phys. Rev. **B46**, 15290.

Asami K., K. Miki, K. Sakamoto, T. Sakamoto and S.-I. Gonnda, 1990, Jap. J. Appl. Phys. **29**, L381.

Aspnes D. E. and A. Frova, 1970, Phys. Rev. **B2**, 1037.

Aspnes D. E., 1972, Surface Science **37**, 418.

Aspnes D. E. and N. Bottka, 1972, in Semiconductors and Semimetals, Vol. 9, eds. R. L. Willardson and A. C. Beer (Academic, New York, 1972), p.457.

Aspnes D. E. and A. A. Studna, 1973, Phys. Rev. **B7**, 4605.

Aspnes D. E., 1974, Phys. Rev. **B10**, 4228.

Aspnes D. E. and M. Cardona, 1978, Phys. Rev. **B17**, 726.

Aspnes D. E., 1980, in Handbook on Semiconductors, Vol. 2, ed. M. Balkanski (North-Holland, New York, 1980), p. 109.

Bar-Joseph I., J. M. Kuo, C. Klingshirn, G. Livescu, T. Y. Chang, d. A. B. Miller,

and D. S. chemla, 1987, Phys. Rev. Lett., **59**, 1357.

Bassani R. and G. Pastori Parravicini, 1973, Electronic States and Optical Transitions in Solids, Pergamon Press, Chapter 6.

Bastard G., 1981, Phys. Rev. **B24**, 5693.

Bastard G., 1982, Phys. Rev. **B25**, 7584.

Bastard G., 1988, Wave Mechanics Applied to Semiconductor Heterostructures, Les Editions de Physique, distributed by John Wiley and Sons, Chapter V and references therein.

Batchelor R. A., A. C. Brown and A. Hammett, 1990a, Phys. Rev. **B41** 1401.

Batchelor R. A. and A. Hamnett, 1990b, Proc. Soc. Photo-Optical Instrum. Engineers (SPIE, Bellingham, 1990) **1286**, 175.

Batchelor R. A. and A. Hamnett, 1992 J. Appl. Phys. **71**, 2414.

Bauer E. G., B. W. Dodson, D. J. Ehrlich, L. C. Feldman, C. Peter Flynn, M. W. Geis, J. P. Harbison, R. J. Matyi, P. S. Peercy, P. M. Petroff, J. M. Phillips, G. B. Stringfellow and A. Zangwill, 1990, J. Mater. Res. **5**, 852.

Bean J. C., L. C. Feldman, A.T. Fiory, S. Nakahars and I.K. Robinson, 1984a, J. Vac. Sci. Technol. **A212**, 436.

Bean J. C., T. T. Sheng, L. C. Feldman, A. T. Fiory and R. T. Lynch, 1984b, Appl. Phys. Lett. **44**, 103.

Bean J. C., 1988, in Advanced Surface Processes for Optoelectronics, ed. by S.L. Bernasek, T. Venkatesen and H. Temkin, MRS Symposia Proceedings No. 126 (Materials Research Society, Pittsburgh, 1988) p. 111.

Behn U. and H. Roppischer, 1988, J. Phys. C: Solid State Phys. **21**, 5507.

Ben-Daniel D. J. and C. B. duke, 1966, Phys. Rev. **152**, 683.

Bevk, J., J.P. Mannaerts, L.C. Feldman, B.A. Davidson, and A. Ourmazd, 1986, Appl. Phys. Lett. **49**, 286.

Bhattacharya R., H. Shen, P. Parayanthal, F. H. Pollak, T. Coutts and H. Aharoni, 1987a, Solar Cells **21**, 371.

Bhattacharya R., H. Shen, P. Parayanthal, F. H. Pollak, T. Coutts and H. Aharoni, 1987b, Proc. Soc. Photo-Optical Instrum. Engineers (SPIE, Bellingham, 1987) **794**, 81.

Bhattacharya R., H. Shen, P. Parayanthal, F. H. Pollak, T. Coutta and H. Sharoni, 1988, Phys. Rev. **B37**, 4044.

Bicelli L. P., 1987, J. Appl. Phys. **62**, 4523.

Bir G. L. and G. E. Pikus, 1974, in Symmetry and Strain-Induced Effects in Semiconductors, John Wiley, New York, 1974.

Bottka N., D. K. Gaskill, R. S. Sillmon, R. Henry and R. Glosser, 1988, J. Electron. Materials **17**, 161.

Bottka N., D. K. Gaskill, P.D. Wright, R. W. Kaliski and D.A. Williams, 1991, J. Cryst. Growth **107**, 893.

Brantley W. A., 1973, J. Appl. Phys. **44**, 534.

Brooks, H., 1955, in Advances in Electronics and Electron Physics, Vol. 8, ed. L. Marton (Academic Press, New York, 1955), 132.

Brierley S. K., W. E. Hoke, P. S. Lyman and H. T. Hendriks, 1991, Appl. Phys. Lett. **59**, 3306.

Camassel J., D. Auvergne, H. Mathieu and B. Pistoulet, 1970, Phys. Stat. Sol. **42**, 147.

Campi, D., C. Cacciatore, C. Coriasso, C. Alibert and A. Regreny, 1990, in E-MRS Nov 27-30, 1990.

Cardona M. and F. H. Pollak, 1966, Phys. Rev. **142**, 530.

Cardona M., 1969, Modulation Spectroscopy (Academic, New York, 1969) and references therein.

Cardona M., 1970, Festkorperprobleme X (Pergamon, Oxford,1970) p. 125.

Chang S. J., M. A. Kallel, K.L. Wang, R. C. Bowman, Jr. and P. Chow, 1988, Proc. Soc. Photo-Optical Instrum. Engineers (SPIE, Bellingham, 1988) **946**, 163.

Chemla D. S., I. Bar-Joseph, C. Klingshirn, D. A. B. Miller, J. M. Kuo, and T. Y. Young, 1987, Appl. Phys. Lett. **50**, 585.

Chemla D. S., I. Bar-Joseph, J. M. Kuo, T. Y. Chang, C. Klingshirn, G. Livescu and D. A. B. Miller, 1988a, IEEE J. of Quantum Eelectronics, **24**, 1664.

Chemla D. S., 1988b, in Laser Optics of Condensed Matter, ed. by J.L. Birman, H.Z. Cummins and A.A. Kaplyanski (Plenum, New York, 1988) p.71.

Chen W., M. Fritze, W. Walecki and A. V. Nurmikko, 1992, Phys. Rev. **B45**, 8464.

Chen Y. J., Emil S. Koteles, B. S. Elman, and C. A. Armiento, 1987, Phys. Rev. **B36**, 4562.

Cohen M. L., 1962, Phys. Rev. **128**, 131.

Coriasso, C., D. Campi, C. Cacciatore, C. Alibert, S. Gaillard, B. Lambert, and A. Regreny, 1990, Euro. Phys. Leets.

Dafesh P. A., V. Arbet and K.L. Wang, 1990a, Appl. Phys. Lett. **56**, 1498.

Dafesh P. A., V. Arbet and K.L. Wang, 1990b, Proc. Soc. Photo-Optical Instrum. Engineers (SPIE, Bellingham) **1286**. 308.

Dafesh P. A. and K. L. Wong, 1992, Phys. Rev. **B45**, 1712.

Delalande C., J. Orgonasi, J.A. Brum, G. Bastard, M. Voos, G. Weimann and W. Schlapp, 1987, Appl. Phys. Lett. **51**, 1346; also, 1986, Phys. Rev. **B34**, 2482.

Delalande C., J. Orgonasi, M. H. Meynardier, J. A. Brum, and G. Bastard, 1986, Solid State Commun. **59**, 613.

Delalande C., G. Bastard, J. Orgonasi, J. A. Brum, H. W. Liu, M. Voos, G. Weimann, and W. Schlapp, 1987, Phys. Rev. Lett. **59**, 2690.

Dingle R., H. L. Stormer, A. C. Gossard and W. Wiegmann, 1978, Appl. Phys. Lett. **33**, 665.

Dodabalapur A., V.P. Kesan, D.P. Neikirk, B.G. Streetman, M.H. Herman and I. D. Ward, 1990, J. Electron. Materials **19**, 265.

Dimoulas A., K. Zekentes, M. Androulidaki, N. Kornelios, C. Michelakis and Z. Hatzopoulos, 1993, Appl. Phys. Lett. **63**, 1417.

Dutartre D., G. Bremont, A. Soufi and T. Benyattou, 1991, Phys. Rev. **B44**, 11525.

Edwards S. F. and Y. B. Gulyaev, 1964, Proc. Phys. Soc. **83**, 495.

Ehrenfreund E., J. Oiknine-Schlesinger, D. Gershoni, D. Ritter, M. B. Panish and R. A. Hamm, 1992, Surface Science **267**, 461.

Elliott, R. J., 1957, Phys. Rev. **108**, 1387.

Enderlein R., R. Keiper, and W. Tausendfreund, 1969, phys. stat. sol. **33**, 69.

Enderlein R., D.-S. Jiang and Y. S. Tang, 1988, Phys. Stat. Solidi **145(b)**, 167.

Enderlein R., 1990, in Proc. Soc. Photo-Optical Instrum. Engineers (SPIE, Bellingham, 1990) **1286**, 188.

Erman M., J. B. Theetan, P. Frijlink, S. Gaillard, F. J. Hia and C. Alibert, 1984, J. Appl. Phys. **56**, 3241.

Esaki, L. and R. Tsu, 1970, IBM J. Res. Develop. **14**, 61.

Esaki, L., 1981, J. Cryst. Growth **52**, 227.

Fan H. Y., 1951, Phys. Rev. **82**, 900.

Ferrieu F., F. Beck and D. Dutartre, 1992, Solid State Commun. **82**, 427.

Frank, F. C. and J. H. Van der Merwe, 1949, Proc. Roy. Soc. London **A198**, 216.

Fritze M., W. Chen, and A. V. Nurmikko, 1992, Phys. Rev. **B45**, 8048.

Froyen, S., S. M. Wood and A. Zunger, 1987, Phys. Rev. **B36**, 4574.

Gal M. and C. Shwe, 1990, Appl. Phys. Lett. **56**, 545.

Garini Y., E. Cohen, E. Ehrenfreund, A. Ron, K.K. Law, J.L. Merz and A.C. Gossard, 1992, Surf. Sci. **263**, 561.

Garland J. W., H. Abad, M. Viccaro and P. M. Raccah, 1988, Appl. Phys. Lett. **52**, 1176.

Gell, M. A., M.H. Herman, K. Elcess, I.D. Ward, C.J. Gibbings and C. G. Tuppen, 1990, Proc. Soc. Photo-Optical Instrum. Engineers (SPIE, Bellingham) **1286**, p.320.

Gilpérez J. M., J. L. Sànchez-Rojas, E. Muñoz, E. Calleja, J. P. R. David, G. Hill and J. Castagné, 1992, Appl. Phys. Lett. **61**, 1225.

Glembocki O. J., B. V. Shanabrook, N. Bottka, W. T. Beard and J. Comas, 1985a, Proc. Soc. Photo-Optical Instrum. Engineers (SPIE, Bellingham,1985) **524**, p.86.

Glembocki O. J., B. V. Shanabrook, N. Bottka, W. T. Beard and J. Comas, 1985b, Appl. Phys. Lett. **46**, 970-972 (1985).

Glembocki O. J. and B. V. Shanabrook, 1987, Superlattices and Microstructures **3**, 235.

Glembocki O. J. and B. V. Shanabrook, 1987, Proc. Soc. Photo-Optical Instrum. Engineers (SPIE, Bellingham, 1987) **794**, 74.

Glembocki O. J. and B. V. Shanabrook, 1989, Superlattices and Microstructures **5**, 603.

Glembocki O. J., 1990a, Mat. Res. Soc. Symp. Proc. **160**, 631.

Glembocki O. J., 1990b, in Proc. Soc. Photo-Optical Instrum. Engineers (SPIE, Bellingham, 1990) **1286**, 2 and references therein.

Glembocki O. J. and B. V. Shanabrook, 1992, in Semiconductors and Semimetals, Vol. 36, ed. D.G. Seiler and C.L. Littler (Academic, New York, 1992) p. 221 and references therein.

Gnutzmann U. and K. Clausecker, 1974, Appl. Phys. **3**, 9.

Godby R. W, M. Schluter and L.J. Sham, 1988, Phys. Rev. **B37**, 10159.

Gopalan S., P. Lautenschlager and M. Cardona, 1987, Phys. Rev. **B35**, 2163.

Gumbs G., D. Huang, Y. Yin, H. Qiang, D. Yan F. H. Pollak and T. F. Noble, 1993, Phys. Rev. **B48**, 18328.

Hamakawa Y. and T. Nishino, 1976, Optical Properties of Solids: New Developments ed. B. O. Seraphin (North-Holland, Amsterdam, 1976) p. 255.

Hamnett A., J. Gilman, and R. A. Batchelor, 1992, Electrochimica Acta, **37**, 949.

Harrison W. A., 1961, Phys. Rev. **123**, 85.

Hawrylak P., 1990, Phys. Rev. **B42**, 8986.

Hawrylak P., 1991, Phys. Rev. **B44**, 6262.

Hensel J. C. and G. Feher, 1963, Phys Rev **129**, 1041.

Herman M. H., I. D. Ward, R.F. Kopf, S.S. Pearton and E.D. Jones, 1990a, Materials Research Society Proceedings. **160**, 655.

Herman M. H., 1990b, Proc. Soc. Photo-Optical Instrum. Engineers (SPIE, Bellingham, 1990) **1286**, 39.

Herring C. and E. Vogt, 1956, Phys. Rev. **101**, 933.

Hopfel R. A., J. Shah, A. C. Gossard and W. Wiegmann, 1985, Appl. Phys. Lett. **47**, 163.

Huang D., R. Houdre, Y. C. Chang, and H. Morkoc, 1987, Bull. Amer. Phys. Soc., **32**, 850.

Huang D., H. Y. Chu, Y. C. Chang, R. Houdre and H. Morkoc, 1988a, Phys. Rev **B38**, 1246.

Huang D., G. Ji, U. K. Reddy, H. Morkoc, F. Xiong and T. A. Tombrello, 1988b, J. Appl. Phys. **63**, 5447.

Huang Y. S., H. Qiang, F. H. Pollak, J. Lee and B. Elman, 1991a, J. Appl. Phys. **70**, 3808 (1991).

Huang Y. S., H. Qiang, F. H. Pollak, G. D. Pettit, R. D. Kirchner, J. M. Woodall, H. Stragier and L.B. Sorensen, 1991b, J. Appl. Phys. **70**, 7537.

Humlicek J., M. Garriga, M.I. Alonso and M. Cardona, 1989, J. Appl. Phys. **65**, 2827.

Hybertsen M. S. and M. Schulter, 1988, Mat. Res. Soc. Symp. Proc. Vol. 102 (Mat. Res. Soc., Pittsburgh, 1988) p. 413.

Isihara A., 1989, in Solid State Physics, advances in Research and Applications, eds. H. Ehrenreich and D. Turnbull (Academic Press, 1989), Vol. 42, 135.

Iyer S. S., G. L. Patton, J.B.C. Stork, B.S. Meyerson and D.L. Harame, 1989, IEEE Tansactions on Electron devices, **36**, 2403.

Jackson P. L. and E. G. Seebauer, 1991, J. Appl. Phys. **69**, 943.

Jesser, W. A. and D. Kuhlmann-Wilsdorf, 1967, Phys. Status Solidi **19**, 95.

Jiang D.-S., Y. S. Tang, J.-B. Xia and R. Enderlein, 1989, Superlattices and Microstructures **6**, 387.

Kallergi M., B. Roughani, J. Aubel and S. Sundaram, 1990, J. Appl. Phys. **68**, 4656.

Kane, E. O., 1966, in Semiconductors and Semimetals, Vol. 1, eds. R. K. Willardson and A. C. Beer (Academic, New York, 1966), p. 75.

Kane, E. O., 1970, Phys. Rev. **178**, 1368.

Kim, C. K., C. P. Lautenschlager and M. Cardona, 1986, Solid State Comm. **59**, 797.

King C. A., J. L. Hoyt and J.F. Gibbons, 1989, IEEE Transactions on Electron Devices, **36**, 2093.

King, F. W., 1978, J. Opt. Soc. Am. **68**, 994.

King, F. W., 1977, J. Phys. **C10**, 3199.

Kleiner W. H. and L. M. Roth, 1959, Phys. Rev. Lett. **2**, 334.

Kline J. S., F. H. Pollak and M. Cardona, 1968, Helv. Phys. Acta **41**, 968.

Klipstein P. C., P. R. Tapster, N. Apsley, D. A. Anderson, M. S. Skolnick, T. Kerr M. and K. Woodbridge, 1986a, J. Phys. C: Solid State Phys. **19**, 857.

Klipstein P. C. and N. Apsley, 1986b, J. Phys. C: Solid State Phys. **19**, 6461.

Knox W. H., D. S. Chemla, and G. Livescu, 1988, Solid State Electron. **31**, 425.

Kohn, W., 1957, in Solid State Physics: Advances in Research and Applications, F. Seitz and D. Turnbull, eds., (Academic, New York, 1957) Vol. 5, p. 257.

Kuech T. F., D.J. Woeford, R. Potemski, J.A. Brodley, K.N. Kelleher, D. Yan, J.P. Farrele, P.M.S. Lesser and F.H. Pollak, 1987, Appl. Phys. Lett. **51**, 505.

Landolt-Börnstein, 1982, Numerical Data and Functional Relationship in Science and Technology, Vols. 17a and 17b, eds. O. Madelung, M. Schulz and H. Weiss, Springer, New York, 1982.

Laude L., F. H. Pollak and M. Cardona, 1971, Phys. Rev. **B3**, 2623.

Lautenschlager, P., P. B. Allen and M. Cardona, 1985, Phys. Rev. **B31**, 2163.

Lautenschlager, P., P. B. Allen and M. Cardona, 1986, Phys. Rev. **B33**, 5501.

Lautenschlager, P., M. Garriga and M. Cardona, 1987a, Phys. Rev. **B35**, 9174.

Lautenschlager, P., M. Garriga and M. Cardona, 1987b, Phys. Rev. **B36**, 4813.

Lee J. S., Y. Iwasa, and N. Miura, 1987, Semiconductor Sci. Technol. **2**, 675.

Lee J. and M. O. Vassell, 1988a, Phys. Rev. **B37**, 8861.

Lee J., C. Jagannath, M.O. Vassel and E. S. Koteles, 1988b, Phys. Rev. **B37**, 4164.

Lee A. Y., A.K. Ramdas, A.L. Moretti, F.A. Chambers, G.P. Devone, L. R. Ram-Mohan, 1990, Phys. Rev. **B41**, 8380.

Liu C. T., S.Y. lin, D.C. Tsui, H. Lee and D. Ackley, 1988, Appl. Phys. Lett. **53**, 2510.

Livescu G., D. A. B. Miller, D. S. Chemla, M. Ramaswamy, T. Y. Chang, N. Sauer, A. C. Gossard, and J. H. English, 1988, IEEE J. of Quantum Electronics **24**, 1677.

Lobentanzer H., H. J. Polland, W. W. Ruhle, W. Stolz and K. Ploog, 1987, Phys. Rev. **B36**, 1136.

Lukes T. and K. T. S. Somaratna, 1970, J. Phys. **C3**, 2044.

Mahan G. D., 1967a, Phys. Rev. **153**, 882.

Mahan G. D., 1967b, Phys. Rev. **163**, 612.

Marzin, J. Y., 1985, in Proc. 85 Les Houches Winterschool Semiconductor Superlattices and Heterojunctions, eds. G.Allan, G. Bastard, N. Boccara, M. Lannoo and M. Voos, Springer-Verlag, Berlin, 161.

Manoogian A. and J. C. Woolley, 1984, Can. J. Phys. **62**, 285.

Marzin, J. Y. and J. M. Gérard, 1990, Semiconductors and Semimetals Vol. 32, ed. T. P. Pearsall (Academic, New York, 1990), p. 55.

Matthews, J. W. and A. E. Blakeslee, 1976, J. Cryst. Growth **32**, 256.

Mencziger U., M. Dahmen, R. Zachai, K. Eberl and G. Abstreiter, 1991, Proc. Soc. Photo-Optical Instrum. Engineers (SPIE, Bellingham) **1361**, 282.

Mendez E. E., L. L. Chang, G. Landgren, R. Ludeke, L. Esaki and F. H. Pollak, 1981, Phys. Rev. Lett. **46**, 1230.

Mendonca C. A. C., L. M. R. scolfaro, J. M. V. Martins, E. A. Meneses and J. R. Leite, 1990, in Proceedings of the Society of Photo-Optical Instrumentation Engineers (SPIE, Bellingham, 1990), **1286**, 370.

Merzbacher, E., 1970, Quauntum Mechanics, 2nd ed. (John Wiley and Sons, New York, 1970), pp. 100-105.

Meseguer F., J. C. Maan, and K. Ploog, 1987, Phys. Rev. **B35**, 2505.

Meynardier M. H., J. Orgonasi, C. Delalande, J. A. Brum, G. Basstard, and M. Voos, 1986, Phys. Rev. **B34**, 2482.

Miller R. C. and D. A. Cleinman, 1985, J. Luminecscence, **30**, 520.

Mioc S. L., P.M. Raccah and J.W. Garland, 1992, Proc. Soc.Photo-Optical Instrum. Engineers (SPIE, Bellingham, 1992) **1678**, 296.

Morkoc, H. and H. Unlu, 1987, in Semiconductors and Semimetals, Vol. 24, ed. by R. dingle (Academic, New York, 1987) p. 135.

Mueller J. F., A. E. Ruckenstein, and S. Schmitt-Rink, 1991, Mod. Phys. Lett. **B2**, 135.

Nakayama M., I. Tanaka, T. Doguchi and H. Nishimura, 1990, Jap. J. Appl. Phys. **29**, L1760.

Novellino R. A., C. Vazquez-Lopez, A. A. Bernussi, C. Schmidt, F. Cerdeira, P. Motisuke, F. H. Pollak, F. Meseguer and K. Ploog, 1991, J. Appl. Phys. **70**, 5577.

Nozieres P. and C. T. De Dominicis, 1969, Phys. Rev. **178**, 1079.

Nye J. F., 1957, Physicsl Properties of Crystals: Their Representation by Tensors and Matrices, Clarendon Press, Oxford, 1957.

O'Donnell, K. P. and X. Chen, 1991, Appl. Phys. Lett. **58**, 2924.

Osbourn, G. C., 1982, J. Vac. Sci. Technol. **21**, 459.

Osbourn, G. C., 1983, in Proc. Int. Conf. Metastable and Modulated Semiconductor Structures,Pasadena, 1982, eds. F. J. Grunthaner and A. Madhukar, J. Vac. Sci. Technol., Vol. B1(2), 379.

Osbourn, G. C., 1985, Superlattices and Microstructures, **1**, 223.

Pan N., X. L. Zheng, H. Hendriks and J. Carter, 1990, J. Appl. Phys. **68**, 2355.

Pan S. H., H. Shen, Z. Hang, F.H. Pollak, W. Zhuang, Q. Xu, A.P. Roth, R.A. Masut, C. Lacelle and D. Morris, 1988, Phys. Rev. **B38**, 3375.

Pearsall T. P., J. Bevk, L.C. Feldman, J.M. Bonar, J.P. Mannaerts, and A. Ourmazd, 1987, Phys. Rev. Lett. **58**, 729.

Pearsall T. P., J. Bevk, J.C. Bean, J. Bonar, J.P. Mannaerts and A. Ourmazd, 1989a, Phys. Rev. **B39**, 3741.

Pearsall T. P., 1989b, in CRC Critical Reviews in Solid State and Materials Sciences, Vol. 15, p. 551.

Pearsall T. P., J. M. Vandenberg, R. Hull and J.M. Bonar, 1989c Phys. Rev. Lett. **63**, 2014.

Pearsall T. P., J. C. Bean and J. M. Bonar, 1989d, Thin Solid Films, **183**, 9.

Pearsall T. P., 1990a, in Semiconductors and Semimetals, Vol. 32, ed. by T.P. Pearsall (Academic, New York, 1990) p. 1.

Pearsall T. P., 1990b, in Preceedings of the Socielty of Photo-Optical Instrumantantion Engineers, edited by F.H. Pollak, M. Cardona, and D.E. Aspnes (SPIE, Bellingham, WA, 1990), Vol. 1286, p. 256.

Pearsall T. P., 1992, Appl. Phys. Lett. **60**, 1712.

Pearsall T. P., 1993, Phys. Rev. **B48**, 2795.

Peiponen K. -E. and E. M. Vartiainen, 1991, Phys Rev. **B44**, 8301.

People R., 1986, IEEE J. Quantum Electronics, **QE-22**, 1696 and references therein.

People R. and S.A. Jackson, 1987, Phys. Rev. **B36**, 1310.

People R. and S. A. Jackson, 1990, in Semiconductors and Semimetals, Vol. 32, ed. T.P. Pearsall (Academic Press, New York, 1990), p. 119.

Petrou A., G. Waytena, X. Liu, J. Ralston, and G. Wicks, 1986, Phy. Rev. **B34**, 7436.

Phillips J. C., 1973, Bonds and Bands in Semiconductors, Academic Press, 1973. Pickering C., R. T. Carline, D. J. Robbins, W. Y. Leong, S. J. Bennet, A. D. Pitt and A. G. Cullis, J. Appl. Phys. **73**, 239 (1993); C. Pickering, personal communication.

Pinczuk A., J. Shah, R. C. Miller, A. C. Gossard and W. Wiegman, 1984, Solid State Commun. **50**, 734.

Pollak F. H., C. W. Higginbotham and M. Cardona, J. Phys. Soc. Japan Suppl. **21**, 20 (1966).

Pollak F. H. and G. W. Rubloff, Phys. Rev. Lett., **29**, 789 (1972).

Pollak F. H., Surface Science **B36**, 863 (1973).

Pollak F. H., 1981, Proc. Soc. Photo-Optical Instrum. Engineers (SPIE, Bellingham, 1981) **276**, 142.

Pollak F. H. and O. J. Glembocki, 1988, Proc. Soc. Photo-Optical Instrum. Engineers, edited by O.J. Glembocki, F.H. Pollak, and F. Ponce (SPIE, Bellingham, WA, 1988), Vol. 946, p. 2.

Pollak F. H. and H. Shen, 1989a, J. Crystal Growth **98**, 53.

Pollak F. H. and H. Shen, 1989b, Superlattices and Microstructures **6**, 203.

Pollak F. H. and H. Shen, 1990a, J. Electron. Materials **19**, 399.

Pollak F. H., 1990b, in Semiconductors and Semimetals, Vol. 32, ed. T. P. Pearsall (Academic, New York, 1990), p. 17.

Pollak F. H., 1991, Superlattices and Microstructures **10**, 333.

Pollak F. H., 1992, Encyclopedia of Materials Characterization: Surfaces, Interfaces and Thin Films , ed. by C. Evans, R. Brundle and S. Wilson (Butterworth-Heinemann, Boston, 1992) p. 385.

Pollak F. H. and H. Shen, 1993, to be published in Materials Science and Engineering R: Reports, 1993.

Press, W. H., B. P. Flannery, S. A. Teukolsky and W. T. Vetterling, 1988,

Numerical Recipes in C, (Cambridge, New York, 1988) p. 398.

Priester, C., G. Allan and M. Lannoo, 1988, Phys. Rev. **B38**, 9870.

Qiang H., F. H. Pollak and G. Heckman, 1990, Solid State Comm. **76**, 108.

Qiang H., F. H. Pollak, C. Mailhiot, G. D. Pettit and J. M. Woodall, 1991, Phys. Rev. **B44**, 9126.

Qiang H., F. H. Pollak, C. Mailhiot, G. D. Pettit and J. M. Woodall, 1992. Surface Science **267**, 103.

Qiang H., 1993, Ph.D. Thesis, The City University of New York, 1993 (unpublished).

Raccanelli M., C.T. Drowley, N.D. Theodore, R.B. Gregory, H.G. Tomkins and D.J. Meyer, 1992, Appl. Phys. Lett. **60**, 2225.

Rees, H. D., 1967, Solid State Commun. **5**, 365.

Rees, H. D., 1968, J. Phys. Chem. Solids **29**, 143.

Richardson, D. and R. Hill, 1971, J. Phys. **C4**, 1339.

Ruckenstein A. E., S. Schmitt-Rink and R. C. Miller, 1986, Phys. Rev. Lett., **56**, 504.

Ruckenstein A. E. and S. Schmitt-Rink, 1987, Phys. Rev. **B35**, 7551.

Schaff W. J., P. J. Tasker, M. C. Foisy and L. F. Eastman, 1990, Semiconductors and Semimetals, Vol. 32, ed. by T.P. Pearsall (Academic, New York, 1990) p.73.

Schmid, U., F. Lukes, N. E. Christensen, M. Alouani, and M. Cardona, 1990, Phys. Rev. Lett. **65**, 1933.

Schmid, U., N. E. Christensen, M. Alouani, and M. Cardona, 1991, Phys. Rev. **B43**, 14597.

Schmid, U., J. Humlicek, F. Lukes, M. Cardona, H. Presting, H. Kibbel, E. Kasper, K. Eberl, W. Wegscheider, and G. Abstreiter, 1992, Phys. Rev. **B45**, 6793.

Schmitt-Rink S., C. Ell and H. Haug, 1983, Phys. Rev. **B33**, 1183.

Seraphin, B. O., 1972, in Semiconductors and Semimetals, Vol. 9, eds. R. L. Willardson and A. C. Beer (Academic, New York, 1972), p. 1.

Shanabrook B. V. and O. J. Glembocki, 1987, Proc. 18th Int. Conf. Phys. Semicond., Stockholm, ed. O. Engstrom (World Scientific, Singapore, 1987) p. 565.

Shanabrook B. V., O. J. Glembocki and W. T. Beard, 1987, Phys. Rev. **B35**, 2540.

Shank C. V., R. L. Fork, R. Yen, J. Shah, B.I. Greene, A.C. Gossard and C. Weisbuch, 1983, Solid State Comm. **47**, 981.

Shen H., X. C. Shen, F.H. Pollak and R.N. Sacks, 1987, Phys. Rev. **B35**, 3487.

Shen H., P. Parayanthal, Y. F. Liu and F. H. Pollak, 1987, Rev. Sci. Instrum. **58**, 1429.

Shen H. and M. Dutta, 1990a, Appl. Phys. Lett. **57**, 587.

Shen H., M. Dutta, L. Fotiadis, P.G. Newman, R.P. Moerkirk, W.H. Chang and R.N. Sacks, 1990b, Appl. Phys. Lett. **57**, 2118.

Shen H., F. H. Pollak, J. M. Woodall and R. N. Sacks, 1990c, J. Electron. Materials **19**, 283.

Shen H. and F.H. Pollak, 1990d, Phys. Rev. **B42**, 7079.

Shields A. J., P. C. Klipstein, and N. Apsley, 1989, Semicond. Sci. Technol. **4**, 476.

Shields A. J. and P. C. Klipstein, 1991, Phys. Rev. **B43**, 9118.

Silberstein R. P. and F. H. Pollak, 1980, Solid State Comm. **33**, 1131.

Skolnick M. S., J. M. Rorison, K. J. Nash, D. J. Mowbray, P. R. Tapster, S. J. Bass and A. d. Pitt, 1987a, Phys. Rev. Lett. **58**, 2130.

Skolnick M. S., K. J. Nash, P. R. Tapster, D. J. Mowbray, S. J. Bass, and A. D. Pitt, 1987b, Phys. Rev. **B35**, 5925.

Skolnick M. S., K. J. Nash, M. K. Saker, S. J. Bass, P. A. Claxton, and J. S. Roberts, 1987c, Appl. Phys. Lett. **50**, 1885.

Smith D. L. and C. Mailhiot, 1987, Phys. Rev. Lett. **58**, 1264.

Smith D. L. and C. Mailhiot, 1990, Rev. Mod. Phys. **62**, 173.

Smith M. C., A. Petrou, C. H. Perry, J. M. Worlock, and r. L. Aggarwal, 1985, in Proc. 17th Int. Conf. Phys. Semiconductors, San Francisco, CA, 1984, Eds. J.D. Chadi

and W. A. Harrison, New York, Sringer-Verlag, 547.

Smith P. M., P. C. Chao, J. M. Ballingall and A. W. Swenson, 1990, in Microwave Journal, May 1990, p. 71.

Snow E. S., O, J. Glembocki and B. V. Shanabrook, 1988, Phys. Rev. **B38**, 12483.

Stern F., 1986, in the Proceedings of the Les Houches Winterschool, edited by G. Allan, G. Bastard, N. Boccara, M. Lannoo and M. Voos (Springer Verlag, Berlin) 1986.

Stormer H. L., R. Dingle, A. C. Gossard, W. Wiegmann and R. A. Logan, 1979, Conf. Ser. --Inst. Phys. Vol. 43, p. 557.

Streit D. C., K. L. Tan, R. M. Dia, J. K. Liu, A. C. Han, J. R. Velcbir, S. K. Wang, T. Q. Trinh, P. D. Chow, P. H. liu and H. C. Yen, 1991, IEEE Electron Device Lett. **12**, 149.

Stroud D. and H. Ehrenreich, 1970, Phys. Rev. **B2**, 2197.

Sydor M., N. Jahren, W.C. Mitchel, W.V. Lampert, T.W. Haas, M.Y. Yen, S.M. Mudare and D.H. Tomich, 1990, J. Appl. Phys. **67**, 7423.

Sydor M. and A. Badakhshan, 1991a, J. Appl. Phys. **70**, 2322.

Sydor M., A. Badakhshan, James R. Engholm and D. A. Dale, 1991b, Appl. Phys. Lett. **58**, 948.

Sydor M. and J. R. Engholm, M. O. Manasreh, K. R. Evans, C. E. Stutz and W. C. Mitchel, 1992, Phys. Rev. **B45**, 13796.

Tan K. L., R. M. Dia, D. C. Streit, T. S. Lin, T. Q. Trinh, A. C. Han, P. H. Liu, P. D. Chow and H. C. Yen, 1990, IEEE Electron Device Lett. **11**, 585.

Tang Y. S., 1991, J. Appl. Phys. **69**, 8298.

Tang Y. S., 1992, Phys. Stat. Sol **129(a)**, 285.

Tauc J. and A. Abrahám, 1961, J. Phys. Chem. Solids **20**, 190.

Theis W. M., G. D. Sanders, C. E. Leak, K. K. Bajaj and H. Morkoc, 1988, Phys. Rev. **B37**, 3042.

Thorn A. P., A. J. Shields, P. C. Klipstein, N. Apsley and T. M. Kerr, 1987, J. Phys.

C: Solid State Phys. **20**, 4229.

Tober R. L., J. Pamulapati, J. E. Oh and P. K. Bhattacharya, 1988, Appl. Phys. Lett. **53**, 883.

Tober R. L., J. Pamulapati, J. E. Oh and P. K. Bhattacharya, 1989, J. Electron. Mat. **18**, 379.

Toyozawa S. Y., 1958, Prog. Theor. Phys. **20**, 53.

Van der Merwe, J. H., 1963, J. Appl. Phys. **34**, 123.

Vandenberg J. M., R. A. Hamm, M.B. Panish and H. Temkin, 1987, J. Appl. Phys. **62**, 1278.

Varshni, Y. P., 1967, Physica(Utrecht) **34**, 149.

Voisin, P., 1984, in Two-Dimensional Systems, Heterostructures and Superlattices, eds. G. Bauer, F. Kuchar, and H. Heinrich, 1984 (Springer-Verlag, Berlin 1984), Springer Series in Solid State Sciences, Vol. 53, p.192.

Voisin, P., J. Bleuse, C. Bouche, S. Gaillard, C. Alibert and A. Regreny, 1988, Phys. Rev. Lett., **61**, 1639.

Voos, M., 1983, J. Vac. Sci. Technol. **B(1)**, 404.

Warren A. C., J. M. Woodall, P. D. Kirchner, X. Yin, X. Guo, F. H. Pollak and M. r. Melloch, 1992, J. Vac. Sci. Technol. **B10**, 1904.

Weisbuch C. and B. Vinter, 1991, in Quantum Semiconductor Structures: Fundamentals and Applications (Academic Press, New York, 1991) p.57.

Weisbuch, C., 1987, Semiconductor and Semimetals, Vol. 24, ed. by R. dingle (Academic, New York, 1987), p. 1.

Yin X., F.H. Pollak, L. Pawlowicz, T. O'Neill and M. Hafizi, 1990a, Appl. Phys. Lett. **56**, 1278.

Yin X., F.H. Pollak, L. Pawlowicz, T. O'Neill and M. Hafizi, 1990b, Proceedings of the Society of Photo-Optical Instrumentation Engineers (SPIE, Bellingham, 1990) **1286**, 404 (1990).

Yin X. and F. H. Pollak, 1991, Appl. Phys. Lett. **59**, 2305.

Yin X., X. Guo, F.H. Pollak, G.D. Pettit, J.M. Woodall, T.P. Chin and C. W. Tu, 1992a, Appl. Phys. Lett. **60**, 1336.

Yin X., X. Guo, F.H. Pollak, G.D. Pettit, J.M. Woodall, and E-H. Cirlin, 1992b Proc. Soc. Photo-Optical Instrum. Engineers (SPIE, Bellingham, 1992) **1678**, 168.

Yin Y., D. Yan, F. H. Pollak, G.D. Pettit and J.M. Woodall, 1991a, Phys. Rev. **B43**, 12138.

Yin Y., D. Yan, F. H. Pollak, M.S. Hybertsen, J.M. Vandenberg, and J.C. Bean, 1991b, Phys. Rev. **B44**, 5955.

Yin Y., H. Qiang, F. H. Pollak, D. C. Streit, and M. Wojtowicz, 1992a, Proceedings of the Society of the Photo-Optical Instrumentation Engineers (SPIE, Bellingham), **1675**,498.

Yin Y., H. Qiang, F. H. Pollak, D. C. Streit, and M. Wojtowicz, 1992b, Appl. Phys. Lett. **61**, 1579.

Yin Y., D. Yan, F. H. Pollak, M.S. Hybertsen, J.M. Vandenberg and J.C. Bean, 1992c, Surface Science **267**, 99.

Yin Y., F. H. Pollak, P. Auvray, D. Dutartre, R. Pantel and J. A. Chroboczek, 1992d, Thin Solid Films, **222**, 85.

Yin Y., F. H. Pollak, P. Auvray, D. Dutartre, R. Pantel and J. A. Chroboczek, to be published.

Yin Y., H. Qiang, D. Yan, F. H. Pollak and T. F. Noble, 1993, Semiconductor Science and Technology, **8**, 1599.

Yin Y., D. Yan, F. H. Pollak, M.S. Hybertsen, J.M. Vandenberg and J.C. Bean, submitted to Phys. Rev..

Zhang S. B., et al., 1988, Solid State Commun **66**, 585.

Zhang Y. H. and K. Ploog, 1992, Phys. Rev. **B45**, 14069.

Zheng X. L., D. Heiman, B. Lax, F.A. Chambers and K.A. Stair, 1988a, Appl. Phys. Lett. **52**, 984.

Zheng X. L., D. Heiman, B. Lax and F. A. Chambers, 1988b, Appl. Phys. Lett. **52**, 287.

Zheng X. L., D. Heiman, B. Lax and F. A. Chambers, 1988c, Proc. Soc. Photo-Optical Engineers (SPIE, Bellingham, 1988) **946**, 43.

Zhan W., C.H. Perry, L. Ma, K-S. Lee, J.M. Worlock, A. Zrenner, F. Koch and K. Ploog, 1991, J. Appl. Phys. **69**, 4075.

Zollner, S., S. Gopalan and M. Cardona, 1991, Solid State Comm. **77**, 485.